Doctoral Dissertation
Doctoral Program in Materials Science and Technology (35th Cycle)

Plasma-based surface treatment for improving joint strength of joined ceramics and ceramic matrix composites

Alessandro De Zanet

* * * * * *

Supervisors

Prof. Valentina Casalegno, Supervisor

Prof. Milena Salvo, Co-Supervisor

Doctoral Examination Committee:

Prof. Thierry Cutard, Referee, Institut Clément ADER – UMR CNRS 5312, IMT Mines Albi, Albi, France

Prof. Joaquin Ramirez Rico, Referee, Universidad de Sevilla, Sevilla, Spain

Politecnico di Torino
September 2023

I hereby declare that the contents and organization of this dissertation constitute my own original work and do not compromise in any way the rights of third parties, including those relating to the security of personal data.

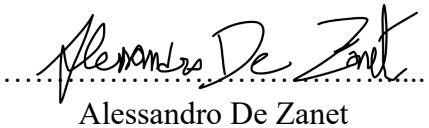

Alessandro De Zanet
Turin, September 2023

Summary

Joining ceramics enables the manufacturing of parts able to face challenging conditions such as high temperatures and corrosive operational environments.

To manufacture a reliable product, promoting optimal adhesion between the parts to be joined and the joining material is critical. This can be promoted by a preliminary preparation of the surface and in particular by modifying the surface texture and chemistry.

Surface texturing of ceramics can be costly, time-consuming, and difficult with traditional techniques like mechanical machining and wet etching because of their hardness, brittleness, and chemical inertness. These limits can be overcome by non-contact surface texturing techniques based on plasma and laser, promising solutions that are recognized as promising, but more research is needed.

This thesis aimed to explore and identify new plasma-based solutions for improving the joint strength of joined ceramics and ceramic matrix composites (CMCs) by inducing a new surface texture able to promote interlocking. Plasma treatments are well-known in the preparation of polymeric surfaces and the manufacturing of semiconductors, but little information is available on their use for increasing the resistance of the joints of ceramics. Therefore, this work gives a contribution to extending the available knowledge and it pays special attention to identifying treatments that can be implemented at an industrial scale.

A commercial corona plasma treater was used as a solution for increasing the joint strength of similar joints of bulk silicon carbide (SiC) bonded with itself using an epoxy adhesive. Such treatment is widely known in the plastic industry, but it was never investigated for improving glue adhesion on SiC. Characterization of the surface before and after the treatment was carried out and it was observed the formation of a corona-induced cauliflower-like silica layer on the surface. Both surface chemistry and texture were modified. Mechanical tests (SLO compressive test) found an increase in joint strength after the corona treatment, from 61.5 ± 5.0 MPa to 68.8 ± 2.3 MPa. Furthermore, the failure mode changed from adhesive to cohesive, pointing out a better adhesion of the glue and the uniformity of the treatment.

For CMCs, the difference in terms of the etching resistance of each constituent was exploited to manufacture a brush-like superficial texture beneficial for enhancing the infiltration of the braze and promoting an interlocking effect.

Fluorine-based Reactive Ion Etching (RIE) is a low-pressure plasma technique extensively used for manufacturing semiconductor devices, but it has never been proposed as a pre-joining treatment for SiC/SiC composites. In this work, an RIE plasma was used to induce a selective removal of fibers in order to obtain the brush-like texture. Several plasma conditions were considered and, after preliminary observations, one of them (CF_4, 20 sscm, 200 W, 30 min) was selected for assessing the effects of the treatment on the joint strength. A commercially available AgCuTi braze was used as the joining material. The joint strength of joined SiC/SiC was recorded to increase by 55% after the treatment (SLO compressive test).

The use of a commercial air-fed Atmospheric Pressure Plasma Jet (APPJ) was evaluated to induce selective removal of fibers and, therefore, manufacturing a brush-like texture on carbon-fiber reinforced carbon (C/C) and carbon-fiber reinforced silicon carbide (C/SiC). In both cases, the treatment resulted in the formation of a brush-like texture since fibers were removed preferentially. This was more remarkable for C/SiC because of the strong difference in terms of oxidation resistance between the carbon fibers and the silicon carbide matrix. The novel

texture promoted the infiltration of the braze (TiCuNi system for C/C and AgCuTi for C/SiC) and the consequent interlocking.

Similar joints of C/C were affected by an intense depletion of joining material given by the presence of existing large and interconnected porosities in the composites, while for dissimilar joints copper-C/C the joint strength was higher for APPJ-treated joined samples (22.8 ± 6.5 MPa) then for the untreated (9.5 ± 7.4 MPa). The joint strength of C/SiC, when joined with itself, increased from 45.5 ± 0.6 MPa to 65.8 ± 2.5 MPa after the APPJ treatment. All values were collected through SLO compressive test.

All the plasma treatments investigated in this thesis proved to be promising as pre-treatment before joining in order to improve the final joint strength and the results set the ground for new research on the topic while contributing to generating new knowledge in a little-explored field that is expected to be critical for unlocking novel technologies in next years.

Thesis Outline

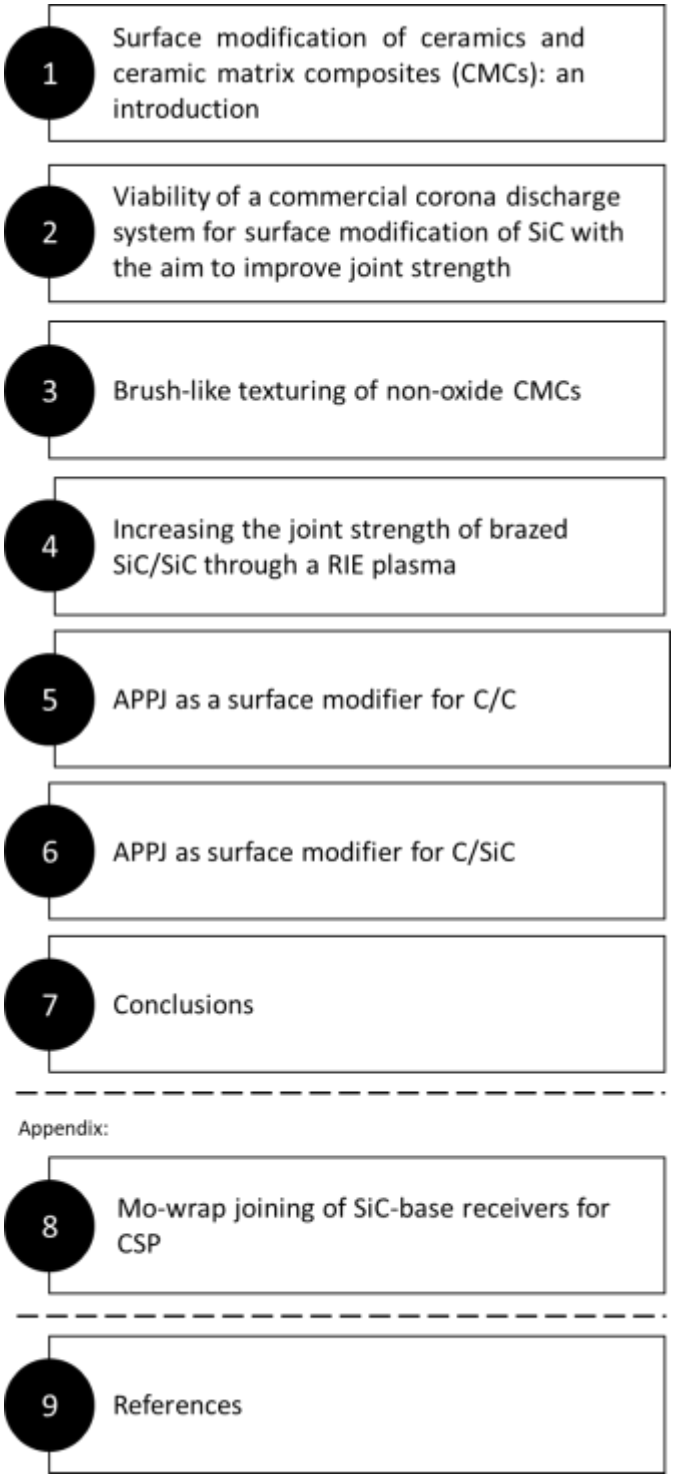

Acknowledgment

I sincerely thank my supervisors, Prof. Valentina Casalegno and Prof. Milena Salvo, for their guidance throughout the entire Ph.D. journey, providing scientific and personal support. I am particularly grateful for their consistent encouragement concerning my research, allowing me to gain confidence and enabling me to grow as both a researcher and an individual. I don't believe I could have asked for better mentors for this experience.

A heartfelt thanks to the entire Glance group for making the journey fantastic. I have encountered wonderful and energized individuals with whom I've been fortunate enough to establish professional and friendship relationships, receiving continuous motivation to push my boundaries and improve through mutual exchange.

A special mention goes to Daniele D'Ambrosio, our laboratory technician, without whom all experimental work wouldn't have been possible, and to Carla Malinverni, with whom I had the pleasure of working closely during the latter part of my Ph.D. on multiple projects. Also, I express gratitude to Antonio Favero for supporting the mechanical tests, and to the team from the interdepartmental center J-TECH, Frediano De Marco, Dr. Mojtaba Alidoost, and Alessandro Benelli, for assisting me with the available instrumentation.

While a Ph.D. is often described as a solitary journey, in my case, it was entirely different, and I am greatly thankful for that. Collaborations are where opportunities for growth and the development of new knowledge and products arise, and I have been fortunate enough to work with incredibly talented and inspiring individuals.

In fact, the research activities presented in this thesis wouldn't have been possible without the valuable contributions of other researchers. Therefore, I would like to sincerely thank Dr. Fabrizio Valenza (CNR-ICMATE, Genoa), Dr. Sofia Gambaro (CNR-ICMATE, Genoa), Dr. Espedito Vassallo (CNR-ISTP, Milan), Dr. Matteo Pedroni (CNR-ISTP, Milan), Dr. Grzegorz Cempura (AGH University, Krakow). Thank you to Prof. Gerard Vignoles (University of Bordeaux) for hosting me at the Laboratoire des Composites Thermo Structuraux and guiding me in approaching modeling.

A loving thank you, finally, to my partner Irene, my family, and my friends for all the love and support I've received throughout this journey.

Contents

List of Tables

List of Figures

1. Surface modification of ceramics and ceramic matrix composites (CMCs): an introduction

The objective of this opening chapter is to provide an overview of the materials targeted by the research work presented in this thesis, non-oxide ceramics and Ceramic Matrix Composites (CMCs), the joining processes available for them, and the importance of the surface when bonding materials. Furthermore, the available surface roughening - and texturing- techniques, with a focus on the most promising for this class of materials, are presented. All these elements will be useful to build the context for this research work's motivation and identify the critical challenges.

CMCs and their application

Traditional ceramics have accompanied humankind since the discovery of pottery approximately 10000 years ago. Everything changed from the beginning of the XIX century when ceramics stopped being seen only as pottery. Indeed, new ceramic materials started to be manufactured to advance industrial applications, such as refractory materials[1]. It was then that technical ceramics made their first appearance, and they experienced fast development.

Nowadays, technical ceramic materials are used for many applications and they have the potential to unlock game-changing technologies. In many cases, they are the only class of materials that can be used to face very high temperatures in harsh environments. However, they have strong limitations. Their brittleness reduces the manufactured components' reliability when employed for structural applications. Ceramic materials are extremely sensitive to the presence of defects and the crack propagation may result in in-service catastrophic failure that is unpredictable. To

overcome this issue, a ductile-like behavior can be triggered through the manufacturing of fiber-reinforced ceramic matrix composites (CMCs). They are made of long ceramic fibers, coated with interphase, and embedded in a ceramic matrix[2]. The orientation of fibers is critical in determining the final mechanical properties of the CMCs and different applications may require different types of composite architecture. They can provide high specific strength and high specific modulus retained at very high temperatures, enabling better performances and weight cuts in the energy and aerospace sectors compared to traditional materials.

Therefore, the global interest in them is progressively increasing since they may unlock new solutions for global challenges, helping to bridge the gap between the current situation and the goals imposed by the 2030 Agenda[3], like energy security and reduction of greenhouse gases emission.

Such interest may be confirmed by the research trend on CMCs that is shown in Fig. 1-1, where the number of articles per year is reported, according to the results for the "ceramic matrix composites" keyword provided by the Scopus Database. The data are not related exclusively to fiber-reinforced CMCs, but they are useful for observing the trend for this class of materials.

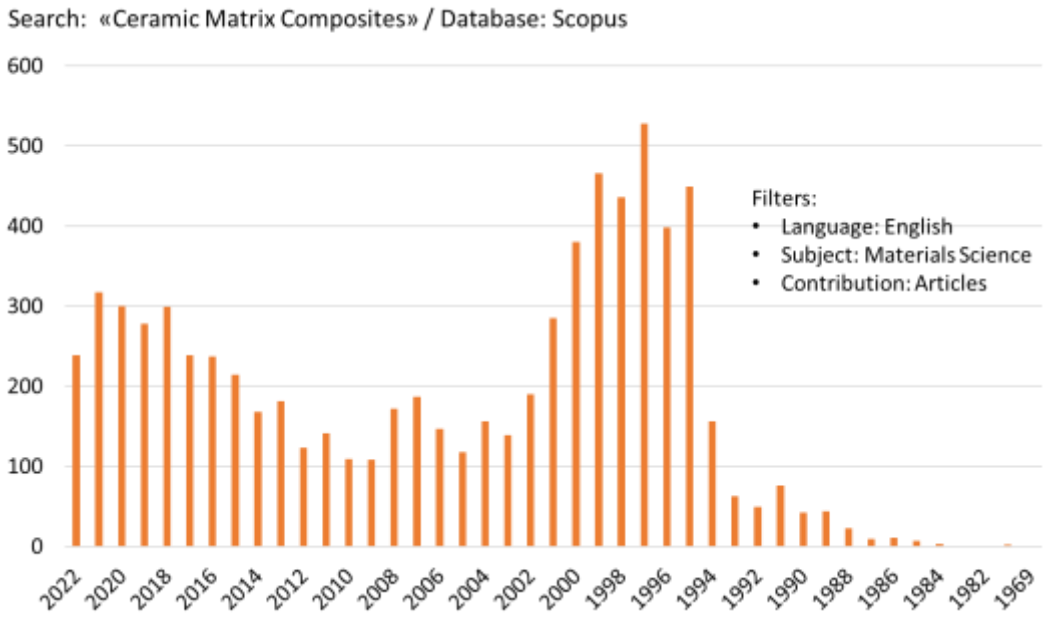

Figure 1-1: Articles per year about "ceramic matrix composites" on Scopus Database (last access: 08/29/2022).

Among all the sectors, together with energy, aerospace is one of the most focused on the utilization of CMC-based solutions to unlock new opportunities and increase performance. In particular, one of the challenges is to achieve a weight reduction of the engine while increasing its efficiency. Fig. 1-2 reports the time evolution of the materials of interest for aerospace engines, starting from 1965. Metals, uncoated and coated with T/EBC (Thermal Barrier Environmental Coating), are the current standard. However, it may be noticed that CMCs are identified as key materials for targeting high-temperature operations. In addition, as introduced, they can retain high mechanical resistance even at high temperatures (over 1000°C), outmatching advanced metallic alloys for aerospace (Fig. 1-3)[4].

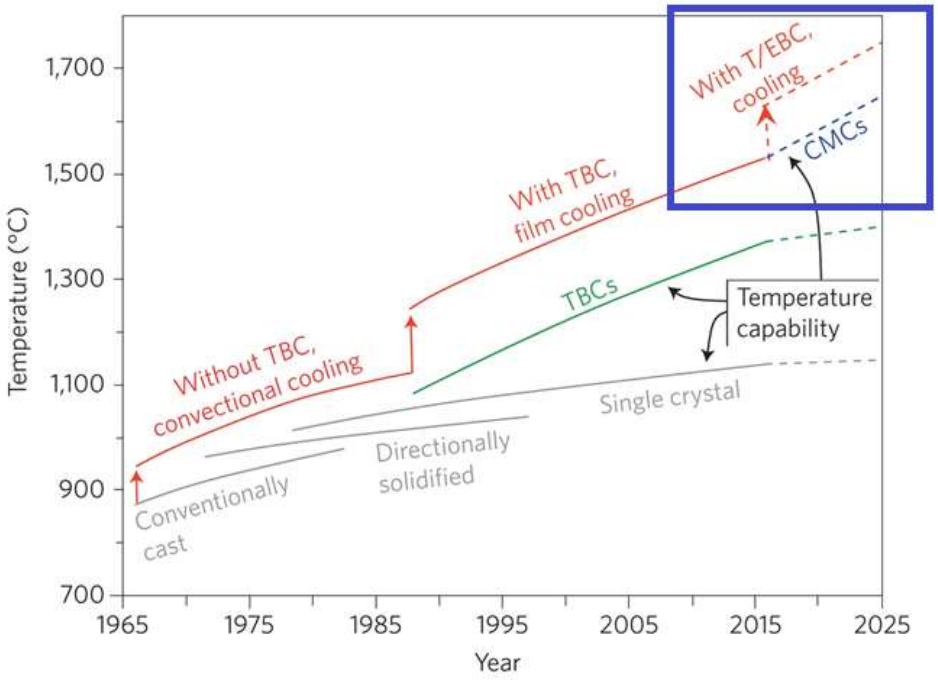

Figure 1-2: Temperature capabilities of several materials for aerospace engines (Adapted from [4]). Green, red and grey colored lines refer to metals, while blue to CMCs.

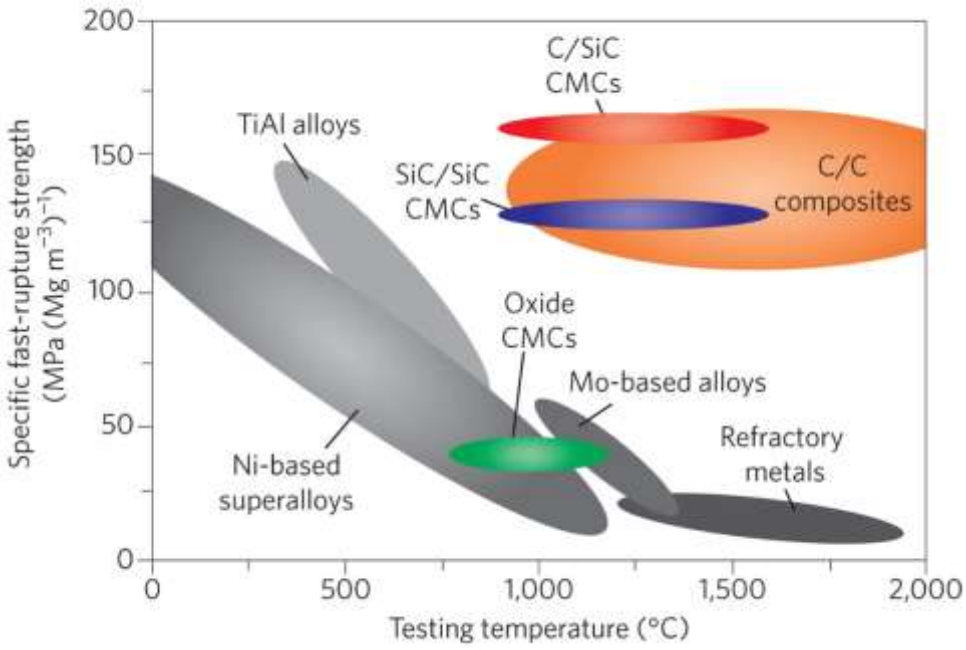

Figure 1-3: Mechanical strength vs temperature behavior for several materials for aerospace engines, including C/C (orange), C/SiC (red), and SiC/SiC (blue). Adapted from [4]).

Since their development between the late 1960s and the early 1970s[5], when high-temperature fibers became available [6,7], researchers more and more focused on advancing the state of the art of these materials to expand their range of applications, in particular, pushed by the aerospace industry.

Indeed, traditionally non-oxide CMCs have found applications in aerospace applications in hot regions like the final stages of turbine engines and rocket nozzles[8,9] or as key materials for Thermal Protective Systems (TPS)[10]. Nowadays, CMCs are considered viable for addressing complex engineering challenges like accident-tolerant fission nuclear reactors[11], nuclear fusion [12], and hypersonic vehicles [13]. Furthermore, CMCs have the potential to replace traditional materials in furnaces for energy-intensive industries like steelmaking to improve the efficiency of the combustion process, thus reducing the GHGs (greenhouse gasses) emission, and extending the lifetime of components[14]. The applications presented are only a fraction of those that may benefit from the use of CMCs. Fig. 1-4 shows the regions of the Pre-X concept X re-entry vehicle where CMCs were proposed.

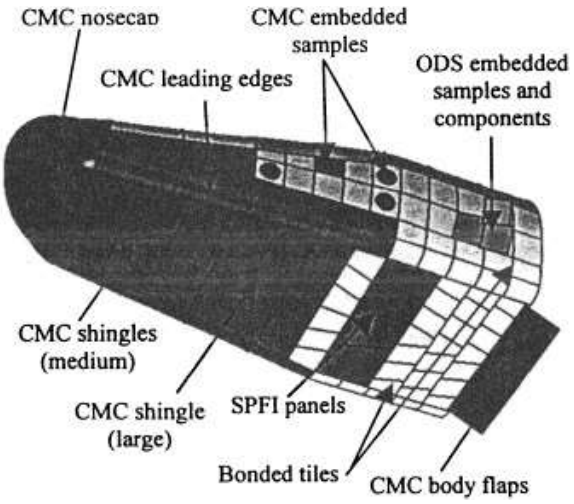

Figure 1-4: Architecture of the TPS for the Pre-X concept re-entry vehicle (adapted from [15])

As can be deducted from Fig. 4 the final product requires assembly to be manufactured. The integration of materials with themselves or other materials is then required. Such a process consists of one or more steps according to the parts to be joined and the complexity of the final component. All these actions constitute the joining process.

Joining is, therefore, a critical and sensitive step that impacts dramatically on the in-service performances since joints are areas of discontinuity where properties are different compared with the rest of the material[16]. Several strategies are available for joining and they have to be evaluated according to the material to be joined and the addressed applications.

Joining of ceramics and CMCs

Joining includes a large variety of processes that may be very different from each other.

Generally, three main categories of joining strategies can be identified: direct joining, mechanical joining, and indirect joining.

Direct joining refers to the technique in which no additional material is used for bonding the two parts. Welding, for example, falls into this category. This is probably the best option because no different material is introduced in the system, but it is quite difficult to perform it on ceramic materials because of their high melting points. Then, very few examples of welding of ceramics have been reported[17]. Some direct bonding techniques based on the diffusion processes have been developed like Spark Plasma Sintering (SPS), but they impose strong limitations on the size and shape of the final product[18].

Mechanical joining is characterized by the use of fasteners to keep the parts in contact with each other. This is a reliable technique, but the parts required preliminary preparation for the insertion of the connectors. For instance, holes may be required for screws.

The hole-making process on ceramics may be risky because of the stress concentration that is produced because of the notch effect[19]. Furthermore, when high temperatures are reached the difference in Coefficient of Thermal Expansion (CTE) can create additional stresses that may be detrimental to the component, in particular when different materials are coupled. The design process has to carefully address this issue to avoid in-service failures.

Fig. 1-5 shows a portion of a TPS system manufactured via mechanical integration of the CMC with the aluminum panel[20]. One of the major advantages given by this approach is that the disassembly of the joined parts is easier and time-effective compared with indirect and direct joining[21].

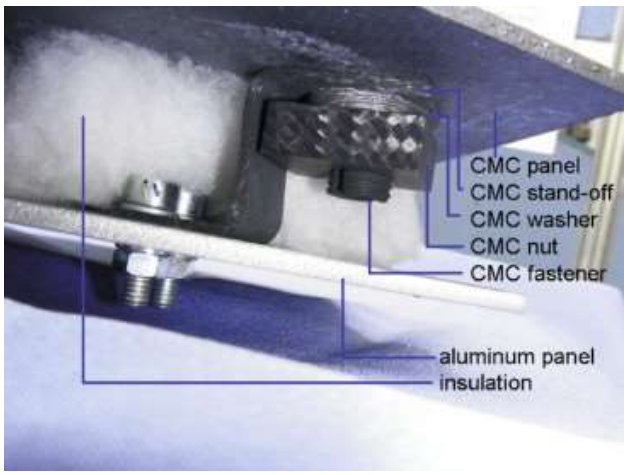

Figure 1-5: Mechanical joining of CMC to an Al panel of a TPS system, Adapted from [20].

Indirect joining includes the techniques that require the use of an additional material, as a bonding agent in order to integrate the parts. The range of materials that can be employed is broad and includes polymers, metals, ceramics, and glasses, chosen according to the parts and the requirements for the application. It is immediate to note how versatile this approach is because of the large variety of solutions that are available. The joining material has to be chosen according to the materials to be joined and to the in-service requirements. For instance, polymeric adhesives are extensively employed at low temperature in all industries and some of them, like epoxy, can be used with most of the materials as substrates[22]. Glasses, instead, are more oriented to high temperature applications in more aggressive environments[23].

It is then possible to merge different approaches. For example, coupling fasteners with a joining material may provide stronger joints and, at the same time, hermeticity.

Concerning CMCs, indirect joining may be considered a viable and versatile technique that enables the manufacturing of large components and meeting the requirements imposed on the products, through the selection of the most suitable technique and material.

The quality of the bonding is strictly dependent on the goodness of the interface between the materials to be joined, which will be indicated as substrate hereafter, and the adhesive. To promote a sound joint, the substrate must have a surface cleaned of contaminants, otherwise, they would act as local barriers to the formation

of an interface compromising the overall joint quality and increasing the risk of detachment.

The substrate and the adhesive must be chemically compatible, if not, no interface may be possible. A first indication can be given by wettability. Poor wettability prevents the formation of a good interface between adherend and bonding material[24]. Reactions between the adhesive and the to-be-joined material may occur, providing strong chemical bonds at the interface. This is the case, for instance, when reactive brazes are used to bond ceramics.

Surface topography is also important since has a dramatic effect on wettability and the substrate/adhesive coupling. If the texture is viable for anchoring between the adherend and the adhesive, a mechanical interlocking effect may occur. This raises when the adhesive infiltrates peaks and valleys accessible on the surface, compenetrating with the substrate (Fig. 6). Those regions behave as anchoring bridges that provide additional strength to the joint [25]. Surface topography is given by three distinct contributions that describe its deviation from an ideal plane: predominant pattern, roughness (distribution of irregularities) and waviness. The higher the deviation from the ideal planar surface, the higher will be the contact area available with the adhesive. For this reason increasing the roughness before bonding can result in improved performance of the joined component. While increasing randomly roughness generally has a positive effect on interlocking, forming a well-distributed texture on the surface is expected to be more effective.

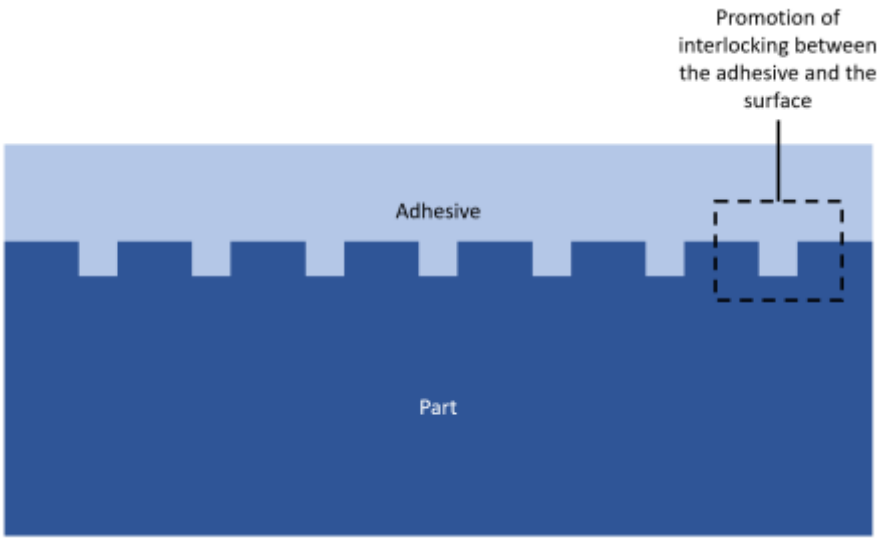

Figure 1-6: sketch of interlocking between adhesive and surface.

Surface preparation is therefore critical for achieving high-quality joints. The surface can be functionalized by introducing chemical groups, can be cleaned from contaminants and its roughness can be changed. Sometimes all these actions are combined to achieve the desired results.

In the next paragraphs, the available technologies for texturing ceramics are described.

Surface texturing of ceramics and CMCs

Several surface processing techniques (schematized in Fig. 1-7) are available for modifying the texture and the roughness of materials, but few may be applied effectively to ceramics, and therefore to ceramic matrix composites. Indeed, their mix of brittleness, inertness, and hardness results in challenges for surface processing.

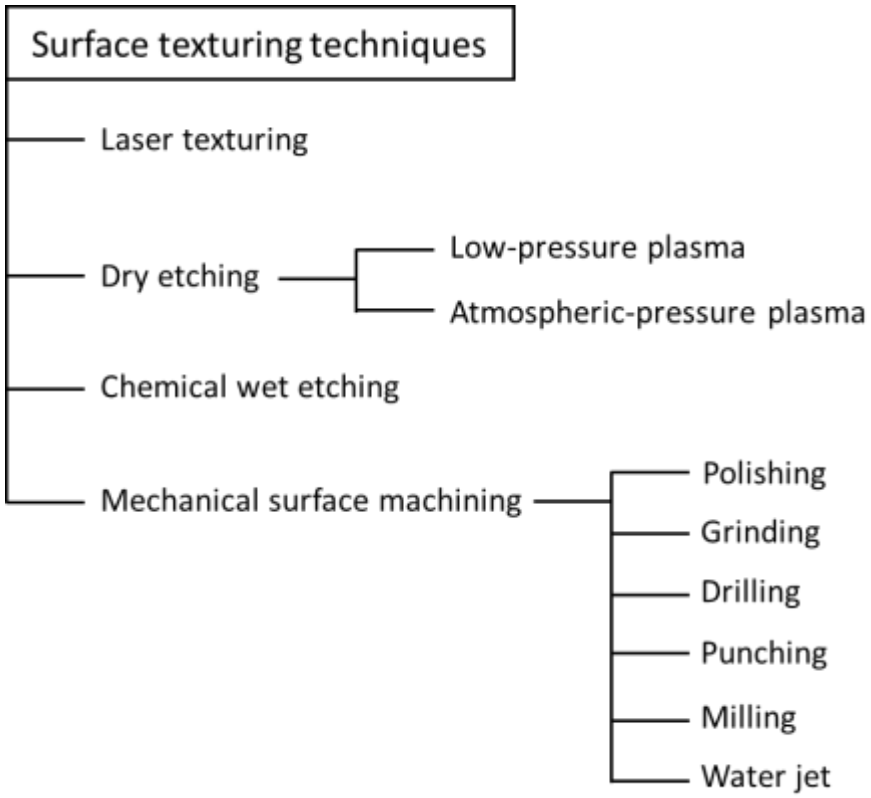

Figure 1-7: scheme of available surface texturing techniques.

Traditional surface roughening and/or texturing rely on mechanical machining and the use of etchants, but they are not very effective for ceramic based materials.

Surface machining may be very difficult to be performed because of the intense wear rate experienced by tools that directly impact costs and the risks of introducing cracks that would propagate later, when in service[26]. However, it is worthy to mention that among mechanical machining techniques, water jet milling has been reported to be a promising technique for surface machining that can be used to tune surface texture while preventing damage to the surface and avoid overheating [27,28].

In traditional wet etching, the material is exposed to a chemically aggressive substance that provides removal by chemical reaction[29]. Ceramics tend to be rather chemically stable and therefore few etchants can be chosen. They usually are not eco-friendly and hazardous for operators. For instance, the main option for etching SiC is molten potassium hydroxide (KOH). Most of the studies available were focused on electronic applications, therefore they reported etching of SiC single crystals. The effectiveness, and therefore the etch rate, increases with the temperature (Fig. 1-8). The main issue is that the etching agent is difficult to handle and the safety concerns are many.

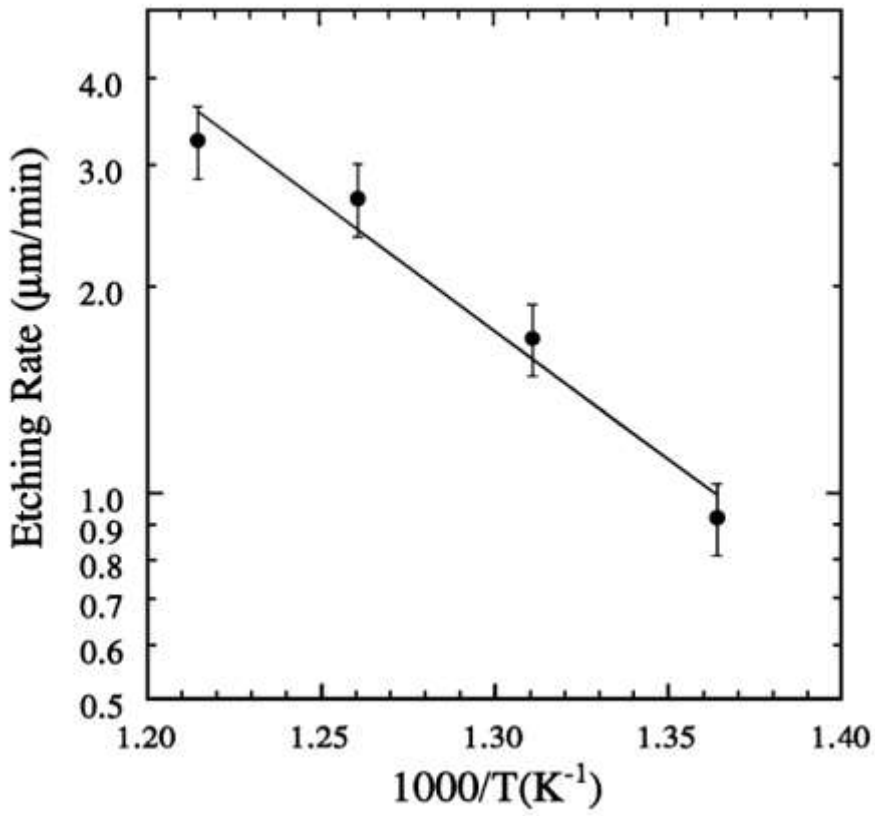

Figure 1-8: etching rate of molten KOH on SiC as function of temperature. Adapted from [30].

Material can be removed even without using a liquid etchant or mechanical operation. In fact, the development of plasma reactors and lasers unlocked new opportunities for the surface preparation of difficult-to-machine hard materials like ceramics. Several techniques are included in these two categories. All of them have the common advantage of avoiding the use of machining tools, therefore no wear occurs, and their high energy makes it easier to carry out chemical reactions and/or to promote physical mechanisms that provide materials removal. Additionally, they can localize the heat at the surface, avoiding detrimental effects on the entire volume of the material.

The removal of matter from a surface is defined as ablation [31] and lasers are extremely promising for this aim because of their versatility and the ability to manufacture very complex and precise patterns once laser-material interactions are optimized.

LASER acronym stands for Light Amplification by Stimulated Emission of Radiation) and the first device was engineered by Theodore Maimann in 1960 [32]. Since then, lasers were improved and they are now targeting a large variety of

applications from medicine to industry. Once laser beam targets the material, the radiation undergoes reflection, absorption and transmission, interacting with electrons and exciting them through the energy exchange [33]. This may lead to heating of surface that can promote local melting or vaporization. If vapor is formed, the presence of the laser-induced electromagnetic field promotes the formation of plasma.

Several types of laser devices exist and they are commercially available. They can work in continuous emission mode or pulsed. Continuous emission lasers provide energy uniformly onto the material surface. Pulsed lasers emit laser light as pulses, resulting in high energy peaks. The emission frequency can vary on a large scale of orders of magnitudes, from seconds to femtoseconds and laser-material interactions change according to the pulse time scale. For exemplification, Fig. 1-9 reports the different effects given by the laser pulse width on fragmentation of silver nanoparticles[34]. As can be seen, the laser-particle interaction completely changes with the pulse time scale.

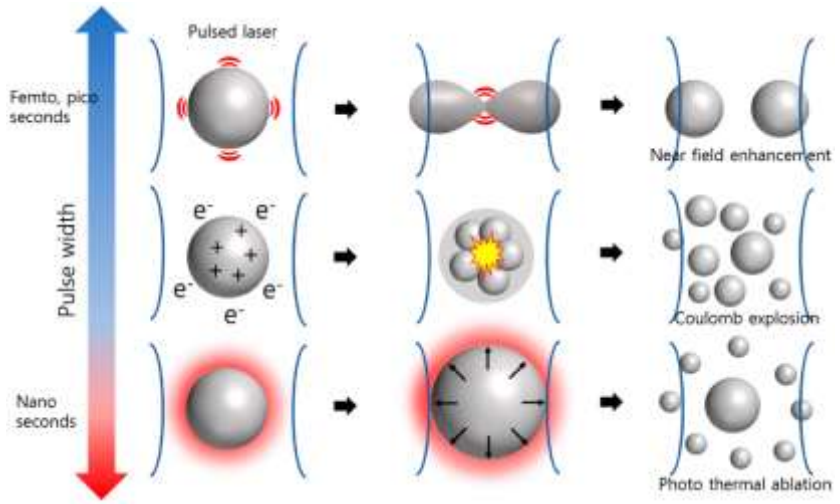

Figure 1-9: different laser-induced effects on silver particles fragmentation depending on pulse width (adapted from* [34]*).

With respect to surface texturing the pulse width and therefore the different laser-material interactions result in a completely different response. Fig. 1-10 summarizes the different macroscopic effects that affect the surface when a long pulse/continuous laser beam and an ultrafast pulsed laser hit the surface. A remarkable difference is the size of the region affected by the beam. In the case of a long-pulsed laser beam, the heat is dissipated by the material and therefore its action is not confined to the application point, thus generating many unwanted side

effects detrimental to successful texturing, such as recast layers, microcracks, melt pool and formation of a heat affected zone around. Instead, the use of an ultrafast laser (pulse shorter than millisecond) can overcome the heat diffusion issue and concentrate the ablation in a very precise area. This is possible because the time scale of the laser emission is shorter than that for the energy transfer to the material lattice, enabling multiphoton absorption and therefore higher energy density in the point hit by the beam [35].

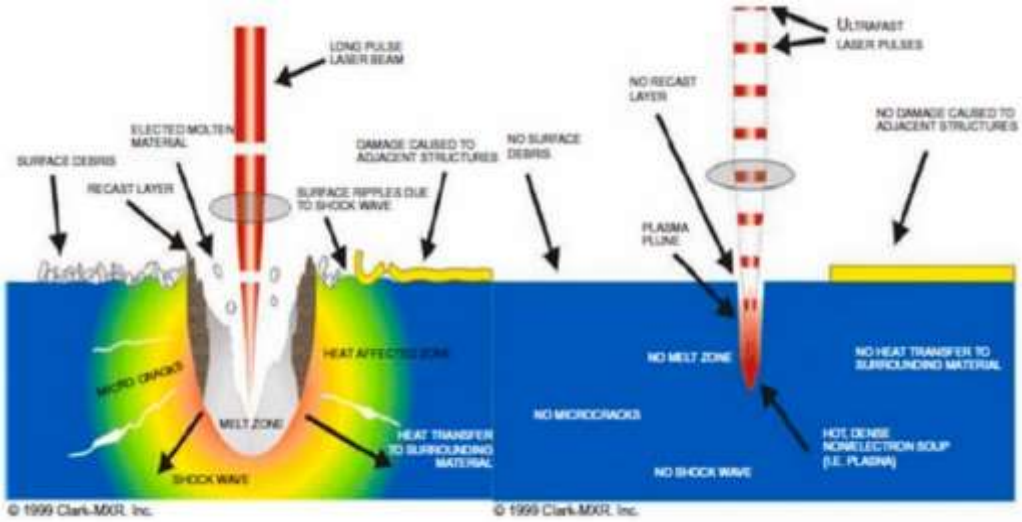

Figure 1-10: comparison between a short-pulsed laser and an ultrafast pulsed laser (adapted from* [36]*).

Three main mechanisms are associated with the laser ablation process: photo-chemical, photo-thermal and photo-physical. They are summarized in Fig. 1-11.

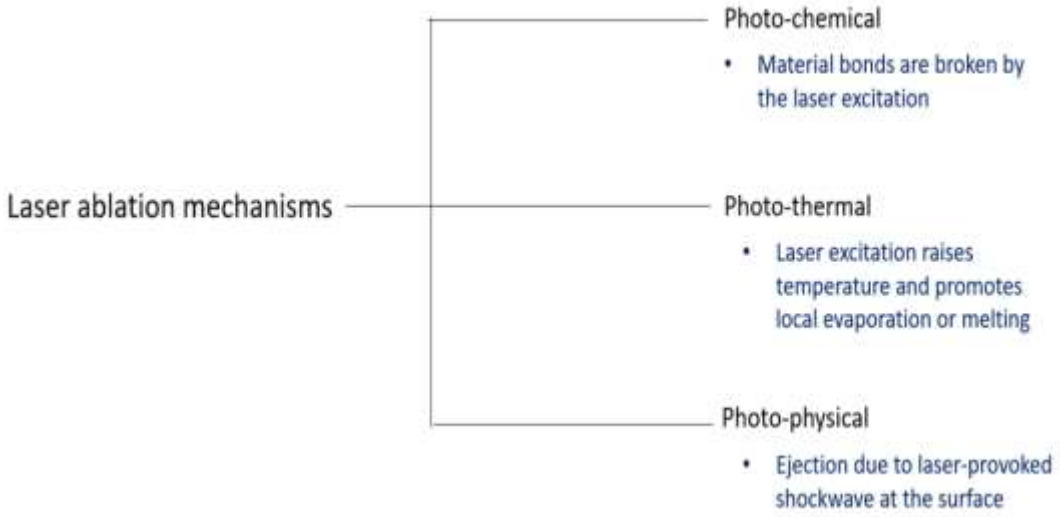

Figure 1-11: summary of laser ablation mechanisms

Photochemical ablation involves breaking material bonds. Bond-breaking can be provoked if laser radiation has a suitable wavelength when long pulsed lasers are used. If ultrafast lasers are employed multiphoton absorption can provide enough energy to break chemical bonds [37]. Multiphoton absorption can enable enough energy to excite an electron from the valence band to the conduction band even in dielectric materials. If enough electrons are promoted, surface properties can change and a transitory metal-like optical behavior can be observed [38].

Fluence is defined by eq. 1. For the low value of radiation fluence provided by ultrafast lasers a photo-physical phenomenon known as Coulomb explosion can take place. Laser-excited highly energetic electrons are pushed out from the lattice which, then, loses the charge balance due to lack of compensation of the contribution of the ions. The ions are then ejected by the strong electric field generated[39]. Alternatively, photo-physical ablation can be caused by shockwave originated by the expansion of the laser induced plasma-plume [40].

$$Fluence\ \left[\frac{J}{cm^2}\right] = \frac{Laser\ pulse\ energy\ [J]}{Effective\ focal\ spot\ area\ [cm^2]} \qquad (1)$$

Photo-thermal ablation takes place because of the laser-induced melting and/or vaporization of the material.

A successful texturing is the result of an optimal match between material and laser parameters, critical for guaranteeing precision and reducing the presence of undesired defects. Ultrashort-pulse lasers, especially picosecond-pulsed and femtosecond-pulsed types, are the most interesting options for the texturing of ceramic materials, in particular, because of their ability to provide local high energy and limit the thermal effect on the entire volume. Therefore, these devices can be considered the most suitable, but they present a major limitation. They are very expensive. A detailed outlook on the application of laser as a surface texturing technique for ceramics and CMCs in several fields is provided in [41]. An example of a fs-pulsed laser texturing of alumina toughened zirconia (ATZ) [42] is shown in Fig. 1-12.

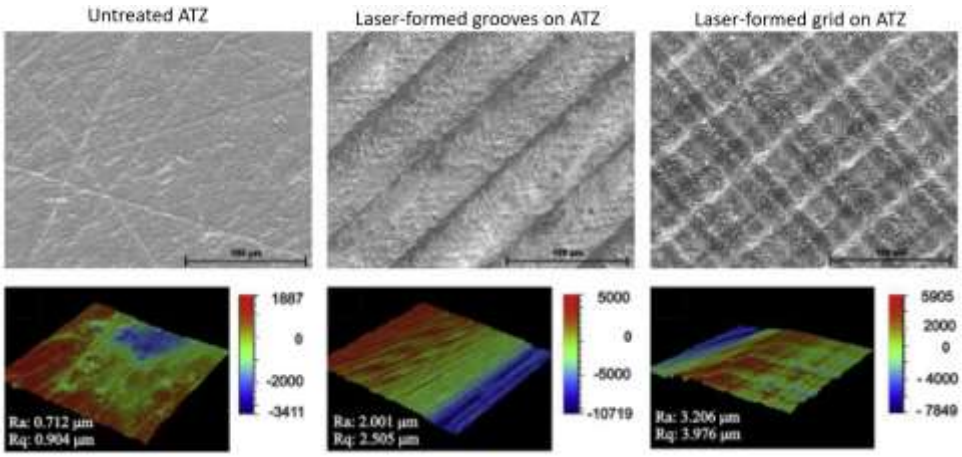

***Figure 1-12: : examples of alumina-toughened zirconia laser-textured surface. Adapted from* [42].**

Few studies have been devoted to the evaluation of laser texturing for non-oxide continuous-fibers CMCs. Wu et al.[43] proposed the use of an excimer laser to induce grooves oriented parallelly and perpendicularly to the fibers of a C/SiC surface. In this case, the ablation mechanism was mainly based on the thermal

effect. They reported an improvement in wettability, a reduction of the anisotropy between different surfaces, and an increase in the oxygen content after laser exposure., Several structures were realized via laser ablation on a C/SiC to investigate changes in wettability given by the process parameters and the laser scanning strategy[44]. In another work[45], the differences between surface texturing of C/SiC manufactured by traditional mechanical machining and laser ablation were studied and they observed that the latter resulted in an increase in the oxygen concentration and a decrease in carbon at the surface. This phenomenon is strongly affected by the surrounding atmosphere that can trigger the redeposition of silica after ablation or oxidation reaction in the heat affected regions[46]. The use of a shielding gas in combination with a femtosecond laser demonstrated good results in preventing these negative effects[47].

As for C/SiC, studies on SiC/SiC laser texturing are still few, but the interest in this topic is increasing as the growing number of scientific papers between 2020 and 2022 can testify. The aim is to build knowledge on the process for these materials and identify the most suitable parameters for successful surface texturing. Several options are under evaluation. For instance, some recent works have focused on continuous-wave lasers [48], femtosecond lasers in air[47], underwater [49] and in reactive atmosphere [50].

Further research has to be carried out in order to make laser texturing of ceramics and CMCs more common, but the trend is encouraging and it may be expected that the next years will be critical for the development of these technologies.

Plasma surface treatment

Besides laser techniques, plasma surface modification methods are another effective option. Plasma processes are not a novelty and are particularly interesting for preparing surfaces. They are used frequently in research and manufacturing for decontamination and cleaning[51,52], surface activation[53], roughening, and texturing[54]. Each industry has contributed to advancing plasma surface technologies. Plastic manufacturers have explored deeply the use of plasma treatment as a means to improve adhesion and promote wettability[55]. The electronic industry has focused on the plasma etching of semiconductor materials for manufacturing integrated circuits. The food and medical industries have focused

on the decontamination properties of plasma for removing hazardous contaminants from food-contact surfaces [56], wounds[57], and tools [58]. The variety of plasma devices available for surface treatment is huge, as well as the applications, but all of them are non-thermal plasmas.

Plasma can be defined as ionized gas, made of light particles, electrons, heavy particles, ions, and neutrons. These charged particles are highly reactive and, as anticipated, they can be exploited to clean the surface by inactivating and removing the contaminants, to etch the surface through physical interactions or chemical reactions, or to depose a coating layer.

To be classified as "plasma" the excited gas has to be quasi-neutral, namely, even if charges are in non-equilibrium locally, they must be globally balanced [59]. Several types of plasmas are included in this definition. They are classified according to their properties. For instance, a first classification can be made considering electron temperature and electron density. Fig. 1-13. shows several types of plasma plotted according to their electron temperature and electron density.

Plasmas can be in thermal equilibrium or not. In thermal-equilibrium plasma heavy particles and light particles have the same energy, global temperature is very high and can be over 10^6 °C[60]. Nuclear fusion is an example. Nonthermal plasmas, instead, are characterized by electrons possessing higher energy than heavy particles. Most of the techniques used for surface processing are based on nonthermal plasmas, also called, cold plasmas, since prevent damage to the entire material, confining the treatment at the surface [61]. Visual classification of plasmas according to the thermal equilibrium of ions/neutrons and electrons is given in Fig. 1-14.

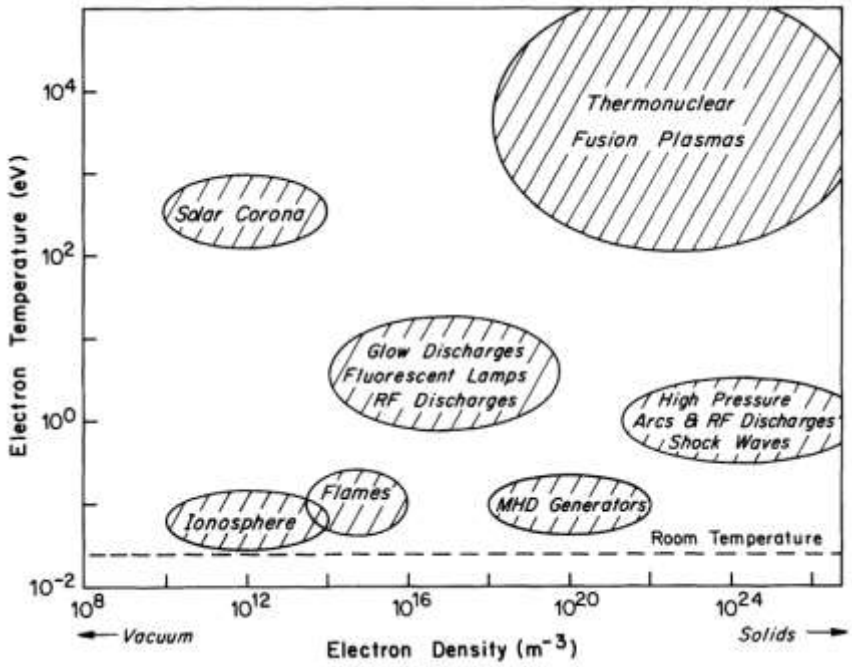

Figure 1-13: plasmas classified according to electron temperature and electron density (adapted from* [62]*).

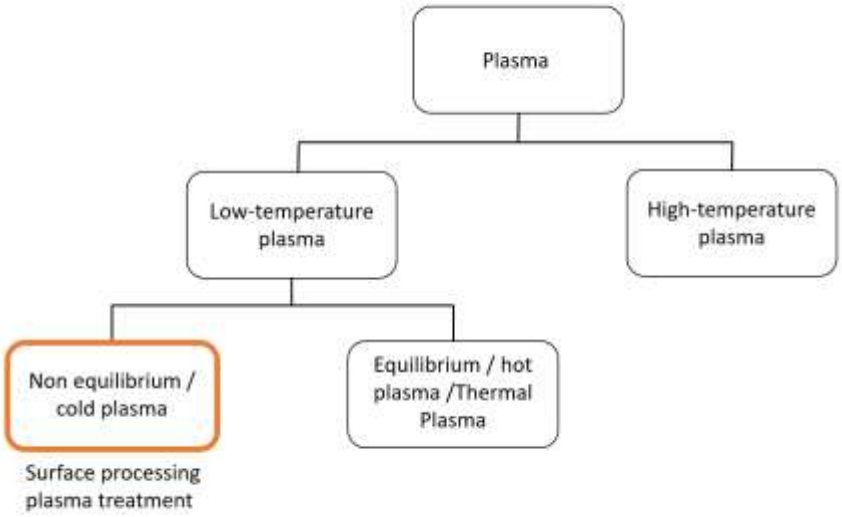

Figure 1-14: classification of plasma according to its temperature.

The literature about plasma is immense, therefore from here on the discussion will be limited to essential information about plasmas for surface modification. To make a plasma, energy for ionization has to be transferred to the gas in order to charge its atoms. To this end, a voltage has to be applied in order to induce a breakdown in the gas.

The entity of the voltage depends on the gas properties, its pressure, and the distance between electrodes. In Fig. 1-15 the dependence of the voltage by gas type, pressur,e and the gap between electrodes is shown. It is evident that the role of pressure is critical because it is one of the main variables for determining the breakdown voltage required for gas ionization. Therefore, plasma techniques can be categorized as low-pressure or atmospheric pressure. Each category has its unique advantages and limitations.

Working at low-pressure makes the gas ionization easier and most effective, as well as to control the uniformity of the glow discharge.

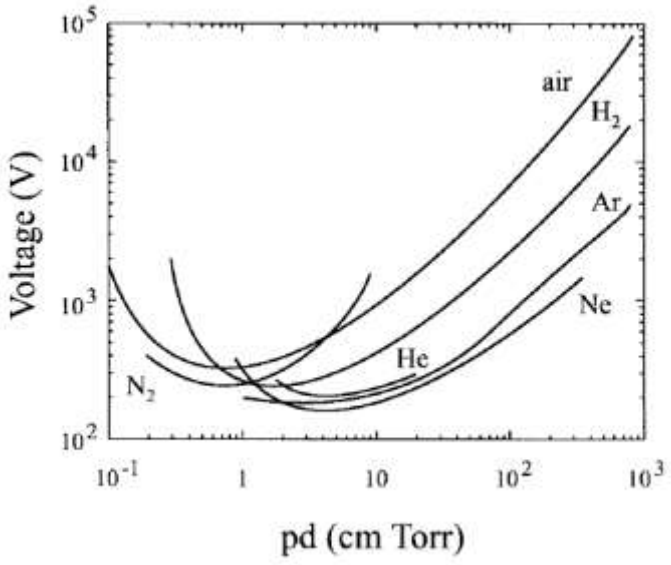

Figure 1-15: relationship between breakdown voltage [V] and the product of pressure and electrode gap [cm Torr] for several gases (adapted from[63]).

Therefore, many low-pressure techniques have been developed. One of the main fields of application is microelectronics where plasma etching was optimized to manufacture semiconductor devices. In order to miniaturize the electronic circuits, an impressive effort has been done to optimize the dry etching of silicon and, later, silicon carbide, which is of interest for power applications. In this case, the texturing is obtained by masking the substrate to enable selective removal of the material from the surface. The etch rate determines the depth of the treatment, enabling also the manufacturing of holes like those generated on Zerodur® (Schott, Germany) shown in Fig. 1-16. Zerodur® is a glass-ceramic system designed for minimizing its coefficient of thermal expansion to enable the production of

advanced optical tools both large like mirrors for telescopes and small like those used for lithography and sensor technology [64,65].

As can be observed in Fig. 1-16 this technique can provide a high accuracy in the manufacturing of the desired texture.

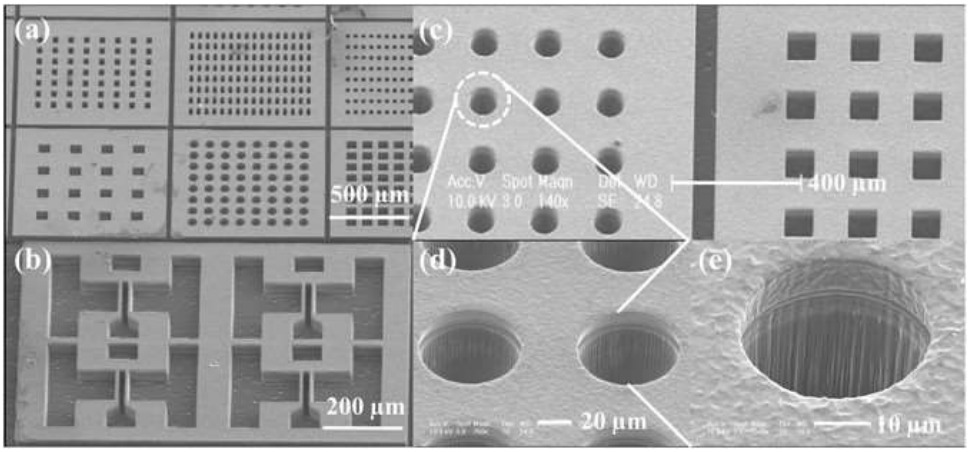

***Figure 1-16: Zerodur structures manufactured via deep etching. Adapted from* [66].**

One of the most relevant etching techniques is Reactive Ion Etching (RIE), a low-pressure process, that enables vertical etching reducing unwanted side etching[67]. This is a very effective methodology for texturing surfaces, mainly in electronics. One or more processe gases are ionized and highly reactive species are generated. When they diffuse to the material, surface reactions take place and volatile by-products are generated and removed from the system, eroding the pristine surface and creating the desired texture thanks to the use of masks. An example of RIE system is shown in Fig. 1-17. As evident, the choice of the process gases is critical for the success of the operation. Common gases used for RIE process are halogen-based (F, Cl, Br, I). For the etching of silicon carbide, SF_6 and CF_4 are the most popular[68], but the use of other gas precursors like NF_3 [69] has been reported. Such gas mixtures have demonstrated also to be successful to dry etch with high accuracy glass-ceramics, like Zerodur® [70,71]. In order to achieve good results, it is rather common to use mixture of gases. By tailoring the gas mixture composition, indeed, it is possible to control the outcome of the process in terms of etch rate, anisotropy, selectivity and surface quality. When high etch rates are required Inductively Coupled Plasma RIE can be used. In this configuration, two plasma sources are coupled to increase the plasma density.

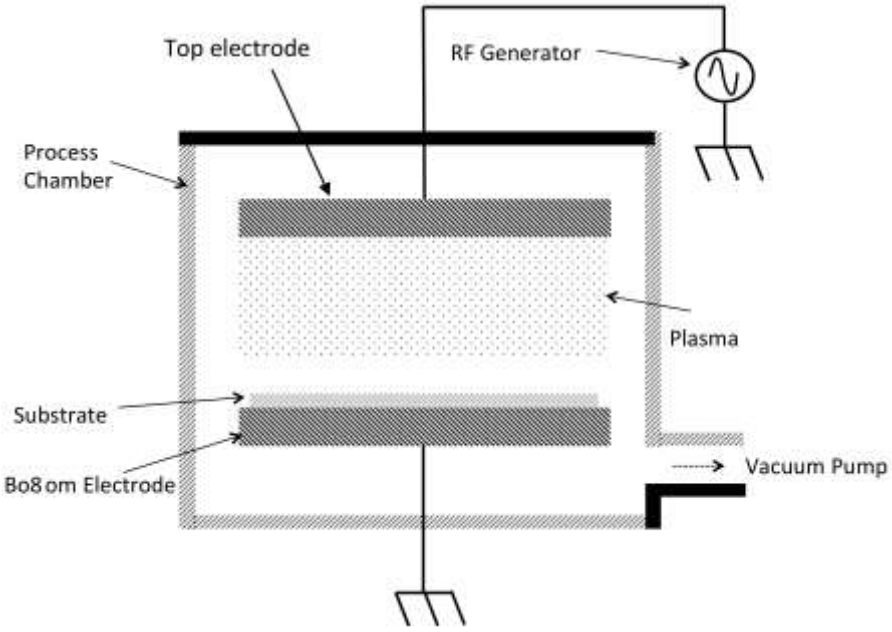

Figure 1-17: schematic representation of RIE (adapted from* [72]*)

Low-pressure plasmas are great for working on small substrates. They provide higher uniformity and good control of the process, but they impose limitations on the size of the samples that can be plasma-treated and they do not make it possible to work continuously.

Atmospheric Pressure Plasmas (APPs) can overcome the issues related to the need for vacuum in low-pressure plasmas, thus, promising cost cuts and higher productivity. In particular, the absence of a vacuum system simplifies the equipment and enables it to work continuously by integrating plasma treatment into the production line. Furthermore, the limitation to the dimensions of the component given by the vacuum chamber is eliminated, making these systems appealing to industry.

APPs are already well-established surface preparation techniques for improving the adhesive bonding of polymers and polymeric matrix composites. One of the most common solutions for this industry is the use of corona plasma devices and, more recently, atmospheric-pressure plasma jets (APPJs)[63]. Polymer surface preparation via corona treatment is a consolidated standard. A filamentary discharge is activated by the application of the voltage between electrodes which results in the partial ionization of the surrounding air. High energy electrons are generated and hit the surface of the material, cleaving bonds.

Furthermore, the ionization of air causes the generation of strong oxidizing species like O_3, atomic oxygen and radicals. The combination of the reactive species together with the bond-breaking results in chemical changes of the surface, promoting the formation of oxygen-rich functional groups. The modification process is sketched in Fig. 1-18. Even if the treatment has proven to be successful, the filamentary nature of the discharge, results in a low plasma density. The use of corona is limited to dielectric materials.

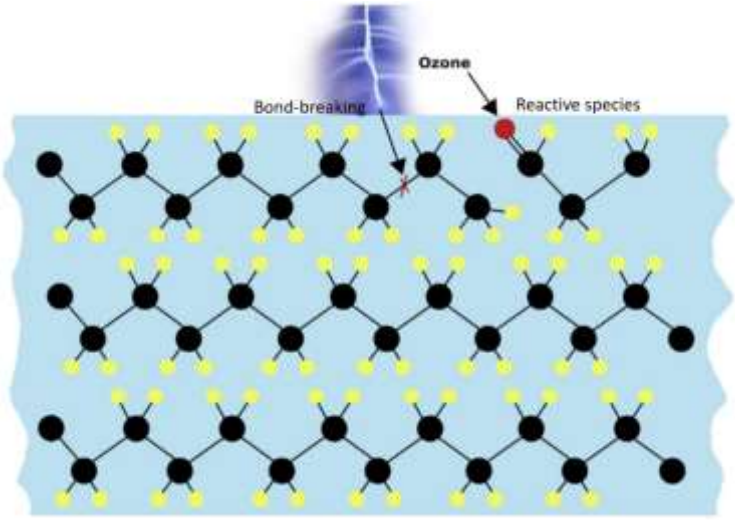

***Figure 1-18: surface modification mechanism induced by corona: bond-breaking and reaction with reactive species like ozone. Adapted from* [73]**

APPJs were developed to increase the plasma density and provide a more efficient and uniform treatment of the material. Plasma is not generated close to the surface to be treated but inside the torch. Then, the gas flow ejects the plasma through the overture. This working principle results in a small area of treatment, but the issue can be solved by scanning the surface to be treated, similarly to laser treatments. On contrary to corona discharge, the APPJ form a stable plasma plume. A typical plasma jet is reported in Fig. 19.

Common plasma gases used in commercial devices are air, nitrogen, argon and oxygen.

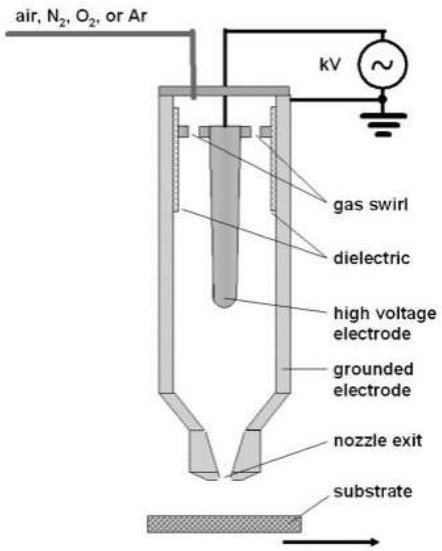

***Figure 1-19: schematic representation of an APPJ. Adapted from* [74].**

Using a different plasma gas mixture is possible to extend the application of APPJ to other materials like glasses [75].

Laser texturing and plasma dry etching are very promising techniques for the processing of the surface of technical ceramics and CMCs, since they are contactless techniques. The amount of information available for plasma etching of ceramics is by far more extensive than for laser texturing, even if no work has been carried out on the etching of CMCs, to the best of our knowledge, but only on bulk ceramics and thin films. However, few studies have addressed the effect of plasma treatments as a preliminary step to prepare the surface for joining.

The research work hereby presented aimed to build knowledge on the viability of existing plasma processes to improve the joint strength for non-oxide CMCs and non-oxide ceramics by providing texturing effect beneficial for interlocking.

Each chapter will be devoted to the use of a plasma surface modification technique on a target material.

2. Viability of a commercial corona discharge system for surface modification of SiC with the aim to improve joint strength

Part of the activity presented in the following chapter was published as a regular article [76] *on Ceramics International (Elsevier).*

Modifying the surface of a ceramic material can be extremely difficult and time-consuming. Non-contact strategies, like lasers and plasma techniques, may be extremely promising to expand the opportunities for sounder joints of ceramics. Addressing needs for aerospace applications, research [77,78] has been carried out within the research group of the author on using a laser and a plasma treatment for inducing a beneficial texture on SiC to provide stronger joints when joined with itself or with other materials (Invar alloy[79]) using an epoxy resin. Both treatments proved to be effective in modifying the surface, but with different effects. The plasma treatment, a low-pressure RIE, did not induce any chemical change and the outcome resulted in a roughness change associated with an improvement in the joint strength and failure mode (from adhesive to cohesive). Rather, the laser treatment carried out in the open air, provided a modification both in terms of chemistry and texture. The novel surface consisted of nanostructured columnar silica with a completely different texture compared with the pristine surface. Laser-treated SiC was expected to provide an improvement in joint strength since the new texture should have improved interlocking, but it performed worse than untreated. This was found to be caused by the laser-formed graphite layer under the silica that weakened the system. The laser-induced structure observed by Suess et al. [78] is reported in Fig. 2-1.

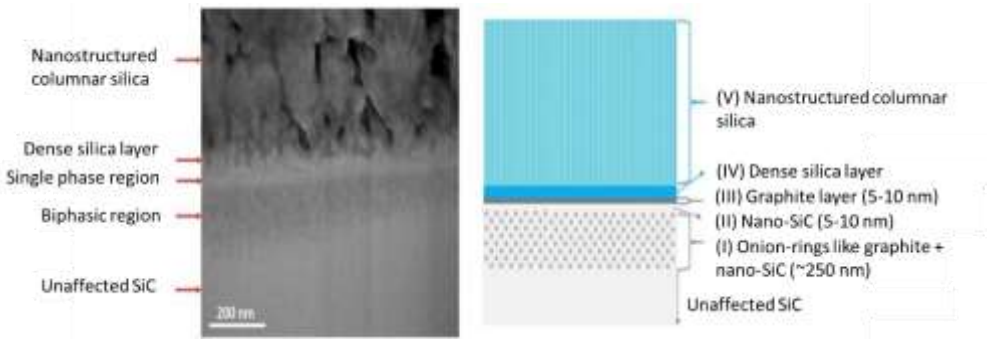

Figure 2-1 Laser-induced surface texture reported by Suess et al. (adapted from* [78]*).

The plasma treatment proposed by Casalegno et al. [77] was effective, but the need for a vacuum can be a barrier to treating large products like space-borne SiC mirrors [80]. The laser treatment may be more of interest for industrial applications if the formation of the graphite layer is avoided. An alternative solution can be taken into consideration: atmospheric pressure plasmas (APPs).

APPs [81] are of industrial interest, in particular when large products or large batches of pieces are manufactured. As mentioned, indeed, this class of plasma surface treaters has some advantages over low-pressure ones. E.g. they can be integrated into the manufacturing line as a continuous process without the restrictions imposed by the presence of a vacuum system and they are well suited for treating large surfaces by working in scanning mode[82], similar to lasers.

Some of the most common APP equipment are Corona discharge [83] systems, which are widely used in the plastic industry for surface activation and the removal of contaminants [73,84]. Such treatment is often performed before printing or bonding operations of polymeric components to improve surface wettability through oxidation. Several geometries are available, and custom-made systems designed for specific requirements can be found in manufacturing lines. The technology is well established and corona generators are stock in the product portfolios of plasma treaters manufacturers, which are accessible online[85–87].

An overview of corona discharge was already given in the previous chapter. The discharge occurs when the gas close to the electrodes is ionized by the applied electric field, and it results in the appearance of a filamentary plasma that stretches from the electrode. The generated plasma is not in thermal equilibrium, since electrons are at higher temperatures than ions, which are almost at room temperature.

Corona treatment, to the best of our knowledge, was never proposed as a surface modifier for advanced ceramics. Previously works reported its evaluation to improve the bond strength of feldspar porcelain.[88] and to generate a high proton superficial concentration on soda-lime glass [89].

The object of this research work was to evaluate the viability of a corona treatment for modifying the surface of SiC and to improve the mechanical performance of epoxy-joined SiC similar joints. For this purpose, a commercial corona generator was used in orde to get interesting insights for the industry. The obtained results were then compared with those reported in [78] and [77]. Next paragraphs will describe the research activity and discuss the chemical-physical changes induced on the SiC surface by the corona treatment.

Material and methods

The SiC selected for this activity, referred to as Boostec, [90] was manufactured through pressureless sintering by Mersen, France, in form of 25 mm x 25 mm x 4 mm tiles. Boostec SiC samples were used as-sintered. The corona treatment was carried out on the 25 mm x 25 mm surface a commercial system, known as *Tantec SpotTEC* [91], manufactured by Tantec, Denmark. The equipment was provided with one treatment head on which were present two electrodes. Air was fluxed between them, projecting the plasma filaments onto the target surface. Settings of the Tantec spotTEC equipment are shown in Table 2-1.

Table 2-1: Tantec SpotTEC settings

Main Voltage/ Frequency	Output power/ Output voltage	Output frequency	Power consumption
230 V, 50 Hz	550 W / 2 x 6,5 kV	25 kHz	600 VA (max. value)

Some preliminary observations were carried out to identify if surface underwent changes when underwent the corona treatment. Two experiments were

carried out with different treatment length: 10 min and 2 min. Sample was kept fixed under the electrodes. Electrodes-SiC surface was set at approximately 5 mm.

According to the observations made for the results of the preliminary activity, the experimental set-up was changed. The treatment head was randomly moved constantly over the sample for 5 min, keeping the distance at 5 mm, to get a uniform treatment. Samples were then prepared for joint shear strength tests adopting these latter conditions (5 mm gap, 5 min)

The surface microstructure was analyzed via Scanning Electron Microscope (SEM) before and after the treatment. The superficial composition was investigated via Energy-dispersive X-ray Spectroscopy (EDS) analysis. The equipment used was a *Benchtop Scanning electron microscopy (JEOL*) and a *MERLIN ZEISS FE-SEM* equipped with an EDS analyzer.

A confocal microscope (*ZEISS LSM 900, ZEN 3.1 software*, Germany) with a 20x magnification served to evaluate the changes on the surface roughness caused by the corona treatment. Average values for roughness parameters were calculated in accordance with ISO 25178 for three different samples for each type (treated and untreated). Parts were joined together using Hysol EA 9321 [92] as the bonding material. This adhesive is a bicomponent epoxy resin reinforced by dispersed aluminum particles and it has been already used in previous works taken as a benchmark [77,78].

Hysol EA 9321 was manually deposited onto each SiC surface and then a sandwich-like sample was manufactured. Joined samples were then curried at 85°C for 1 h in a drying oven (*Heraeus*).

Cross-sections of joined samples were investigated by means of a Transmission Electron Microscope (Titan Cube 2 60-300, FEI) at AGH University of Science and Technology (Krakow, Poland). Such activity was funded by ESTEEM3 program.

Steel plates were used to keep the alignment during the curing. A 6 KPa pressure was applied on the joining area while curing.

At least 3 joined treated and untreated samples were tested by means of the single lap offset (SLO) test under compression in order to measure the apparent shear strength. A sketch of the SLO test configuration, taken from [93], is provided in Fig. 2-2. The mechanical tests were carried out at room temperature by means of a *universal testing machine SINTEC D/10*, equipped with a 50 kN load cell. The

crosshead speed was set at 1 mm/min. After failure, fracture surfaces were inspected visually.

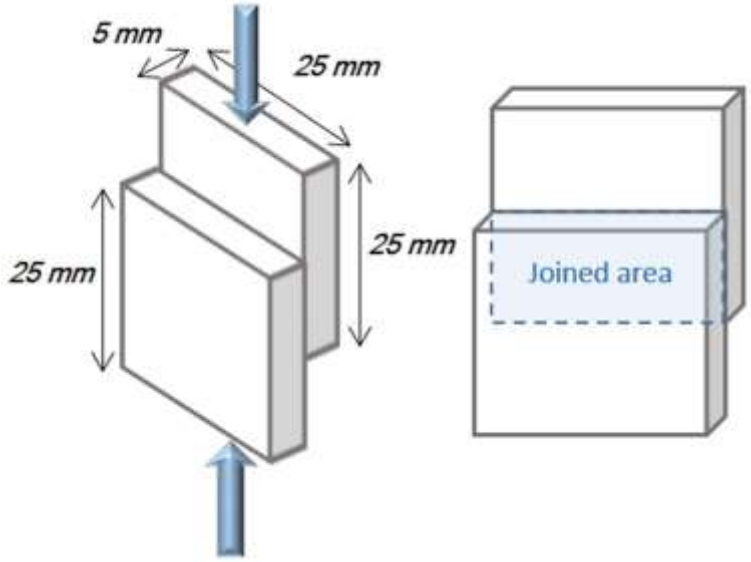

Figure 2-2: SLO test configuration (adapted from*[93]*).

In order to get more insights on the nature of the chemical affinity between the surface and the epoxy adhesive before and after the treatment, zeta potential analysis [94] was proposed as a characterization method. To date, this technique has been exploited to evaluate the superficial charge of nanoparticles and the stability of dispersions. Moreover, over the last decades, it has been extended to the investigation of treated surfaces for several applications like biomaterials, semiconductors, and polymer activation, to determine their characteristic functional groups, their acidity or basicity and even their reactivity [95,96]. However, it has not yet been used in the characterization of surfaces for joining applications and to investigate the chemical compatibility between the adhesive and the adherend. This activity has also the goal to evaluate zeta potential as a characterization method for getting information on surface chemistry, before and after treatment, and get indications on the chemical affinity with the adhesive.

Results and discussion

Changes on the SiC surface were considerable after the 10-min exposure to corona plasma. Large, pitted areas, in contrast with the surrounding glossy SiC, appeared on the surface as a result of the discharge on the surface of the tile, above all near the edges. These changes were very visible to the naked eye (Fig. 2-3).

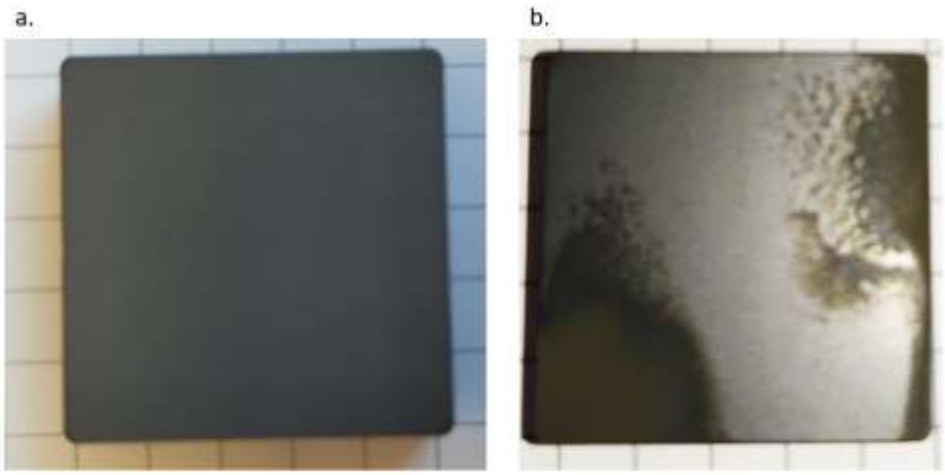

Figure 2-3: SiC before (a) and after 10 min of corona treatment (b).

One of the edges of the SiC tile is shown in Fig. 2-4 before (a) and after (b) the corona plasma treatment, as observed by means of an electron microscope. A locally well-distributed white layer was formed on the surface after 10 minutes of corona discharge, with the electrodes approximately at 5 mm from the surface. The brighter appearance of the surface after corona exposure may be attributed to an accumulation of the charge during the
SEM
analysis (the SEM images were acquired using the same brightness and contrast parameters). This change in the electrical properties suggested the formation of an oxide layer.

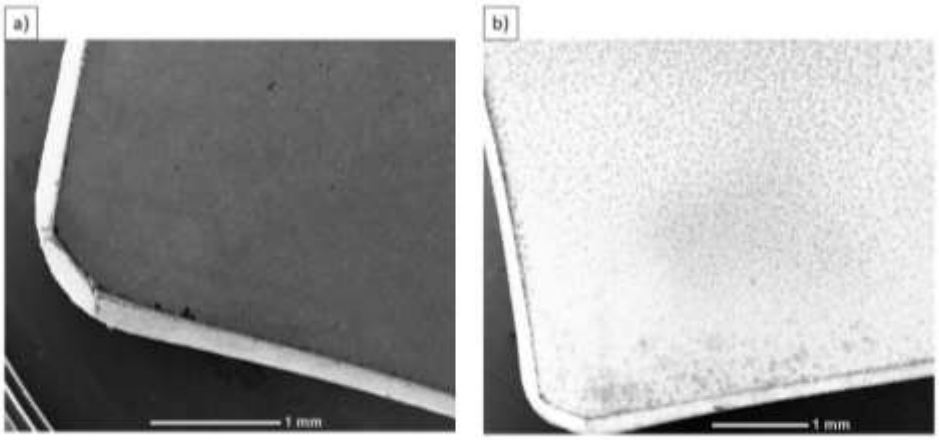

Figure 2-4: SEM top-view of SiC before (a) and after 10 min of corona treatment (b).

The result of the EDS analysis carried out near the edge is shown in Fig. 2-5; only Si, O and C were found in the analyzed regions (Fig.2-5.b). The amount of each element was coherent with the presence of a silica (SiO_2) layer on the SiC surface and was within the expected accuracy of a few percent for EDS quantification. The presence of large amounts of oxygen and silicon, together with the higher tendency of charge accumulation observed by means of electron microscopy, indicate the formation of an oxide layer on the surface. However, carbon is still present, except in site 2, probably due to the contribution of the underlying and surrounding unreacted silicon carbide and/or the contamination of the surface during handling.

a.

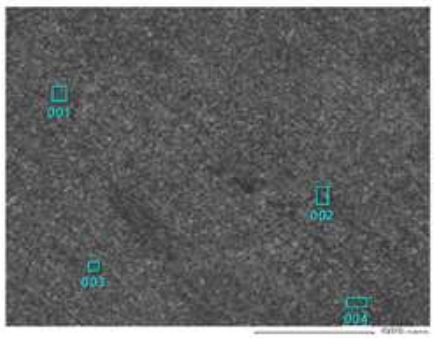

Site 1			Site 2		
Si (%at)	C (%at)	O (%at)	Si (%at)	C (%at)	O (%at)
61.66	35.93	2.41	48.44	48.02	3.55
Site 3			Site 4		
Si (%at)	C (%at)	O (%at)	Si (%at)	C (%at)	O (%at)
55.25	40.50	4.25	48.63	47.63	3.74

b.

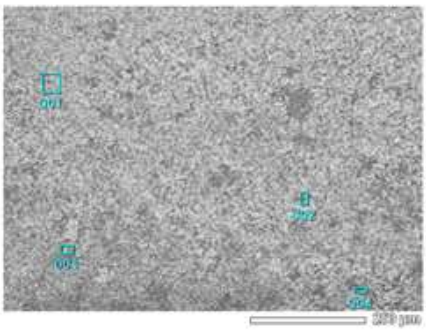

Site 1			Site 2		
Si (%at)	C (%at)	O (%at)	Si (%at)	C (%at)	O (%at)
34.32	14.46	51.22	43	-	57
Site 3			Site 4		
Si (%at)	C (%at)	O (%at)	Si (%at)	C (%at)	O (%at)
38.01	19.77	42.22	37.90	17.34	44.76

Figure 2-5: EDS Analysis on untreated SiC (a) and after corona treatment (b).

During the treatment, the distribution of the plasma filaments was inhomogeneous and some preferential discharge areas were observed. Filaments, in fact, looked to accumulate around the tile's edges. This behavior can be explained by the well-known tendency of charge to accumulate around sharper regions. This phenomenon made the treatment inhomogeneous and large superficial areas, in particular at the center, were not modified.

Shortening the corona treatment to 2 min did not lead to any perceivable differences, thus suggesting that the exposure time might not be a critical variable for the formation of oxide and that the oxide might form in a short time because of the energy released by the discharge. This can be attributed to the energy transferred to the SiC surface by the corona discharge filaments when they reach the surface. Indeed, areas were identified where dark pits of oxide were visible to the naked eye and they seemed to coincide with the impact sites of the corona streamers. Furthermore, it is worth noticing that the corona filament path was not confined to

between the two electrodes, but diverged and formed two different plasma streams that originated at the electrodes and ended up on the SiC surface (Fig. 2.6), thus suggesting an electrical conductance.

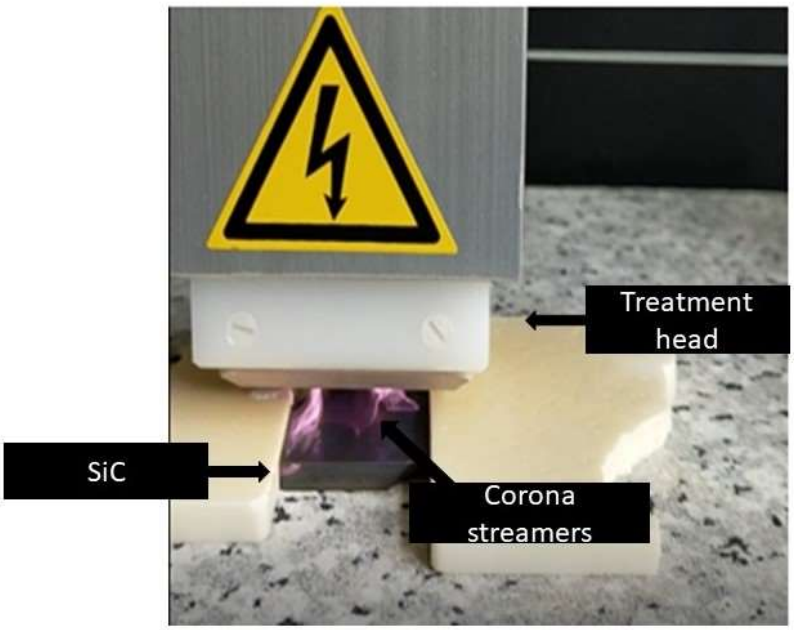

Figure 2-6: ***Corona treatment on SiC.***

As a result of the insights collected during the preliminary tests, electrodes were moved randomly over the surface for 5 minutes to improve the homogeneity of the treatment. The introduction of random motion of the electrode head over the sample mitigated the accumulation tendency at the edges and resulted in a more homogenous distribution of the silica-grown region over the entire surface. This higher homogeneity was, first, visible by naked eye, observing the color variation on the surface and then confirmed by the investigation at SEM.

The silica structures (composition confirmed by EDS analysis) grown on silicon carbide showed a cauliflower structure (Fig. 2-7) that suggested a possible improvement in the joint strength, given by the better anchoring of the joining material through the infiltration of the glue inside the superficial texture. A similar structure was observed also for the laser-treated SiC [78].

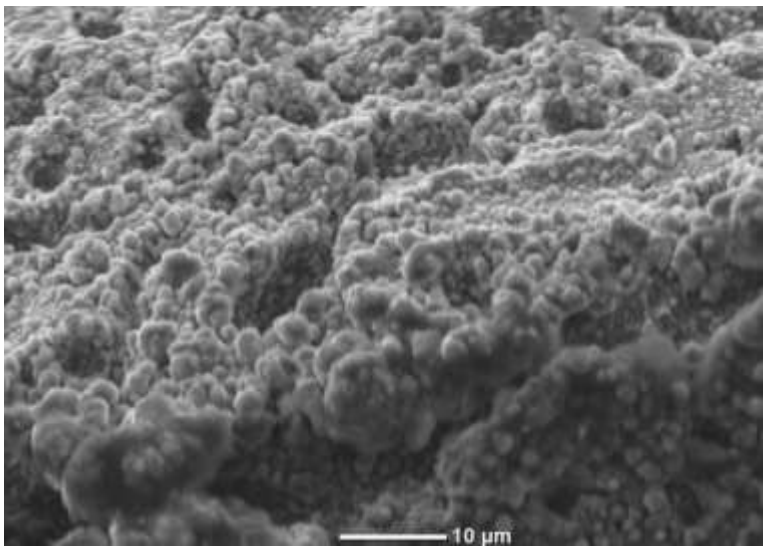

Figure 2-7: cauliflower-like silica layer on the surface (lateral view).

Moreover, an adhesive, and in general any joining material with low viscosity, can penetrate this structure and create a mechanical anchoring system that can be expected to increase the mechanical performance of a joint.

The oxidizing effect of the corona is well-known and, apart from being exploited for cleaning and polymer surface activation, it has also been reported for a silicon wafer [97]. However, it is difficult to find a reliable explanation for the reaction of SiC to oxygen, which has only been reported previously in literature for much higher energy beams (e.g. laser) or higher temperatures, but never in conditions such as these. At this stage, the SiC corona-induced oxidation may be explained by considering a punctual huge increase in temperature provided by the plasma filaments, but a rigorous and focused investigation is needed to fully understand this mechanism. The growth of silicon oxide has been reported in dry air in a temperature range between 800°C and 1400°C, but oxygen plasma already proved to promote oxidation at room temperature [98]. Indeed, it should be taken into consideration that the species generated by the ionization of air induced by the corona discharge, such as oxygen ions, are highly reactive[99]. These reactive ions may promote oxidation at temperatures much lower than 800°C. Therefore, the combination of plasma filaments that are high in energy and the presence of highly reactive ions might therefore explain the oxidation of the SiC.

An open porosity of the silica structure can clearly be observed in Figure 2-8; the pores are homogenously distributed in both orientations, that is, parallel and

perpendicular to the surface. Such a structure leads to an extensive increase in the surface area.

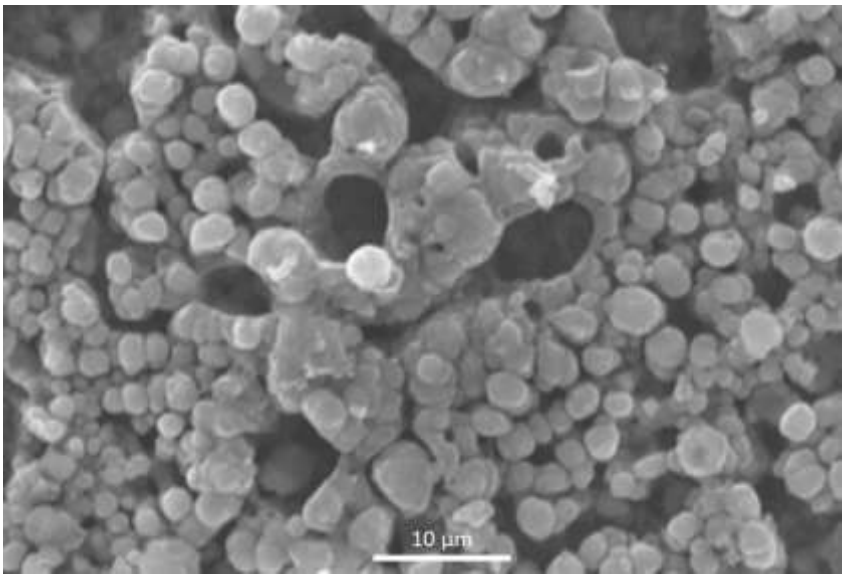

Figure 2-8: cauliflower-like silica layer on the SiC surface (top view).

Measurements carried out with confocal microscopy provided information on the surface roughness. Roughness maps are provided in Fig. 2-9. The arithmetical mean height (Sa) increased after the treatment, from 0.045 ± 0.001 µm to 0.120 ± 0.008 µm, together with maximum height (Sz), (from 1.31 ± 0.185 µm to 3.82 ± 0.56 µm). These results pointed out that the new texture given by the formation of the cauliflower-like silica layer increased the surface roughness, which was higher than before the corona treatment. .

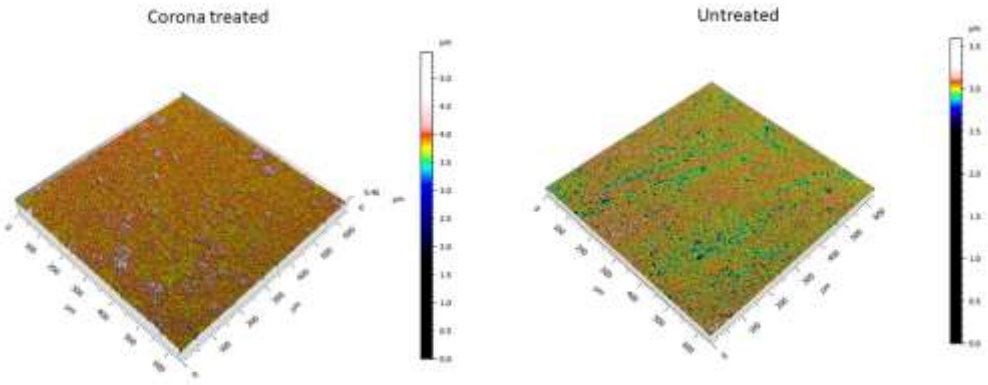

Figure 2-9: confocal roughness map of a corona treated (left) and untreated SiC (right).

In addition, the Sdr value (the ratio between the calculated area and the projected area) was calculated to be, on average, around 1% for the untreated surface and approximately 6% for the corona treated, indicating a slight increase in the surface area given by the superficial textured layer.

The cauliflower-structured silica layer induced by the corona discharge was found to be stable. No noticeable changes were observed with the electron microscope or EDS, even more than one year after the treatment. Analyzed non-joined samples had been stored in sealed laboratory bags.

TEM inspection carried out on the cross-section of the Hysol-joined SiC (untreated and corona-treated) showed insightful results. The observation on untreated joined SiC (Fig. 2-10) showed distinctly the presence of the epoxy adhesive and the underlying SiC. Silica was not observed on the surface before the treatment. Fig. 2-11, Fig. 2-12, Fig. 2-13 show the TEM inspection of the Hysol-joined corona-treated SiC. The presence of the silica layer, formed by the corona treatment on the surface of SiC, is clearly visible (Fig. 2-11). The Selective Area Diffraction (SAED) indicated that the corona-induced silica was amorphous as pointed out by the amorphous halo.

The interface between silica and the adhesive was sound and homogeneous. The Hysol epoxy infiltrated effectively the silica structure providing anchoring, as expected.SAED was also performed on the adhesive (Fig. 2-12) and the SiC substrate (Fig. 2-13). The epoxy was found to be amorphous (amorphous halo),

coherently with being a thermosetting polymer. SiC, instead, was confirmed to be crystalline.

The critical issue of the laser treatment used for SiC in [78] was the formation of a thin graphite layer that was detrimental for the joint strength. In the present work, the composition of the underlying layer of material was analyzed by TEM (Fig. 2-14). The line analysis is shown in Fig. 2-14.b. It can be noticed that under the SiO_2 layer a small region can be identified where the carbon concentration is slightly higher. However, compared with the research reported by Suess et al. [78], there is not the formation of a graphite layer. Further investigation will be adressed to verify the possible formation of a SiOC layer below SiO_2 amorphous layer.

EDS maps of the cross-section of the corona-treated SiC surface is shown in Fig. 2-15.

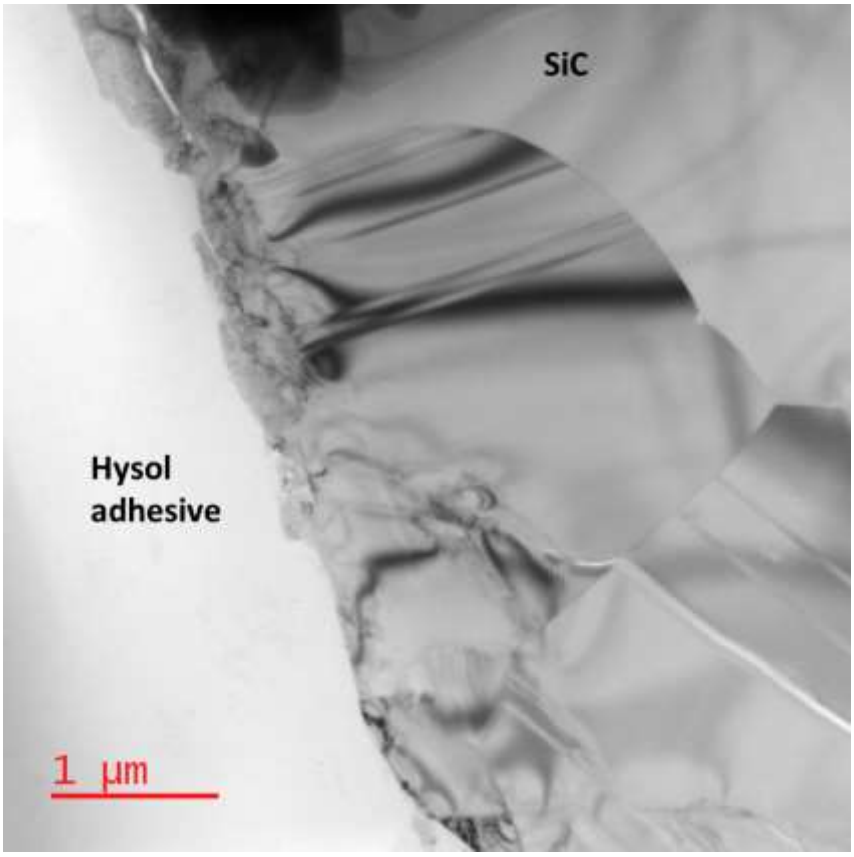

Figure 2-10: TEM investigation on the cross-section of a Hysol-joined SiC (bright field mode).

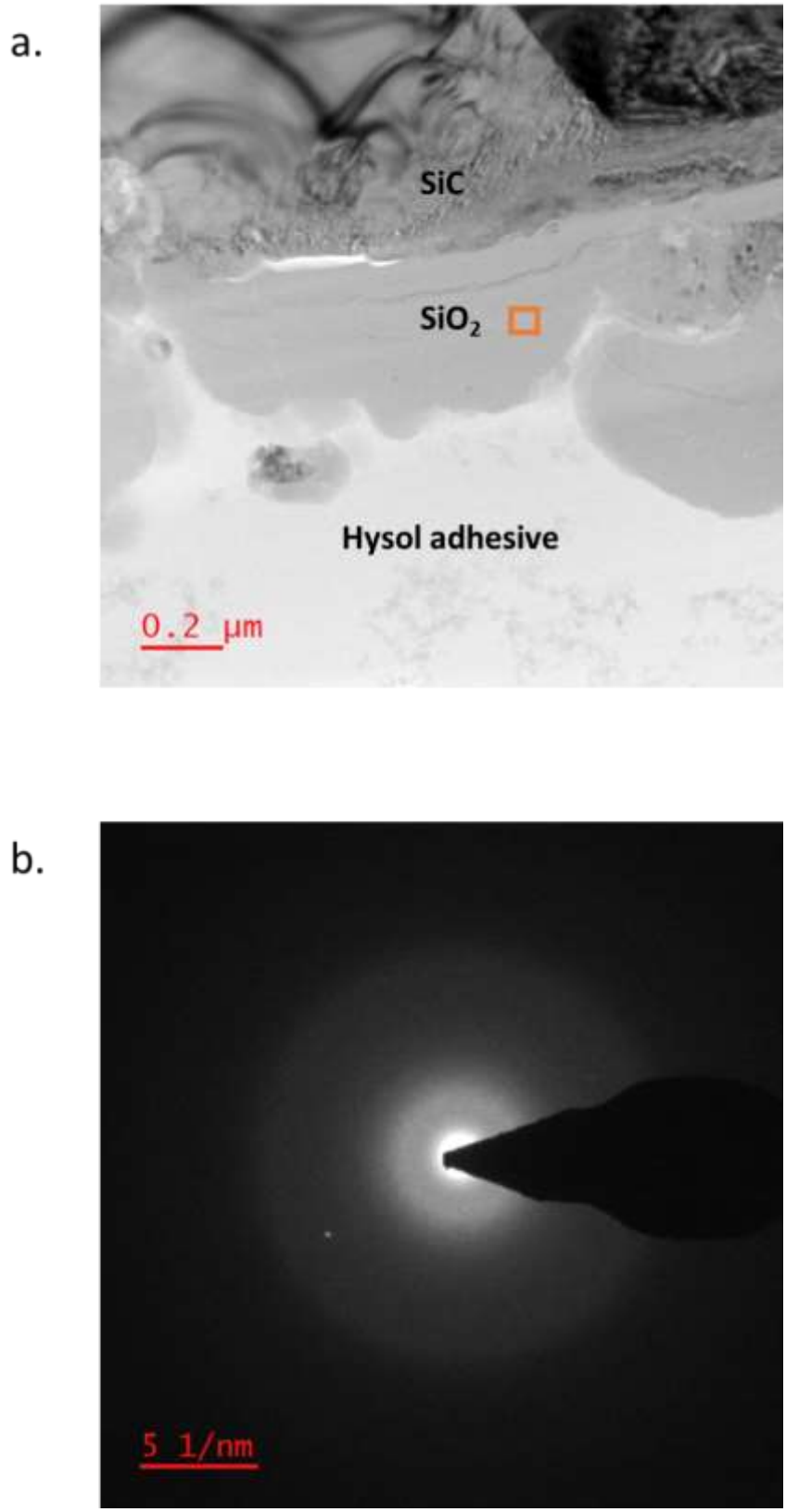

Figure 2-11:TEM investigation on the cross-section of a Hysol-joined corona treated SiC (bright field mode) (a) and the amorphous halo given by the SAED (b) carried out in the region indicated by the orange box in Fig. 2.10.a.

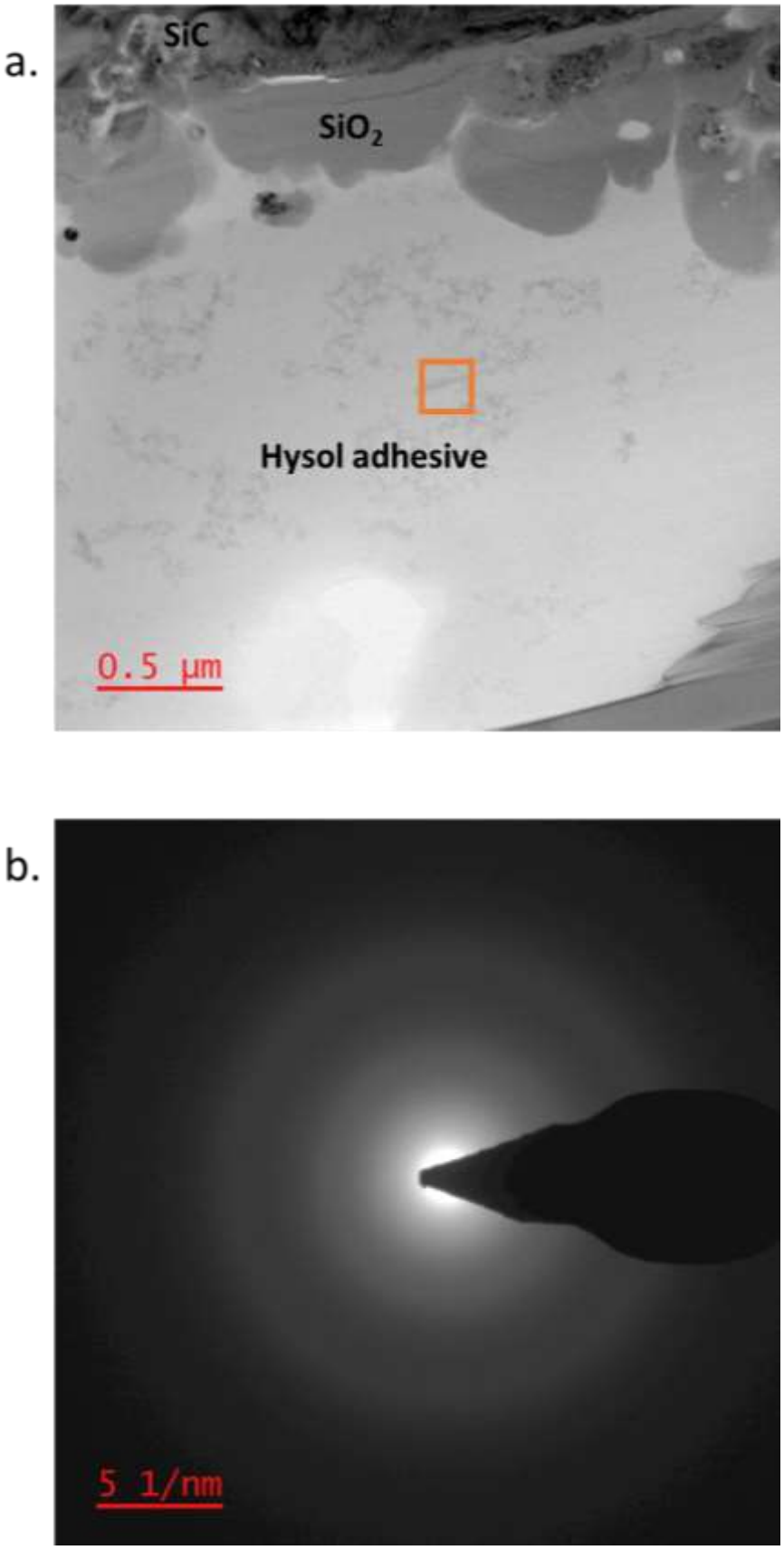

Figure 2-12: TEM investigation on the cross-section of a Hysol-joined corona treated SiC (bright field mode) (a) and the amorphous halo given by the SAED (b) carried out in the region indicated by the orange box in Fig. 2.11.a.

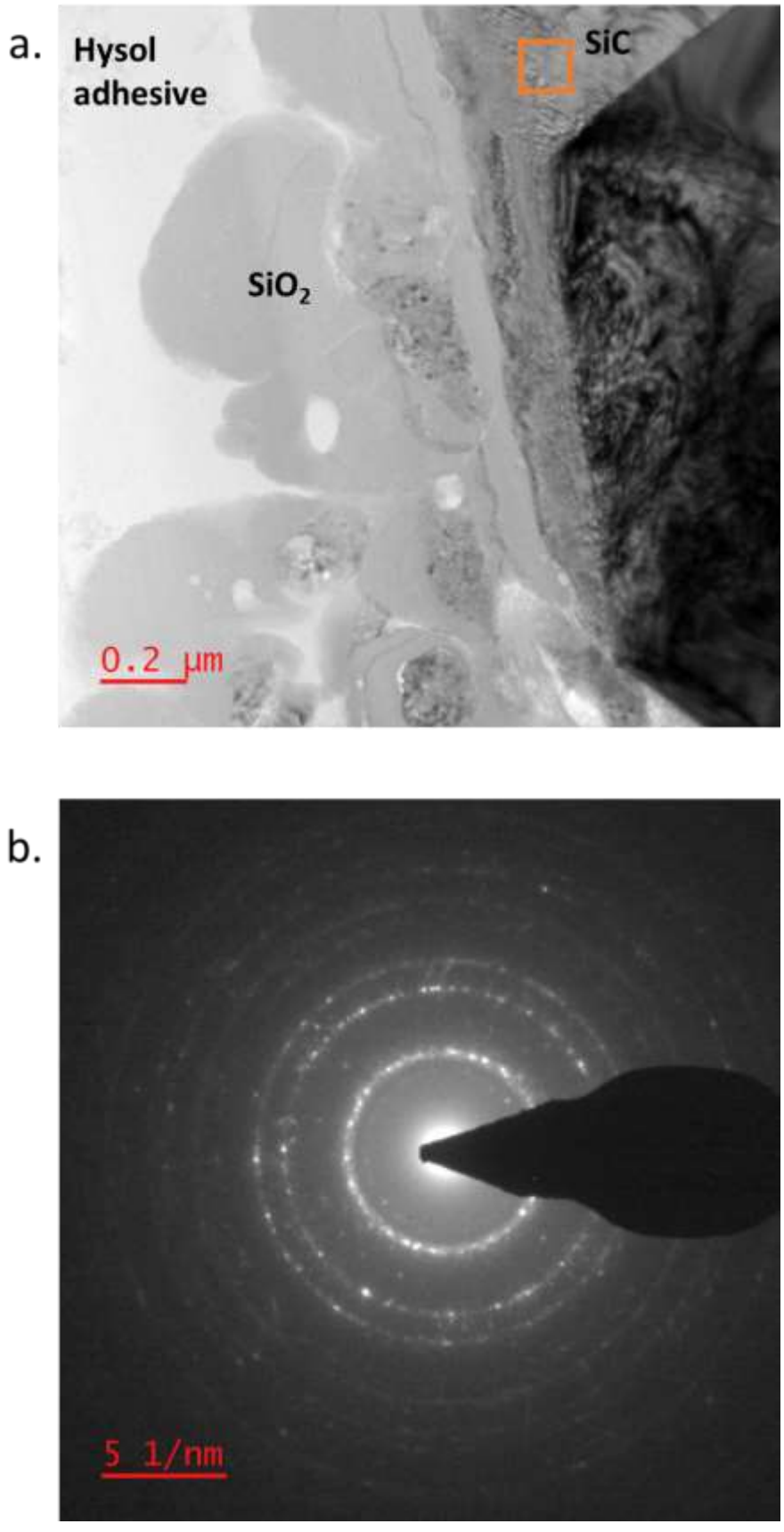

Figure 2-13: TEM investigation on the cross-section of a Hysol-joined corona treated SiC (bright field mode) (a) and polycrystalline pattern given by the SAED (b) carried out in the region indicated by the orange box in Fig. 2.13.a.

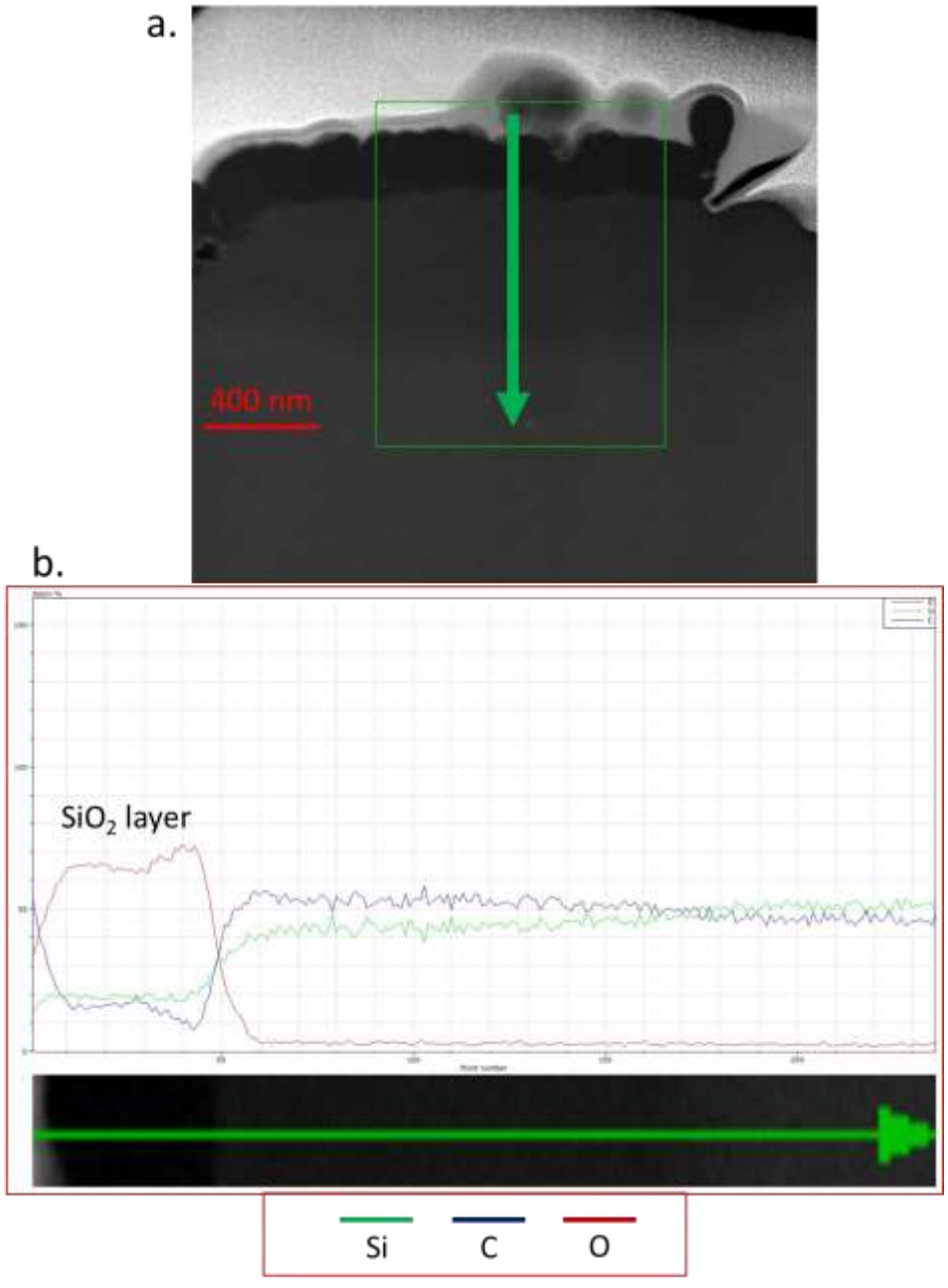

Figure 2-14: EDS Line Analysis carried out along the green arrow shown in (a), taken by TEM.

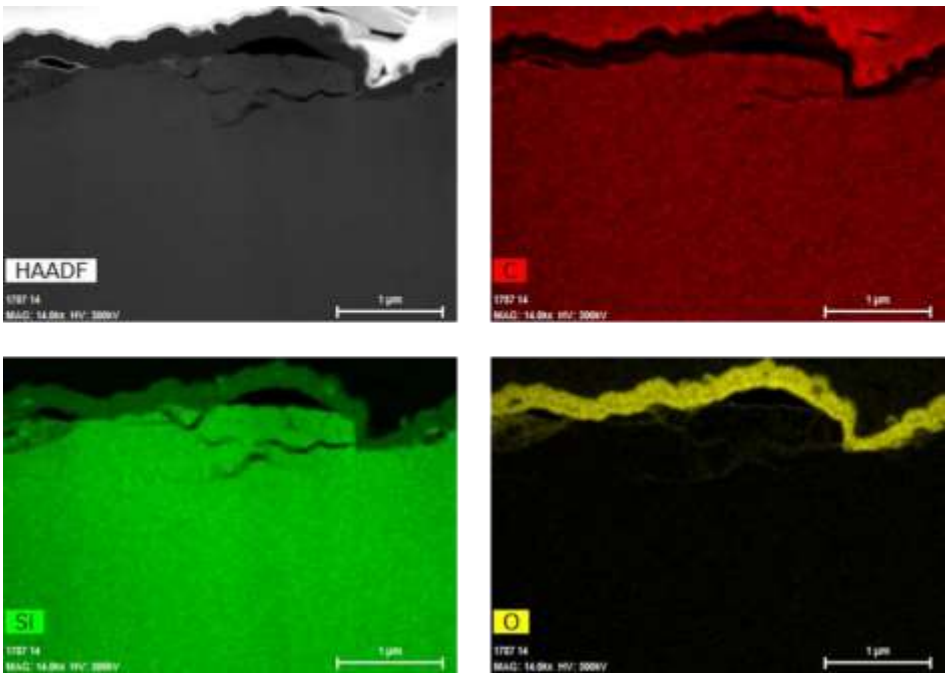

Figure 2-15: EDS maps of cross-sections of corona-treated SiC surfaces.

Single-lap offset shear strength tests were carried out to assess whether the corona-induced textured SiO_2 layer was effective in increasing the joint strength.

Average joint strength for the corona-treated joined components was approximately 68.8 ±2.3 MPa, while the values registered for the untreated samples was about 61.5 ± 5.0 MPa. More than 10% increase in the joint strength was reported after the corona plasma treatment of the SiC surface, compared to the untreated samples. However, the most interesting results concerned the joint failure mode. In this specific case, it was observed that all the corona-treated samples underwent cohesive failure, while the untreated samples underwent adhesive failure. A comparison between two samples, one treated and one untreated, is shown in Fig. 2-16. The difference in the failure mode is easily observable by the naked eye.

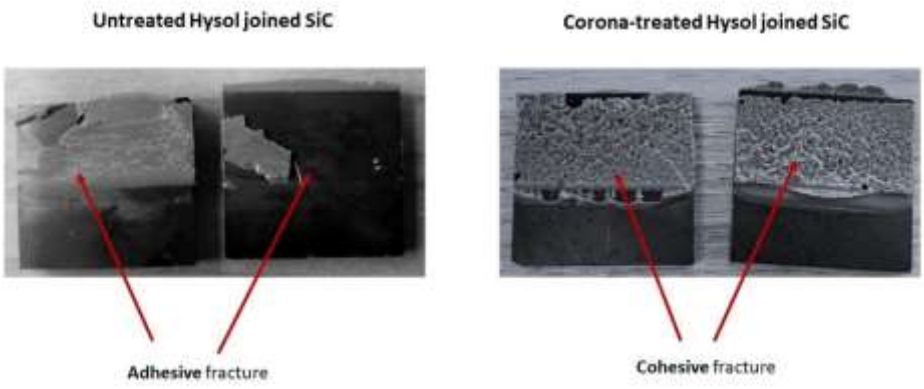

Figure 2-16: fracture surfaces of Hysol-joined untreated SiC (left) and Hysol-joined corona treated SiC (right).

One of the goals of adopting adhesive joining strategies is to maximize the probability of the fracture occurring within the adhesive. Cohesive fracturing is usually a sign of the good quality of the joining process because it suggests that the mechanical strength at the joining interface is higher than that of the joining material itself [77].

Since the adhesive failed cohesively over the entire joining area of the treated samples, the surface was modified quite uniformly by the corona treatment. The enhanced mechanical behavior of joints after the corona treatment can be the result of the induced texture together with the formation of silica at the surface. Harris et al.[100] observed that the formation of a laser-induced silica layer on SiC provided a better chemical bonding with the epoxy adhesive due to the presence of hydroxyl groups. Therefore, the corona-induced cauliflower silica layer obtained in this work can play a significant role in providing a stronger mechanical and chemical bonding.

Comparing the obtained values with those collected in [78] (34.8 ± 3.4 MPa) and in [77] (44.3 ± 2.4 MPa), for laser and low-pressure plasma treated SiC joined with the same adhesive, it is possible to draw two conclusions.

First, the joint strength values in the present study are higher than those found in the previous studies, for both the untreated and corona-treated samples. This difference may be attributed to the different curing treatments: 85 °C for 1h in the present work compared to 7 days at room temperature in the other two studies. This

is a remarkable result because, besides providing higher joint strength, this curing treatment is much shorter (1 h compared to 7 day).

Second, the corona plasma treatment here resulted in cohesive failure, just like the low-pressure plasma treatment proposed in [77], and performed better than pulsed laser irradiated SiC [78], which led to adhesive failure. This result is promising since it reinforces the hypothesis of the validity of a corona plasma treatment as an effective and low-cost treatment that can be used before joining.

A comparison of the different results obtained for the Hysol-joined SiC samples after the corona discharge plasma treatment, the laser treatment, and the low-pressure plasma treatment, together with the recorded untreated SiC joint values, is provided in Table 2-2.

Table 2-2: comparison between results recorded for Hysol-joined SiC from this work and those from previous articles [75,76].

	Corona plasma treatment	Pulsed laser irradiation [78]	Low-pressure plasma treatment [77]	Untreated	Untreated [78]
Apparent Shear Strength [MPa]	68.8 ±2.3	34.8 ± 3.4	44.3 ± 2.4	61.5 ± 5	41.6 ± 0.9
Failure mode	Cohesive	Adhesive	Cohesive	Adhesive	Adhesive
Curing treatment	85°C, 1 h	R.T, 7 days	R.T, 7 days	85°C, 1 h	R.T, 7 days

In order to understand the effect of the corona treatment on the chemical compatibility between the substrate and the adhesive, zeta potential measurements were carried out. This analysis method provided information on the charge of the surface and its acidic or basic behavior, commonly it is used for characterizing nanoparticles, but in this work it was utilized for the first time with the goal to assess the chemical affinity of adhesive and the surface.The titration curves are reported

in Fig. 2-17 for untreated SiC, corona-treated SiC (5 min, 5 mm) and cured Hysol (85°C, 1 h).

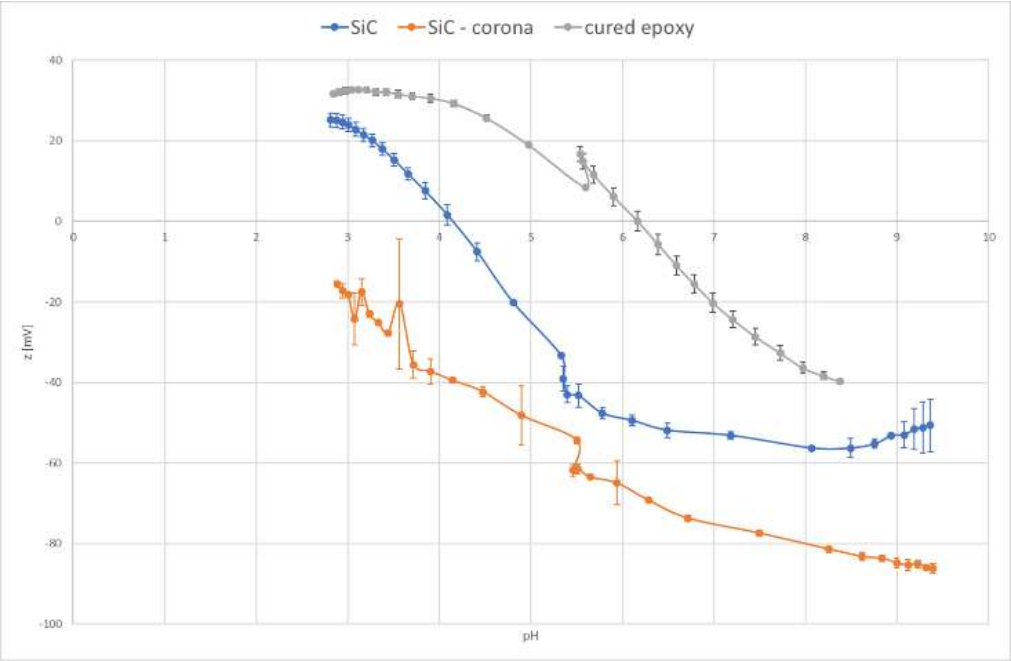

Figure 2-17: Zeta potential titration curves: untreated SiC (blue), corona-treated SiC (orange) and cured Hysol (grey).

In the absence of superficial functional groups, the isoelectric point (IEP) for SiC is close to 4 (blue curve). The corona-treatment changed the surface chemistry and the isoelectric point shifted to a stronger acidity (orange curve). The isoelectric point was not identified for corona-treated because the instruments cannot measure values lower than 3 and it fell in this interval according to the trend of the curve. Acidic functional groups were therefore formed on the surface. Such findings were coherent with the growth of the silica layer. Indeed, silica has an acidic behavior with an IEP at around pH 2 [101]. The change on the surface was successfully detected via zeta potential measurements, confirming that this may be a valid technique for the characterization of surfaces.

Concerning the chemical affinity between the Hysol epoxy resin and the surface, the zeta potential curves provided an interesting result. The IEP of the resin is higher (6.17) than that of SiC, both corona-treated and untreated. Furthermore, the titration curve of the resin (orange) shows also a plateau in the acidic region. This, together with the IEP, indicates the presence of basic groups for Hysol, which is coherent with its declared composition which contains amines[102,103].

Since the epoxy resin disposes of basic functional groups and the corona treatment induced a more acidic behavior on the SiC surface, it can be expected that the chemical bonding will be stronger compared with untreated SiC.

Conclusions

The work presented in this chapter was devoted to the evaluation of the viability of using a commercial corona plasma generator to improve the mechanical performances of adhesive bonded SiC. The corona treatment was demonstrated to be effective in modifying the SiC surface, by inducing an amorphous silica cauliflower structure, suitable to promote the infiltration of the joining material, as observed by TEM, and a stronger bonding with the adhesive. The surface, therefore, underwent to a chemical and physical modification.

The mechanical tests performed on the epoxy-joined SiC confirmed the beneficial effect of the corona treatment. The failure resulted in an adhesive fracture for the joined untreated SiC and in a cohesive fracture for the joined corona-treated SiC. In addition, the treated samples failed at higher stress values and the cohesive failure involved the entire surface, thus suggesting the treatment produced a uniform effect. Such results confirmed the effectiveness of the corona treatment in improving the mechanical performances of joints.

It is noteworthy that the curing treatment proposed in this paper (1h, 85°C) for the epoxy resin resulted in a remarkable increase in the bonding strength compared with previous works.

Finally, the measurement of the zeta potential provided more information on the chemical compatibility between the surface and the adhesive. This technique proved to have the potential to be successfully applied in the characterization of the material before and after the treatment, expanding its range of applications.

3. Brush-like texturing of non-oxide CMCs

As introduced in Chapter 1 the promotion of the interlocking effect can provide improvements in terms of the mechanical properties of joints. Roughness has a critical role, but the introduction of a specific texture can result in an even more remarkable effect. Indeed, it is critical to provide suitable anchoring points between the joining material and the surface.

In chapter 2, the effect of the corona-induced modification of the texture and chemistry of a SiC surface was described. In that case, only one constituent (sintered SiC) was present and the treatment was homogeneous on the surface.

For composites, things are different because there is more than one component and each has different properties. Even when fibers and matrix are made of the same material, slight differences may exist because of the different manufacturing processes.

Plasma-based texturing, usually, requires masking to produce the desired structure on the surface, but the presence of multiple constituents in composites unlocks new opportunities. Since, different properties means different response to the environment, when composites undergo treatments each constituent may behave differently.

By identifying a viable treatment, it is possible to promote the selective removal of one of the constituents from the surface of the composite. Indeed, when composites, in the case of this work CMCs, are exposed to a physical or chemical action, fibers and matrix will respond differently to it. The weaker phase will be removed faster, leaving cavities on the surfaces and inducing a brush-like texture. A schematic representation is shown in Fig. 3-1.

Such a texture can be tricky and complex to manufacture otherwise and can boost dramatically the joint strength when CMC are joined. In fact, the cavities

formed onto the surface can provide regions for infiltration of the joining material that later will enable interlocking.

Brush-like texturing of CMCs is expected to be promising as a pre-joining operation, but to date few works are available. One of this works, carried out by Valenza et al.[104], set the ground for the research work on the plasma-based brush-like texturing of CMCs presented in this thesis.

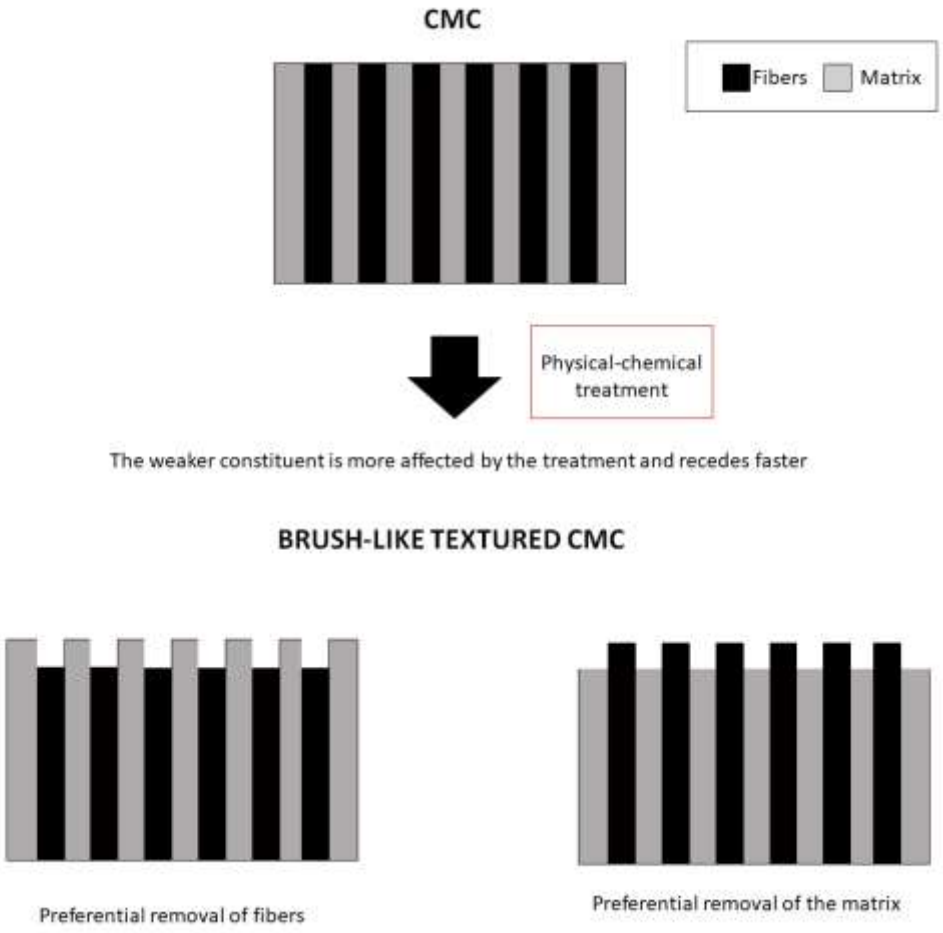

Figure 3-1: brush-like texturing of CMCs

The formation of a brush-like texture on SiC/SiC was achieved on SiC/SiC via a selective thermal treatment proposed by Valenza et al.[104]. Samples were treated for 2h at 1400°C in argon and, as can be seen in Fig 3-2 and Fig 3-3, the surface texture changes due to the preferential removal of the fibers. The fiber erosion resulted in the formation of well-distributed and regular cavities in the areas with fibers perpendicular to the surface, which act as points for infiltration of the brazing

alloys. The fibers were then more affected by the thermal stimulus and the brush-like texture was formed.

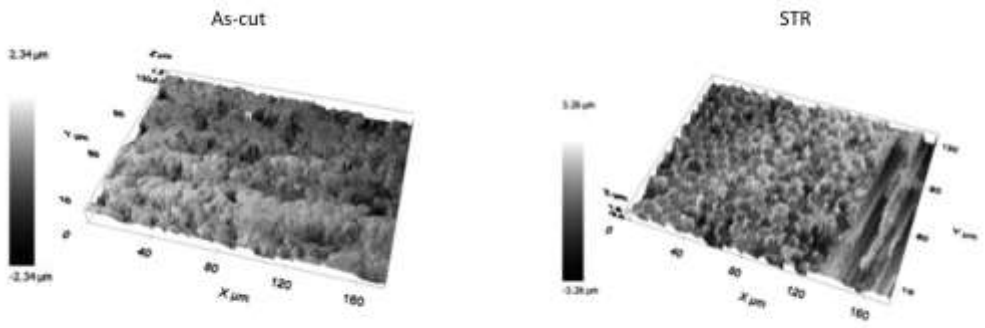

Figure 3-2: Roughness maps of as-cut SiC/SiC surface (left) and after STR (right). Adapted from [104]**.**

The treatment successfully induced the desired texture, but it had a negative outcome on the overall mechanical performance. The composites lost the 60% of their flexural tests after being heat treated[105]. This occurred because the entire volume of the material underwent the treatment, the thermal effects were not confined to the surface. Furthermore, the treatment was time consuming.

However, these results showed that it was possible to take advantage of the different responses of fibers and matrix to produce a complex texture on the CMC, tracing the path for further research.

Plasma technologies have the potential to confine the selective removal action on the surface without damaging the material.

Next chapters (from 4 to 6) will describe the research work done to replicate a similar texture on CMC without the detrimental effect on the bulk and its contribution to the joint strength. These activities are schematized in Fig. 3-3.

The brush-like texturing effect on perpendicular fibers was the most prominent effect. Also, parallel-to-surface fibers were slightly affected by the treatment, but no patterning was observed. Therefore the discussion will focus on perpendicular fibers

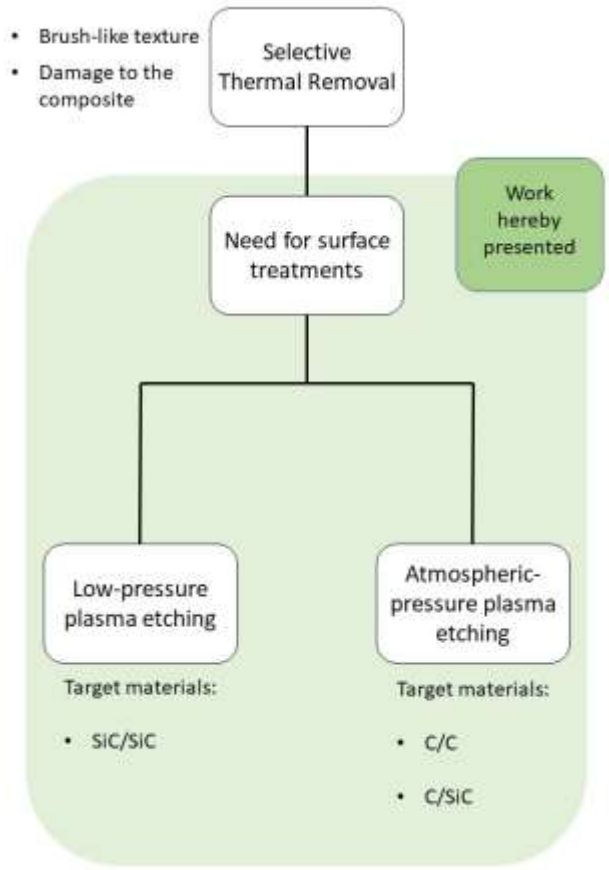

Figure 3-3: research activities derived from Selective Thermal Removal (STR) treatment.

More specifically, existing plasma techniques were investigated.

Reactive Ion Etching was proposed for inducing a brush-like structure on SiC/SiC surface, while an Atmospheric Pressure Plasma Jet system was employed for C/C and C/SiC composites.

4. Increasing the joint strength of brazed SiC/SiC through a RIE plasma

Part of the activity presented in the following chapter was published as a regular article [106] *on Ceramics International (Elsevier).*

RIE plasmas are a key state-of-the-art technology for surface etching for silicon carbide in the manufacturing of integrated circuits, as described previously in chapter 1. This technology enables to manufacture of very precise patterns when masks are used.

In the case of CMCs, however, the presence of multiple constituents unlocks new texturing opportunities since the response of each phase is expected to be different as introduced in chapter 3. In fact, fibers and matrix can experience various etching rates according to their properties and therefore a brush-like texture, as a result of the selective removal, can be manufactured.

The use of plasma etching limits the effects of the treatment to the surface, overcoming the detrimental effect reported for the Selective Thermal Removal (STR) treatment [104,105]. It is, therefore, possible to obtain similar results, but without compromising the mechanical resistance of the material.

This is the reason why a RIE was investigated as a surface texturing treatment for SiC/SiC. The aim was to manufacture the brush-like structure and to evaluate its effectiveness in improving the joint strength when a reactive brazing alloy is used for joining.

To the best of author's knowledge, RIE has been never proposed as preliminary treatment for CMCs to texture the surface before bonding.

Materials and methods

2D Keraman SiC/SiC composites (BJS composites (Germany)), were used as materials to be joined. SiC/SiC architecture consisted of piled Tyranno S fibers, a pyrolytic carbon interphase, and a chemical vapor infiltrated (CVI) SiC matrix. The plies of Tyranno S fibers are arranged along the thickness of the composite in a 0°/90° piling. These fibers oriented perpendicular to the surface are viable to manufacture a brush-like structure. A cross-section of this SiC/SiC is provided in Fig. 4-1 for clarity.

SiC/SiC composites were purchased in the form of 100 x 100 x 4,5 mm tiles. Then, they were cut into smaller samples (approximately 10 x 10 x 4,5 mm) by means of a precision cutting machine (*ATM Brilliant 220, Germany*). Once cut, the 10 x 4,5 mm surfaces were mirror-polished using SiC grinding paper, with a grit of up to P2400. After polishing samples underwent ultrasonic bath in ethanol for 20 min at room temperature.

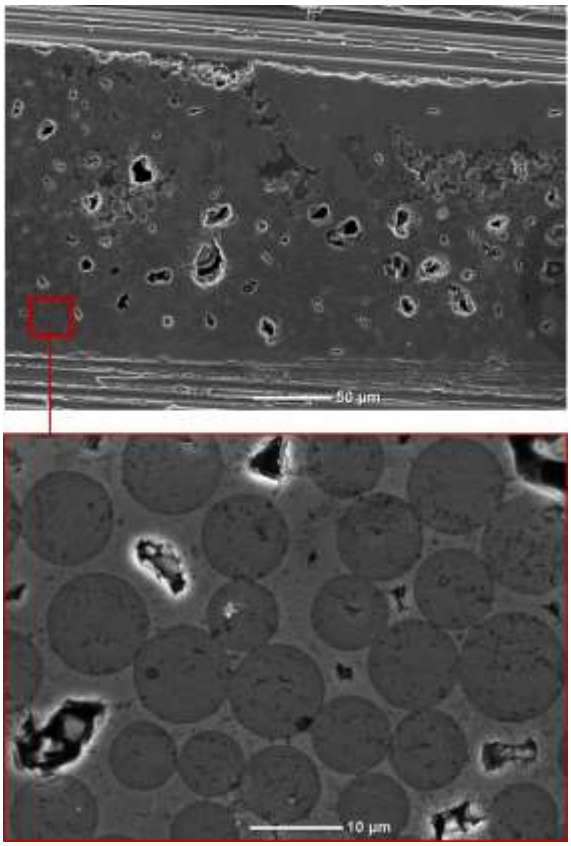

Figure 4-1: cross-section of 2D Keraman SiC/SiC.

The plasma treatment was carried out on one of the 10 x 4.5 mm surfaces. Those were placed under the powered electrode of an RF (13.56 MHz) plasma system available at CNR-ISPF (Milano). Two reactive atmospheres were used: CF_4 alone and in a mixture with H_2 (10%)[107]. The power and working pressure were kept at 200 W and 9 x 10^{-2} mbar, respectively. Treatment lengths varied from 5 to 30 minutes. Conditions for each treatment are summarized in Table 4-1.

Table 4-1: Plasma treatment conditions

Treatment	Gas	Flow	Power	Exposure Time
A	CF_4	20 sscm	200 W	15 min
B	CF_4/H_2	18/2 sscm	200 W	15 min
C	CF_4	20 sscm	200 W	30 min
D	CF_4/H_2	18/2 sscm	200 W	30 min
E	CF_4	20 sscm	200 W	5 min

Untreated and treated surfaces were characterized using a SEM-EDS scanning electron microscope (*JEOL Benchtop Scanning electron microscope equipped with an EDS Analyzer* and *SUPRA ZEISS FE-SEM),* to evaluate superficial changes given by each etching treatment. EDS analysis was conducted to investigate the presence of fluorine on the surface after the plasma etching.

The selected joining material was Cusil-ABA®[108], a silver-copper-titanium system (63 wt% Ag, 35.25 wt% Cu, 1,75 wt% Ti). Such material was chosen because Ag-Cu-Ti alloys have been extensively employed in joining SiC based materials because of their ability to form reaction layers [109–112]. In particular, Cusil-ABA® braze is known to be effective as joining material for SiC substrate and several works on the evaluation of its properties are available [112–114].

Since the objective of this research activity was to evaluate the viability of a plasma treatment to improve the SiC/SiC joint strength, a consolidated braze was needed.

Each joint was produced by piling three 80-µm Cusil-ABA foils between the surfaces to join in order to reduce the depletion of braze due to presence of voids in the composite due to its manufacturing process.

Samples were joined with a thermal treatment conducted at 850°C for 15 min in vacuum (10^{-5} mbar) to prevent oxidation. Peak temperature was chosen in accordance with the prescriptions given by Cusil-ABA® data sheet [108]. The joining process was pressure-less.

Cusil-ABA joined SiC/SiC cross-sections were investigated using SEM for evaluating the global quality of the manufacturing joint, the braze-composite interface and hints for the presence of anchoring points induced by the plasma treatment. The composition of the joint was evaluated via EDS analysis.

The apparent shear stress strength of the joined SiC/SiC (untreated and plasma-treated) was calculated for 4 samples per type using a compressive single lap offset (SLO) test. The tests were conducted at room temperature using a universal testing machine (SINTEC D/10), equipped with a 50 kN load cell. The crosshead speed was 1 mm/min. Further information on the SLO set-up is available in ref. [115].

Fracture surfaces were then inspected by eye and by SEM to identify differences in the failure mode for treated and untreated joined samples.

Results and discussion

Fig. 4-2.a and Fig. 4-2.b confront the SiC/SiC surfaces before and after each plasma treatment at different magnifications.

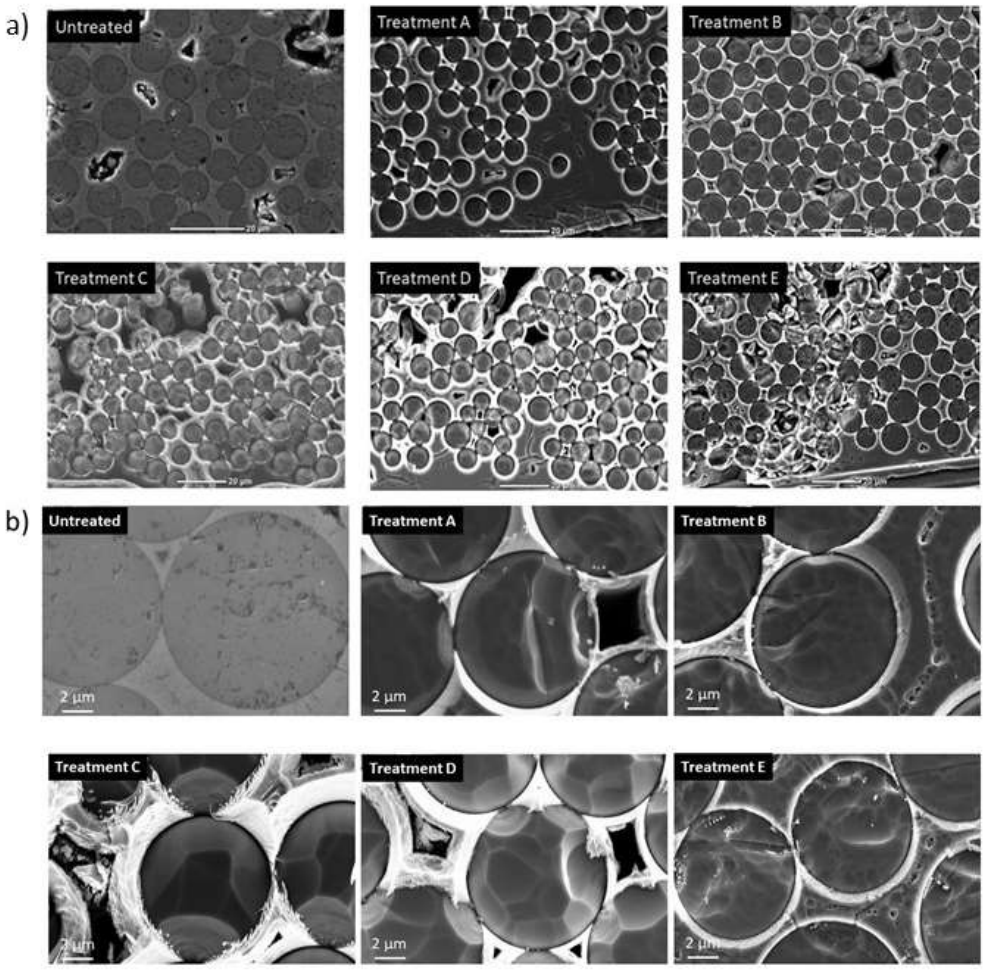

Figure 4-2: comparison of the surfaces before and after the plasma treatment at lower (a) and higher (b) magnification.

It can be noted that the plasma treatment resulted in a preferential recession of the fibers on the flat polished surface that produced the target brush-like structure, expected to be beneficial for the improvement of the SiC/SiC joint strength (Fig. 4-2). The matrix was etched too, but in a much less evident way than for fibers. As assumed, even though both fibers and matrix consisted of SiC, their properties slightly varied because of their manufacturing processes [116]. They therefore had different etching resistance, similarly to what was reported for the STR treatment [104].

The matrix consists of crystalline and near-stoichiometric SiC deposited via CVI. On the other hand, Tyranno S fibers (first generation type) are made of SiC nanocrystallites and residual carbon particles embedded in an amorphous SiOC matrix [117]. Tyranno S composition is far from stoichiometric Si/C ratio; the Tyranno S fiber structure is reported for clarity in Fig. 4-3.

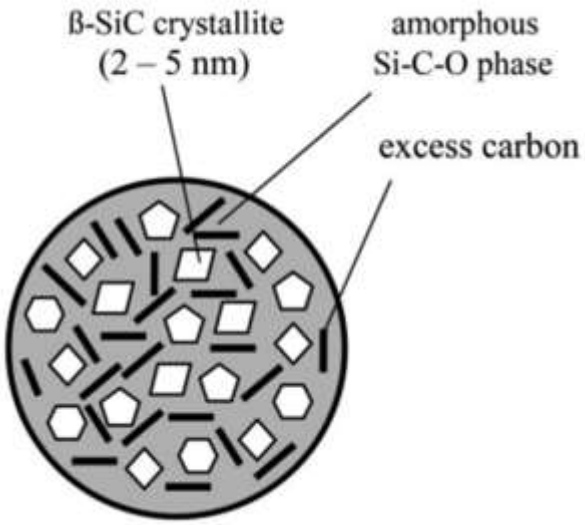

Figure 4-3: typical structure of first-generation fibers like Tyranno S (adapted from [117]***).***

This diversity in crystallinity and composition between fibers and matrix can justify the differences in etching resistance.

Different combinations of treatment length and gas mixture gave diverse results (Fig. 4-2.b). 5 minutes (treatment E, CF_4, 5 min), was enough to induce observable changes on the surface. The tnterphase was not visible anymore and the fibers began to look slightly corrugated. After 15 min (-treatments A and B), the SiC/SiC surface was similar to that observed after treatment E. The differences in gas mixture between A (CF_4) and B (CF_4/H_2) did not resulted in a marked diversity of the surfaces (Fig. 4-2.b).

30 minutes of plasma treatment (treatments C and D) resulted in more remarkable effects. Fibers were sharpened moderately because of their faster recession occurring close to the fiber/matrix boundary. In addition, the CF_4-alone plasma treatment (C) looked more aggressive than the CF_4/H_2 one (D). This confirmed what has been reported over the years for the dry etching of SiC. In fact, the etch rate of SiC is strongly dependent on plasma conditions and, in particular, on the mixture of the etch gas. By-products of the etching of SiC are SiF_x and they are the result of the reaction of fluorine radicals (also ions in minority form) and silicon atoms of the material attacked. The pure CF_4 treatment may be more aggressive than the treatment by the mixture of CF_4/H_2 because of the effect given by hydrogen. H_2 injection in plasma discharge produces hydrogen atoms (radicals),

which can intercept fluorine radicals (generated by the fragmentation of the CF_4 molecules in the plasma phase) reacting to form hydrofluoric acid. In this way, the concentration of fluorine in plasma is reduced, and the less fluorine radicals react with the SiC surface [118].

The concentration of fluorine recorded by EDS on the treated surface was close to the detection limit for this analysis (<0,1 %wt) [119]. No significant chemical changes were identified on the SiC/SiC surface. Hence, the surface composition may be considered to have been unaffected by the treatment and changes in the joint properties should be attributed exclusively to the evolution of the surface structure.

As a result of the preliminary characterization activity, plasma treatment C was identified as the most effective in texturing the SiC/SiC surface after electron microscope characterization since the fibers looked more eroded.Therefore it was selected to study the effect of the plasma treatment of SiC/SiC joints. Surface before and after the -treatment C is shown in Fig. 4-4).

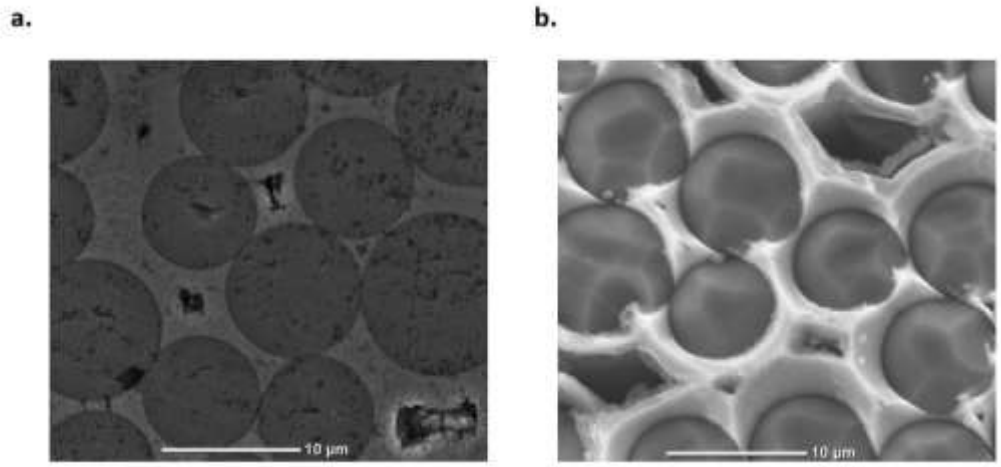

Figure 4-4: SiC/SiC surface before (left) and after plasma treatment C (right).

Cross-sections of Cusil-ABA® joined SiC/SiC, untreated and pre-treated (treatment C) are reported in Fig. 4-5. The joint looked sound, with a continuous and homogeneous Cusil-ABA-SiC/SiC interface in both cases. This was expected since the braze – a Ag-Cu-Ti type - is known to be an effective reactive joining material for SiC-based material. Cusil-ABA provided a high wettability on both SiC fibers and SiC matrix. Furthermore, no porosities were observed in the joint.

The composition of the alloy in the joint, analysed with EDS, was in accordance with data from the literature [112–114]: Cu-rich and Ag-rich regions are distributed

in the joining region, while Ti was detected close to the SiC/SiC surface where it formed a reaction layer, probably TiC.

Cusil-ABA filled all pores and voids present on the SiC/SiC surface even if no pressure was applied to the joining process, suggesting a very low viscosity of the braze at the process temperature. Such cavities, pointed out by black arrows in Figs. 4-5, are due to the composite architecture and the porous deposited matrix.

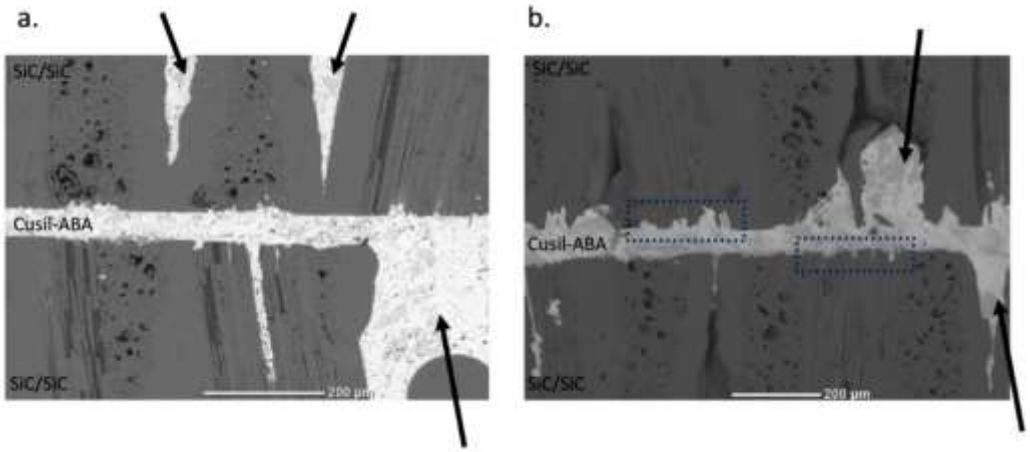

Figure 4-5: cross-sections of Cusil-ABA joined untreated SiC/SiC(a) and Cusil-ABA joined plasma treated SiC/SiC (b). Blue boxes in b. identify the plasma-induced brush-like structures. Black arrows indicate the cavities present in the as-received composites.

The existing cavities in the as-received SiC/SiC enabled an intense infiltration of Cusil-ABA in the composite, forming anchoring points locally. The braze infiltrated for tens of microns in the composite. Such phenomenon was observed also for plasma-treated SiC/SiC, being those cavities due to the manufacturing process of the composite. Therefore, both as-received and plasma-treated SiC/SiC got an interlocking contribution because of this alloy infiltration in the existing randomly distributed porosities.

However, the plasma treatment provided an additional contribution. Indeed, as can be observed in Fig. 4-5.b, as a result of the plasma treatment, the surface looked brush-like (indicated by the dotted blue boxes), in the regions where fibers are perpendicular to the surface. This new superficial texture provided more anchoring points because of the new cavities left by the erosion of fibers, which are regularly distributed along the joints and available for infiltration of the braze. Therefore, the global interlocking effect for plasma-treated SiC/SiC was given by the sum of the two contributions: the presence of random cavities (depth of tens microns) and the

plasma-induced brush-like texture regularly distributed on the surface (depths of a few microns).

The Cusil-ABA infiltration in the superficial brush-like textured regions is clearly visible in Fig. 4-5.b at the highest magnification.

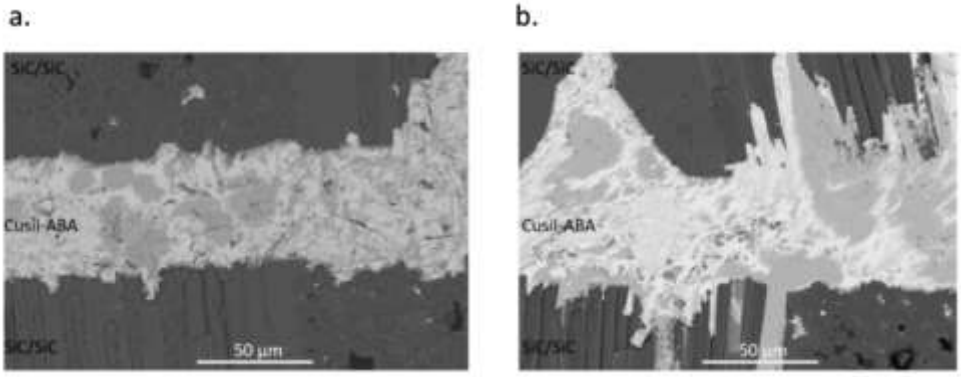

Figure 4-6: cross-sections of Cusil-ABA joined untreated SiC/SiC(a) and Cusil-ABA joined plasma pre-treated SiC/SiC (b) at higher magnification.

The good spreading of Cusil-ABA and the presence of the morphology in the joint for both untreated and treated SiC/SiC surfaces suggested that the plasma modification of the surface topography did not affect the good interfacial behavior of the brazing alloy.

SEM analysis of the cross-sections of the joined specimens showed that the plasma treatment introduced new anchoring points, prone to provide joint reinforcement through additional interlocking. Mechanical tests were carried out to assess the presence of such a beneficial effect on the apparent shear strength of the SiC/SiC joints.

Joined samples, made of both untreated and plasma-treated SiC/SiC, failed showing a mixed cohesive fracture surface, thus confirming the good quality of the joints, expected after the investigation on cross-section. Macro shots of the fracture surface are reported in Fig. 4-7.a-b).

Cross-sections of the fracture surfaces (Fig. 4-7.c-d) were inspected through SEM. Such characterization provided additional confirmation of the improved interlocking given by the presence of brush-like structure manufactured by the plasma pre-treatment. Looking at the top-view of fracture surfaces (Fig 4-7.e-f shows), it can be noted that a larger amount of Cusil-ABA is visible on the fracture surface of plasma-treated samples. This is coherent since the availability of more anchoring points, originated by the preferential etching of fibers, led to higher

adhesion at the braze/composite interface and a higher tendency of the joint to fail cohesively.

At higher magnification (Figure 4-8), the investigation on fibers provided further insights. Untreated fibers were clean after failure (Figure 4-7.a), suggesting that adhesive failure occurred at the braze/fiber interface. On the contrary, plasma-treated fibers were still covered by Cusil-ABA (Figure 4-7.b with attached EDS analysis), thus suggesting a cohesive failure at the fiber/braze interface.

The joint strength measured for the Cusil-ABA joined untreated SiC/SiC was 76 ± 27 MPa, whereas for joined samples produced with plasma-treated SiC/SiC was 118 ± 33 MPa. Failure loads were different, but no remarkable differences were recorded between the load-displacement curves of the two types of joints.

The coefficient of variance (standard deviation/mean value) was calculated to be around 0.25 for the plasma-treated joints and 0.31 for the untreated joints. Thus, it was similar for both cases, which could be related to the joining process, influenced by the operator. Indeed, bonding SiC/SiC along their thickness (only 4.5 mm) is a rather complicated operation and this may slightly affect the distribution of values of the joint strengths, but not their general trend.

The improved interlocking effect given by the the brush-like surface texture on SiC/SiC via plasma treatment treatment C in Table 4-1) led to a remarkable 55% increase in the apparent shear strength of the joined samples. The good adhesion of Cusil-ABA was enhanced by the presence of the new plasma-induced anchoring points interlocking mechanism and similar results can be expected for other Ag-Cu-Ti reactive brazing systems.

It is important to keep in mind that these results are valid for the SiC/SiC examined. Indeed, the type of composite strongly influences the final texture, since the architecture and the nature of each constituent (chemistry, physical properties, crystalline structure) would result in a different response to the treatment. For instance, 3rd generation SiC fibers that are highly stoichiometric and crystalline, can show a much higher resistance to chemical etching compared with the 1st generation of the SiC/SiC used in this work.

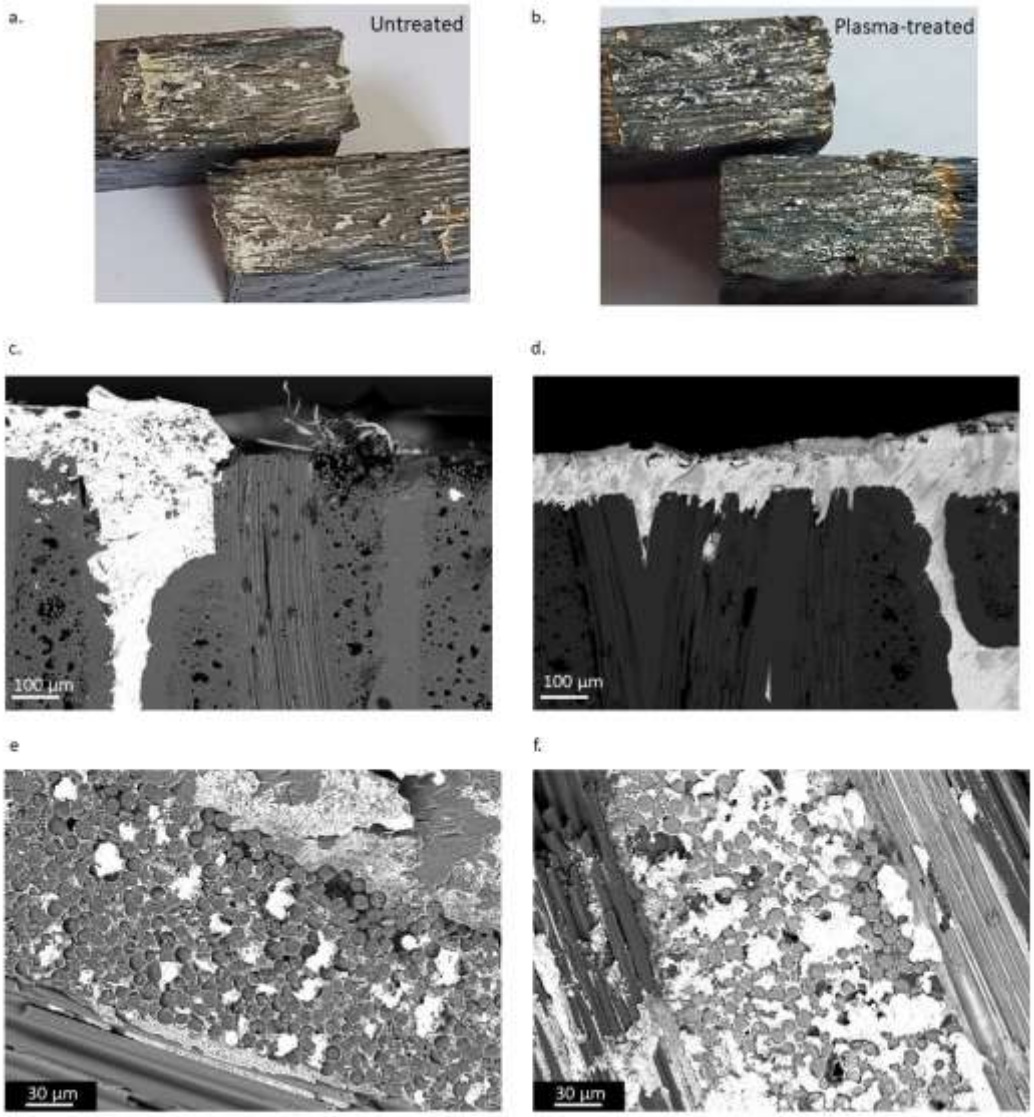

Figure 4-7: Macro shotsof the fracture surfaces of the joined SiC/SiC after SLO test untreated (a) and plasma-treated (b). The cross-sectional and top views taken by SEM for untreated (c,e) and plasma-treated (d,f) fracture surfaces.

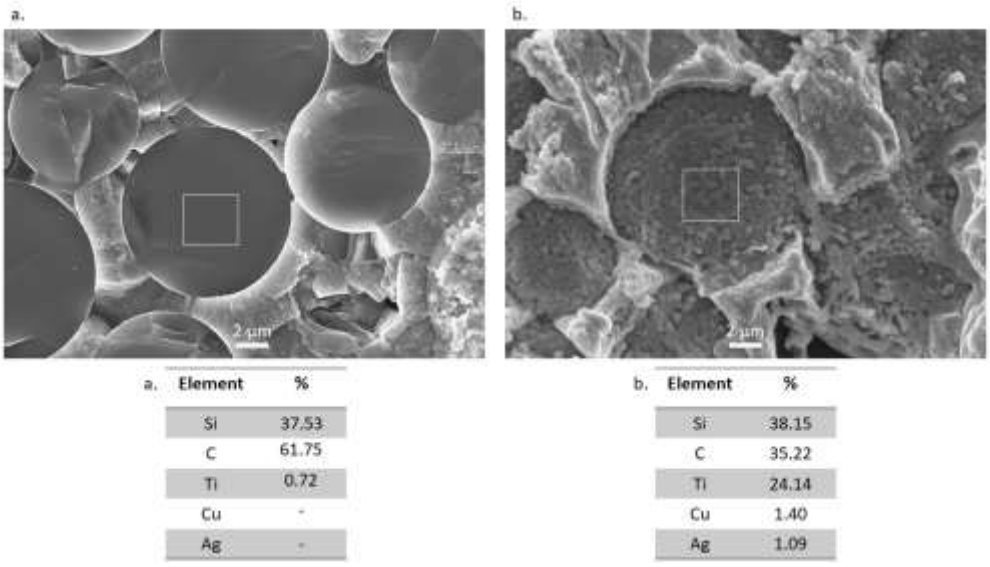

Figure 4-8: : SiC fibers on the failure surface of the untreated (a) and plasma-treated (b) SiC/SiC, together with the associated EDS analysis. EDS tables refer to the region enclosed by the white box.

Conclusions and future works

The research work presented in this chapter demonstrated the effectiveness of a fluorine-based low-pressure plasma in texturing the surface of SiC/SiC by taking advantage of the different etching resistance of each constituent. In particular, the treatment successfully produced a brush-like superficial texture by preferential erosion of fibers, similar to the one proposed by Valenza et al. [104], but its effect were confined at the surface without damages to the entire volume of material.

Most promising results for texturing were obtained operating with these plasma conditions: CF_4, 20 sscm, with 200 W for 30 min

SiC/SiC joints were manufactured using Cusil-ABA (a Ag-Cu-Ti reactive braze). The braze infiltration was improved by the presence of the plasma-induced brush-like structure, providing more interlocking, and the expected beneficial effect was confirmed by the mechanical testing results. In fact, 55% higher joint strengths were recorded for the plasma-treated SiC/SiC than for the untreated composites and higher retention of braze on the fracture surface was observed when the brush-like was present.

Future works may be focused on optimizing the process parameters and on getting more precise insights on the different etching rates between constituents.

Furthermore, other types of composites with different fibers may be investigated to evaluate if more advanced fibers (e.g. 3rd generation types) respond in the same way to fluorine-based plasma etching.

Finally, the opportunity for industrialization of the treatment may be considered.

5. APPJ as a surface modifier for C/C

Carbon-fiber reinforced carbon composites (C/C) are of interest for high-temperature applications, up to 2800°C, if preserved from oxidation. Their remarkable resistance to thermal shock, retention of mechanical strength even when serving at very high temperatures, high thermal conductivity, and low density, made them interesting as plasma-facing material for nuclear fusion in ITER divertor armor[120], but because of other limitations, they were then replaced by tungsten[121]. However, between the 1990s and 2000s, a huge collective research effort was done in developing suitable CFCs [122,123] and in coupling them with a copper alloy heat sink, in order to guarantee heat removal. Some mock-ups were manufactured according to different designs (Fig. 5-1)[124] and the challenge to provide effective bonding and high thermal transfer from CFC to copper pushed the research on feasible joining techniques. In fact, brazing was considered the best option for withstanding the high heat flux within the joint since mechanical solutions would not be effective for heat dissipation. The copper-C/C joint has been carefully investigated in several works [125–127]. Interest in dissimilar joints has not been limited to this application but extends to the aerospace field. As anticipated in the introductory chapter, C/C composites can target the harsh thermal conditions endured during space missions, from thermal management of the nozzles to re-entry operations. Therefore, even after pausing their development as plasma-facing armor material in the ITER project, the work on joining has been carried out. New brazing processes and optimization of more consolidated methods have been investigated over recent years [128–130].

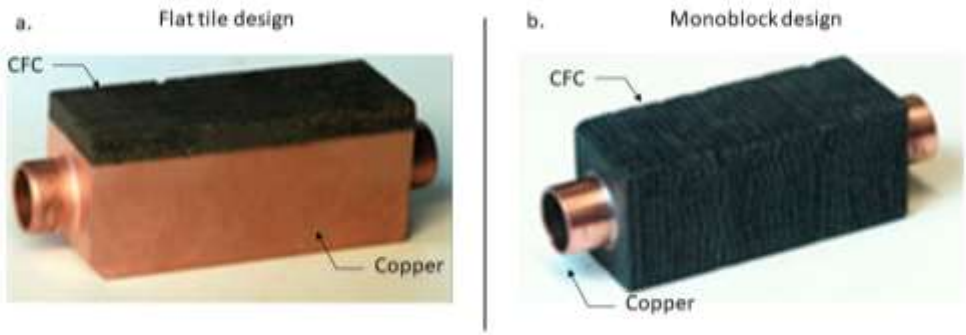

Figure 5-1: mock-ups of two designs for joining CFC to copper for the heat-sink of ITER divertors: flat tile (a) and monoblock (b). Adapted from [124].

The architecture of C/C can change according to the targeted application. For instance, the C/C developed for the ITER fusion reactor were manufactured in a 3D configuration in order to maximize the thermal transfer.

Several carbon fibers are available and their properties vary across a wide range, depending on the preliminary material and the process they undergo[131]. Common precursors fibers are made of polyacrylonitrile (PAN), pitch, and rayon, with the first two being the most common. The preliminary materials have to possess numerous aromatic groups in order to enable the graphitization process, critical for ensuring the desired mechanical properties. Precursor fibers undergo carbonization and graphitization steps necessary to transform the starting material close to graphite. Graphite is known to have strong covalent bonds along the plane and weak molecular bonds between planes. Carbon fibers, after the graphitization process, are made of ribbon carbon crystallites folded together and with the graphitic planes aligned along the axis of the fiber. A typical three-dimensional structure of a PAN-fiber is shown in Fig. 5-2. Final properties of fibers are strongly dependent on defects along the graphitic plane and the alignment between planes. When graphitic planes are randomly misaligned, the material is referred to as turbostratic carbon instead of graphite. The latter, indeed, is characterized by a long-range order in the stack. A comparison between turbostratic carbon and graphite is provided in Fig. 5-3.

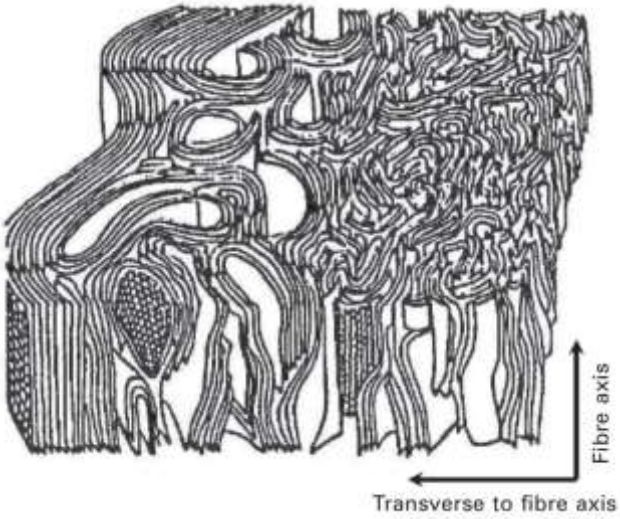

Figure 5-2: lamellar structure of a carbon fiber. (Adapted from [132]***)***

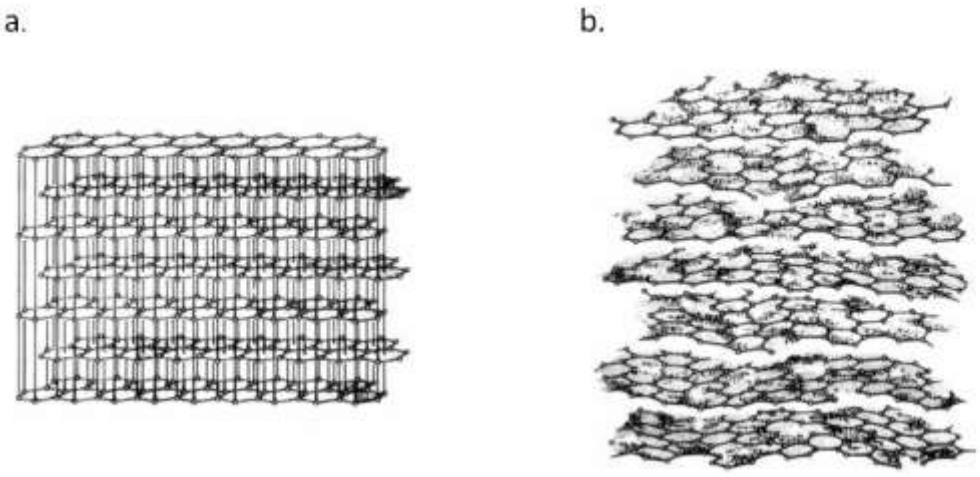

Figure 5-3: alignment of graphite (a) and turbostratic carbon (b). Adapted from [133]**.**

Carbon fibers are nowadays found in all field of applications as reinforcement for polymeric matrix composites addressing demanding applications. C/C are more a niche. In order to manufacture them, fibers have to be embedded in a carbon matrix. Two main matrix-forming processes are available: Chemical Vapor Deposition (CVD), based on reactions between precursor gases, and Resin Impregnation, followed by carbonization treatment. They often are used in combination to foster densification and reduce the porosity of the C/C composite. Eventually, matrix can be consolidated starting from powders, e.g. coke and pitch[134]. In the CVI processes, the matrix, in form of pyrolytic carbon, is

deposited onto fibers, forming concentric layered structures around fibers. The quality of the matrix is strongly influenced by deposition parameters[135].

The overall contribution of the properties of each constituent, the volume of fibers, their distribution, the architecture and the presence of pores influence the final thermo-mechanical properties of the C/C composites.

As already mentioned, carbon-based materials are extremely sensitive to oxidation. Their behavior has been deeply investigated given the importance of carbon in the global economy. Concerning C/C, great attention has been given to the understanding of their ablation behavior during the re-entry phase [136]. Carbon experiences oxidation in air, starting from 400°C, slowly, and then increasing when the temperature exceeds 500 °C. Fig. 5-4reports the oxidation rate calculated for nuclear-grade graphite [137]. The oxidation rate is far higher when temperature overcomes 800°C. Oxidation is a weakness for C/C, therefore coatings are required to preserve the material and guarantee its performance. Alternatively, uncoated C/C must work in a protective atmosphere.

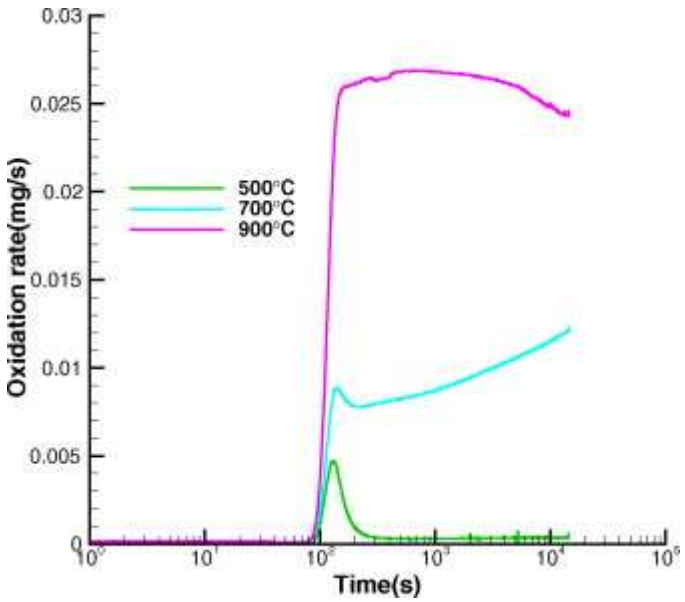

Figure 5-4: oxidation rates of nuclear-grade graphite at different temperatures. Adapted from [137]**.**

However, the oxidation sensitivity of carbon can be exploited to remove materials from the surface and induce texturing. In particular, it can be used to promote the formation of a brush-like texture taking advantage of the slightly different properties between fibers and matrix, given by the manufacturing process.

To the best of our knowledge, the only work carried out on C/C for texturing their surface to improve the joint strength was done by Yang et al.[138]. The reinforcement of the interfacial joint structure was achieved by a combination of a pre-oxidation surface treatment followed by a Chemical Vapor Deposition (CVD) process for grafting Carbon NanoTubes (CNTs) on the surface. The process is reported in Fig. 5-5. The first step (pre-oxidation) generated cavities for infiltration through the growth of annular gaps around fibers. The second (CVD growth of CNTs) served to increase the sites for reaction with the braze along the surface.

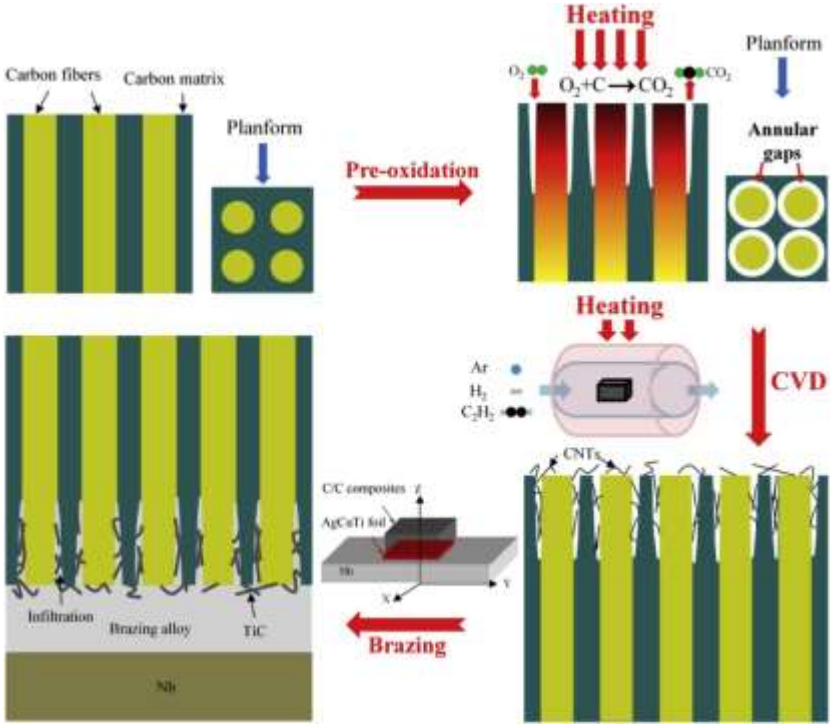

Figure 5-5: pre-oxidation treatment and NTs grafting on C/C proposed by Yang et al. for improving joint strength. Adapted from [138]**.**

The choice of using an oxidation treatment to induce surface treatment is particularly interesting for the scope of this work. The motivation behind this relies on the different oxidation of the fibers and the pyrolytic matrix; the experiments were carried in air, exposing the entire C/C sample for 5 min at several temperatures (between 700°C and 850 °C). The concept recalls the Selective Thermal Treatment (STR) proposed for SiC/SiC composites[104], but the conditions were, of course, different. Findings from this study are hereby reported because useful for comparison. The authors did not report any relevant damage to the C/C after the oxidation treatment (rather unusual since the oxidation of carbon is intense in such conditions, as introduced at the beginning of the chapter) and the annular gaps

generated around fibers was successful in providing infiltration channels for the brazing alloy. The best conditions for the treatment were identified as 800°C for 5 min and they gave an increase of the joint strength of the braze component from 29 MPa to 57 MPa. A second study was conducted, expanding the investigation of the pre-oxidation process even at lower temperature[139].

The aim of the present thesis is to engineer structure on the surface of a C/C composite to obtain a brush-like structure, useful for improving the mechanical interlocking with the joining material. This can be achieved through a selective removal, as already done with SiC/SiC composites in the previous chapter. Since C/C are sensitive to oxidation, the idea hereby proposed is to exploit a commercial Atmospheric Pressure Plasma Jet (APPJ) as an etching tool. This equipment is common in the industry, where it is exploited for the surface activation of polymers. Examples are available on the website of manufacturers of those plasma systems [140–142].

APPJ can provide several advantages since it comes with a simple equipment, contrary to low-pressure plasma systems. The cost is relatively low, the treatment is confined to the surface and the process can be applied to large-size components and big batches, enabling automation and continuous operation.

Surface activation for plastics is induced by the oxidation effect given by the plasma. The introduction of oxygen-rich groups, the removal of contaminants and roughness changes are the main effects of surface modification. Plasma-induced oxidation may be effective in texturing the surface of C/C since the properties of fibers and matrix are slightly different because of the manufacturing process and it can induce the brush-like structure. To the best of our knowledge, no work concerning plasma surface modification of C/C has been carried out with a focus on improving adhesion. APPJ systems have been reported as suitable for improving the adhesion of carbon fibers with polymers to manufacture Polymer Matrix Composites (PMCs)[143]. Working at low temperatures (around 100 °C), the APPJ was effective in introducing oxygen-containing groups on the carbon fibers, beneficial for improving wettability by matrix, and in roughening[144].

Thermal treatment has some limitations because it exposed the entire volume of material to oxidation and a heating furnace can be more impacting than APPJ in terms of energy cost. However, the results from Yang's study[138] were interesting

and therefore the experimental activity included attempts to replicate the process in order to compare it with the APPJ.

Materials and methods

The material chosen for the activity is a C/C composite material known as a NB31 C/C manufactured by SNECMA (FRANCE). The composite 3D architecture is shown in Figure 5-6. The constituents are:

- X direction: Pitch-derived fibers.
- Y direction: PAN-derived fibers.
- Z direction: PAN-derived needles.
- Carbon matrix: a first CVI step was carried out to depose pyrolytic carbon, then a following heat treatment was conducted at 2800 °C. Later, a second CVI deposition took place. Pitch impregnation (100 MPa, 1000°C) was performed as final step[145].

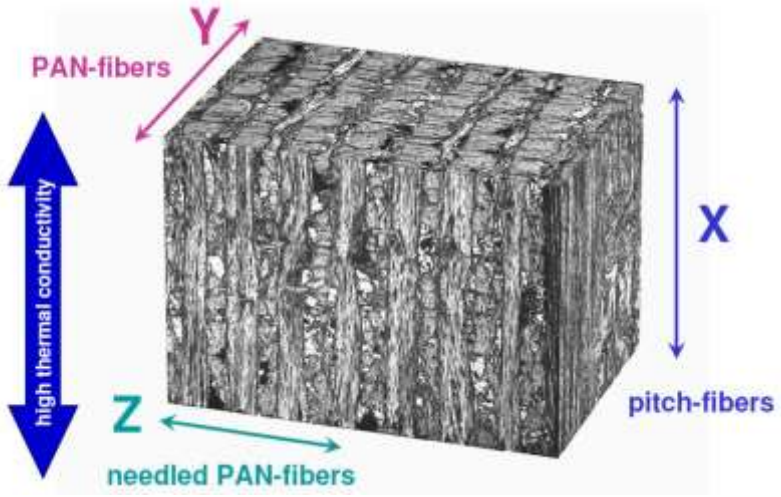

Figure 5-6: Composite architecture for C/C NB31 (Snecma, France).

NB31 tiles were cut in smaller samples, approximately 10 mm x 10 mm with a thickness of 5 mm. The surface that underwent the APPJ treatment was the one identified by the YZ plane, perpendicular to the x-aligned pitch-fibers. Joints were manufactured along this surface in previous works [146] dedicated to joining C/C for ITER applications considering that the X axis provided the highest thermal

conductivity. Therefore, YZ surface was chosen for collecting results that may be perhaps compared with those reported. The YZ was then polished up to P2400 to standardize the surface roughness of samples and evaluate the evolution due to the plasma exposure.

Some samples were oxidized via thermal treatment setting the conditions reported by Yang et al. in their work. YZ surface was left uncovered in order to expose it to oxidation, while the other surfaces were covered using alumina plates to protect them. A chamber furnace (Carbolite Gero, Germany) was set at several temperatures: 600 °C, 650 °C, 700 °C, 750 °C, and 800 °C. Each sample was exposed for 5 minutes. Weight loss was measured by weighting samples before and after the treatment via analytical balance.

The surface plasma treatment was carried out using a PlasmaTec-X plasma generator, equipped with a treatment nozzle, manufactured by Tantec, Denmark. This is a commercial system that is widely available. Technical specifications are reported in table 5-1 (available on the manufacturer's website [142]). Process parameters are exposure time, airflow (L/h), and distance between the nozzle aperture and the sample. The plasma gas is air, under. The minimum value for the air flow suggested by the manufacturer is 1000 L/h. Since the aim of this work was to carry out a preliminary assessment of the effect of this technique on the surface evolution, only one of the parameters was modified and studied: the exposure time. The nozzle-sample distance was kept constant at around 5 mm and the airflow was fixed at 1750 l/h. The exposure lengths evaluated were: 30 s, 1 min, 5 min, 10 min, 15 min, and 20 min. Before and after each plasma treatment C/C samples were weighted using an analytical balance to collect information on the weight loss. Three samples for each time length were evaluated.

Table 5-1: Technical specifications of PlasmaTec-X system (adapted from [147]***).***

Technical Specifications	PlasmaTEC-X Generator	PlasmaREMOTE	PlasmaTEC-X Nozzle
Mains Voltage and Frequency	100-250VAC – 50/60Hz (Universal power input)	N/A	N/A
Output Voltage/Power	550VA	N/A	425 watt
Ramp up time	10 ms	N/A	N/A
Shut down time	< 1 ms	N/A	N/A
Control interface	M12 (8 pole)	M12 (4 pole)	N/A
Dimensions (WxLxH) mm	150x470x198	125x169x167	OD30x206mm
Weight in kg	6,1	2,0	1,1 (w. 2 mtr hose)
Treatment width in mm	N/A	N/A	6 - 12 mm
Compressed air supply	4-8 bar, dry and clean	N/A	N/A
Compressed air connection	OD8mm - Quick connection	N/A	N/A
Air consumption	N/A	N/A	33 ltr/min
Units per PlasmaREMOTE	N/A	1-8 PlasmaTEC-X generators	N/A
Regulation compliance	CE - RoHS - WEEE	CE - RoHS - WEEE	CE - RoHS - WEEE

Electron microscopy (JEOL benchtop equipped with EDS) was carried out to investigate the effect on the ZY surface before and after the thermal oxidation and the APPJ surface treatment to observe how the morphology changed as function of the treatment length. SEM characterization was used as a preliminary screening strategy to select the most interesting conditions for the next steps. In order to evaluate the etching rate of the material, the treatment was confined to a specific area of the CFC sample (as shown in Fig. 5-7) and then the etching depths were calculated through a contact profilometer (Taylor Hobson) for three samples for each treatment condition. The average etching depth was then calculated.

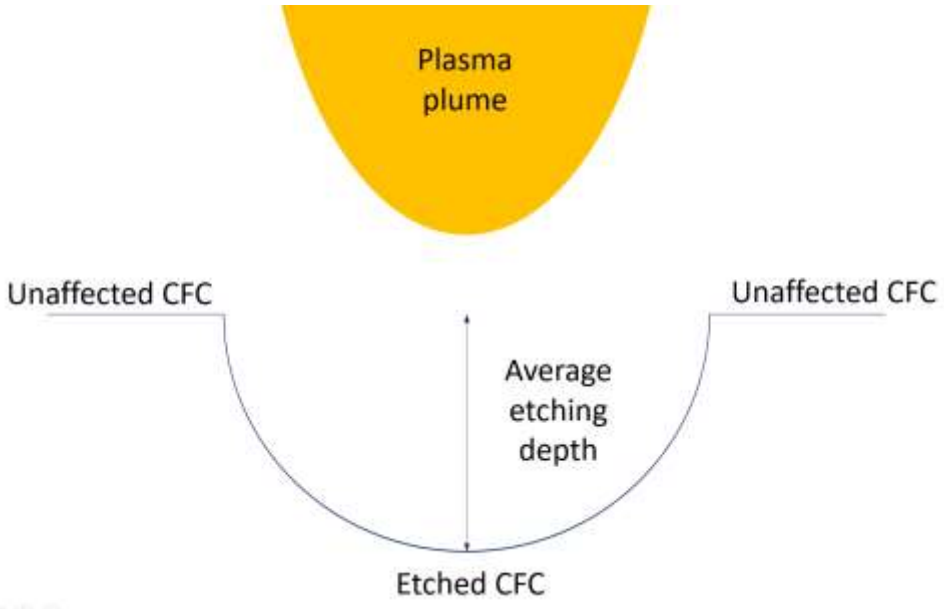

Figure 5-7: sketch of the test for evaluating etching depth.

Samples were then prepared according to the conditions identified as the most interesting: 30 s, 1750 l/h, and 5-mm gap. APPJ scanned the surface, treating each region for 30 s.

Samples were investigated via electron microscopy and EDS were performed to get information on changes in the composition. Confocal microscope (Sensofar S-neox) analysis followed to collect further information on the surface texture and to double-check SEM results. Two objectives were utilized: 20x and 100x (CF-60 Nikon).

The material chosen as joining material is TiCuNi (70 wt% Ti, 15 wt% Cu, 15 wt% Ni) braze, manufactured in the form of foils of thickness 50 μm by Wesgo (Germany). This is a reactive alloy that is well-known as braze for non-oxide ceramics[129,148,149].

Wetting tests were carried out to evaluate the effect of the treatment on the C/C surface-braze interactions. A metallic sphere, with the same composition of TiCuNi, was manufactured via an arc melting furnace and then placed on the top of the C/C composite. Samples were then inserted in a vacuum furnace and monitored using an internal camera to evaluate contact angle evolution (Fig 5-8).

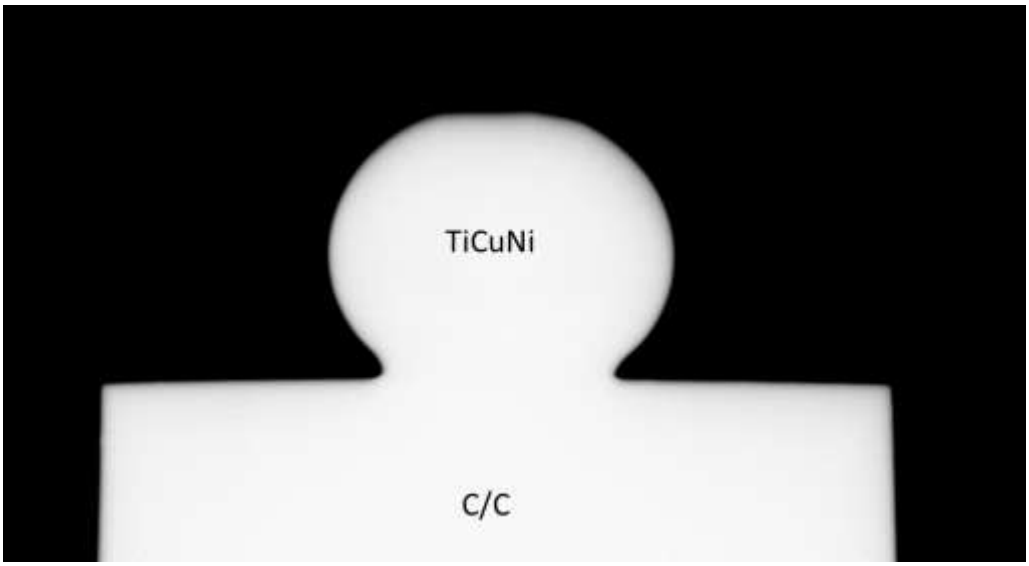

Figure 5-8: wetting test: TiCuNi sphere on the C/C (snapshot).

The temperature was set at 1000 °C. After the wetting tests, cross-sections were prepared to evaluate the braze-composite interface and the infiltration given by the brush-like appearance.

Joints were then manufactured using 3 foils of TiCuNi, to mitigate infiltration due to pre-existing residual voids in the composite. Samples to be joined were heated up to 1000°C and kept at that temperature for 10 min. The heating and cooling rate was set at 10°C/min. The treatment was carried out in a vacuum, according to the indications given by the manufacturer and to prevent oxidation of C/C composites and the braze. Similar (C/C-C/C) and dissimilar joints (C/C-Copper) were prepared and then tested in Single Lap Offset (SLO) shear stress configuration to get information on the joint strength for untreated and treated samples. A universal testing machine SINTEC D/10 equipped with a 50 kN load cell was used to perform the SLO test. Crosshead speed was set at 1 mm/min.

Fracture surfaces were then investigated by visual inspection and their cross-sections were investigated by electron microscopy.

Results and Discussion

Pre-oxidation treatments were coherent with the oxidation rate expected for carbon (graphite)[137]. The 5-min thermal process resulted in a higher weight loss as function of the temperature. The highest mass removal was reported at 800°C, indicated by Yang et al., as the optimal condition for improving the joint strength.

Table 5-2: weight loss recorded for thermal oxidation tests.

Temperature (°C)	Weight loss (%)
600	0.56
650	0.89
700	2.15
750	5.84
800	7.75

The oxidation treatment carried out in air replicating the conditions proposed by Yang et al. resulted in an intense weight loss that is undesired, since in order to prevent any damages to the material that may compromise the in-service performances the volume affected by the treatment has to be limited to the surface. Fig. 5-9 shows the top-views for the samples after the pre-oxidation treatment at 600°C (a), 650°C (b), 700°C (c), 750°C (d), 800°C (e) for 5 minutes. After 5 min

at 600°C no remarkable differences between matrix and fibers can be observed, while annular gaps are visible for exposure at 650°C and 700°C. Pre-oxidation at 750°C and 800°C, associated with relevant weight loss resulted in a strong removal of both matrix and fibers. These treatments provided different results compared with the reference study since the effect of the thermal treatment is detrimental to the integrity of the composite. However, the type of C/C used for this thesis are different and this may explain the variations in the experimental outputs.

The possibility of selective thermal treatment was therefore excluded because of these results and the economy of the process. Indeed, even if no mechanical tests were done on the C/C after the heat treatment, the mass loss recorded pointed out that the composite was severely affected.Plasma treatments have the potential of cutting costs and time compared with thermal processes , and, even more important, they confine the effects at the surface without undermining the integrity of the composites

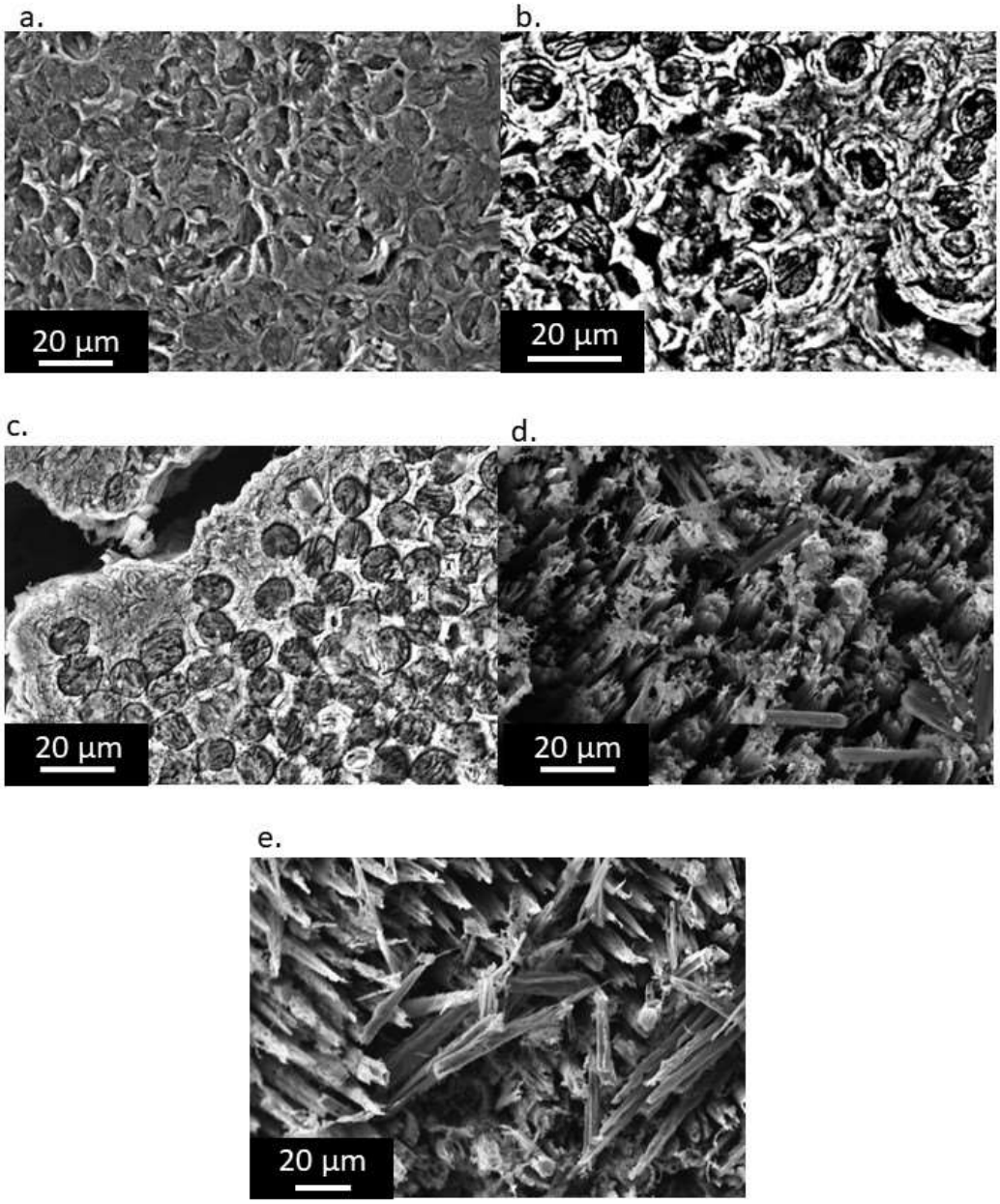

Figure 5-9: top-views of C/C after thermal oxidation treatments: 600°C (a), 650 °C (b), 700 °C (c), 750 °C (d), 800 °C (e) for 5 minutes

The atmospheric pressure plasma jet exposure of the ZY surface of the NB31 C/C provided an interesting weight loss trend that can be approximated by a linear behavior (Fig. 5-10). The mechanism behind the etching of carbon composited by APPJ can be explained through oxidation, even if the temperature is expected to be

lower than the lower limit for oxidation at atmospheric pressure (> 400°C), according to manufacturers' indications.

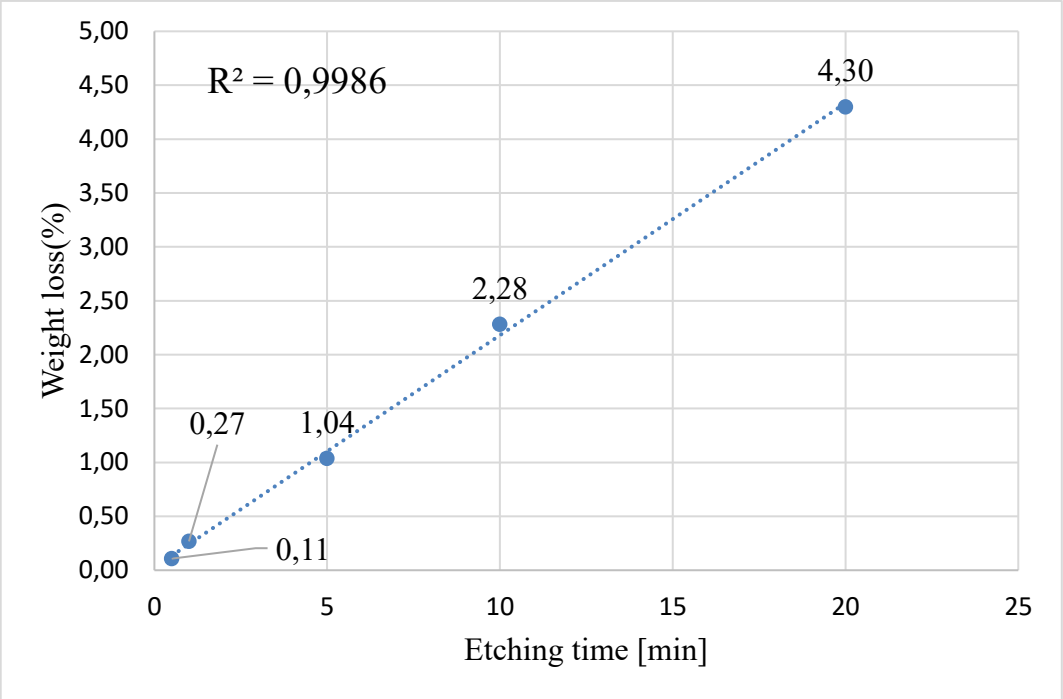

Figure 5-10: Weight loss of CFC under APPJ plasma treatment.

The temperature in the surroundings of the APPJ nozzle was recorded to be around 250 °C using a thermal image camera (Fig 5-10) for all treatment lengths. The K thermocouple in contact with the sample never registered temperatures exceeding 200 °C. The temperatures recorded cannot be considered very accurate, but they are valuable to get information on the overall thermal conditions. The temperature is far lower than the threshold for thermal oxidation.

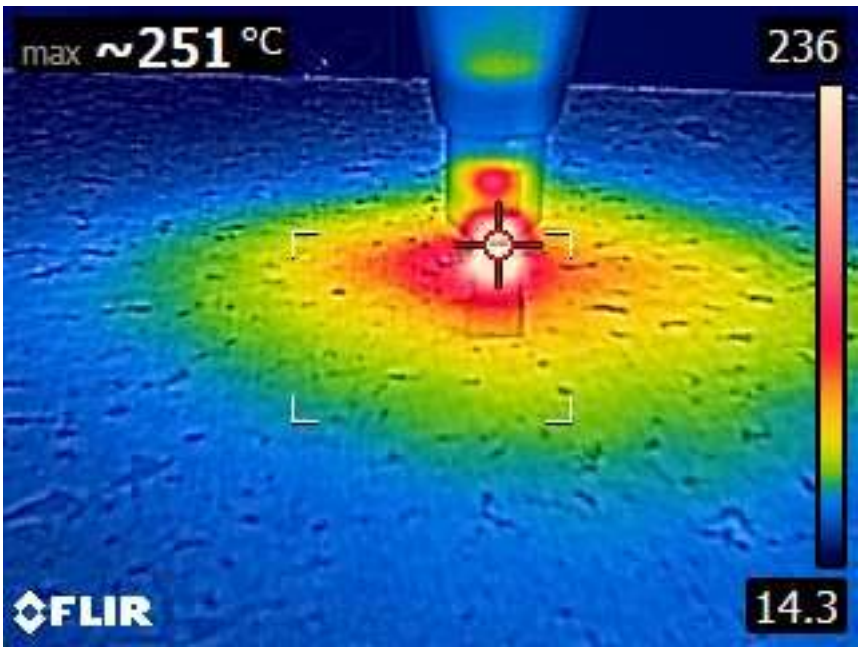

Figure 5-11: thermal image taken during an APPJ treatment

Oxidation can take place because of the presence of highly reactive species that can lower the energetic threshold for the reaction. In this work, no investigation was carried out on the composition of the plasma plume. Since the plasma gas was air, it can be supposed that the ROS (Reactive Oxygen Species) responsible for the low-temperature oxidation are O_3, NO_x, atomic oxygen, OH, etc, which were reported in other studies carried out using air-based APPJs [150,151]. Such species are very effective as oxidizing agents even at temperatures close to R.T. as reported by Kostov et al. [152] in their work on the surface modification of polymeric materials.

The objective was to use the plasma as surface treatment and acceptable weight loss was between 30 s and 1 min. Further exposure resulted in a too-harsh material removal that is undesired and may compromise the integrity of the composite. Fig. 5-13 shows the surface morphology observed by SEM of untreated samples and treated ones for several time lengths. Generally, the fibers looked more sensitive to oxidation compared to matrix, but both of them are fast removed by the plasma as noticeable by the weight loss trend.

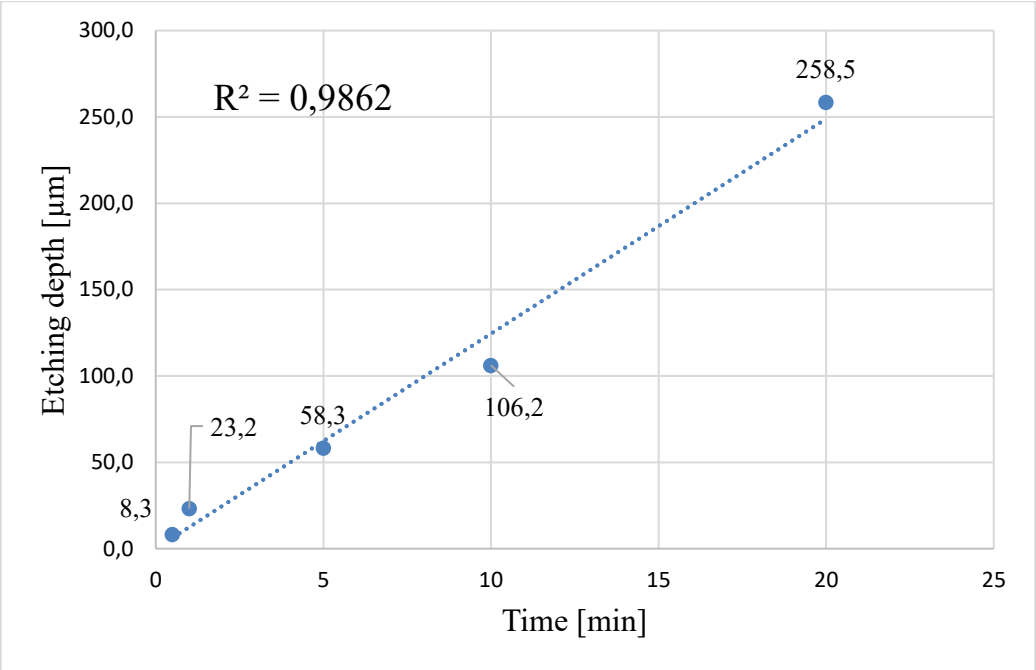

Figure 5-12: Etching depth for CFC under APPJ plasma treatment.

More in detail, the evolution of the surface microstructure observed by SEM showed preferential erosion of fibers compared with the matrix. Considering that the etching rate was calculated to be ~ 0.3 µm/s, the original surface was completely ablated by the treatment. The new surface, generated by the plasma exposure, provided fibers slightly on a lower plane than matrix, thus suggesting a little lower resistance of the fibers to the oxidizing effect of APPJ. It is worth to be noted that fibers, parallel to the APPJ jet, had an unusual look. Annular gaps were formed, as commonly reported as a consequence of the oxidation, but fibers did not show any sharpening. Instead, they were characterized by an almost flat irregular surface with porous channels inside. In all cases, the APPJ treatment provided a similar surface texture. This suggested that after a transitory time, the novel surface texture was formed and then maintained during the progressive plasma-induced erosion. Thus, for a longer time, the volume removed was higher, but the texture was still the same. The ablation of matrix and fibers occurred steadily, slightly faster for the latter. Therefore, extended APPJ exposures may not be effective in modifying further the surface, but they result in a significant material removal as recorded by weight loss and etching tests. Since the goal was to identify a treatment that can be effective, short and non-detrimental for the material, the 30 s condition was identified as the closest to these requirements according to collected data.

In order to get better information on the presence of differences between fibers and matrix in terms of removal, the profilometry was needed. Confocal microscope profilometry analysis provided insightful results that confirmed the preferential etching. As a reference, the SEM top views of the samples before and after the treatment are reported in Fig. 5-14. Fig. 5-15 compares the roughness maps for polished C/C before and after a 30-s plasma treatment. There is an accordance between the deductions suggested by microscope investigation and the roughness maps. In fact, the change in texturing given by the APPJ exposure is remarkable. The fibers looked at a lower height compared with matrix points. The erosion of the fibers seemed to be quite uniform on the surface, resulting in distributed cavities.

An insightful parameter to evaluate changes on the surface is the developed interfacial area ratio (Sdr) given by eq (1):

$$Sdr = \frac{Real\ surface - Ideal\ surface}{Ideal\ surface}$$

This parameter provides a first indication of the roughness evolution of the surface and the increase of the specific area. For totally flat surfaces the Sdr value is zero. To monitor the evolution of the roughness on the surface knowing this parameter before and after the treatment it is critical.

Fig. 5-15 shows the Sdr value before and after treatment. The pristine surface has a value of Sdr of 11%. After the 30 seconds of plasma, the Sdr value is 190%, which indicates a quite remarkable increase of the surface area.

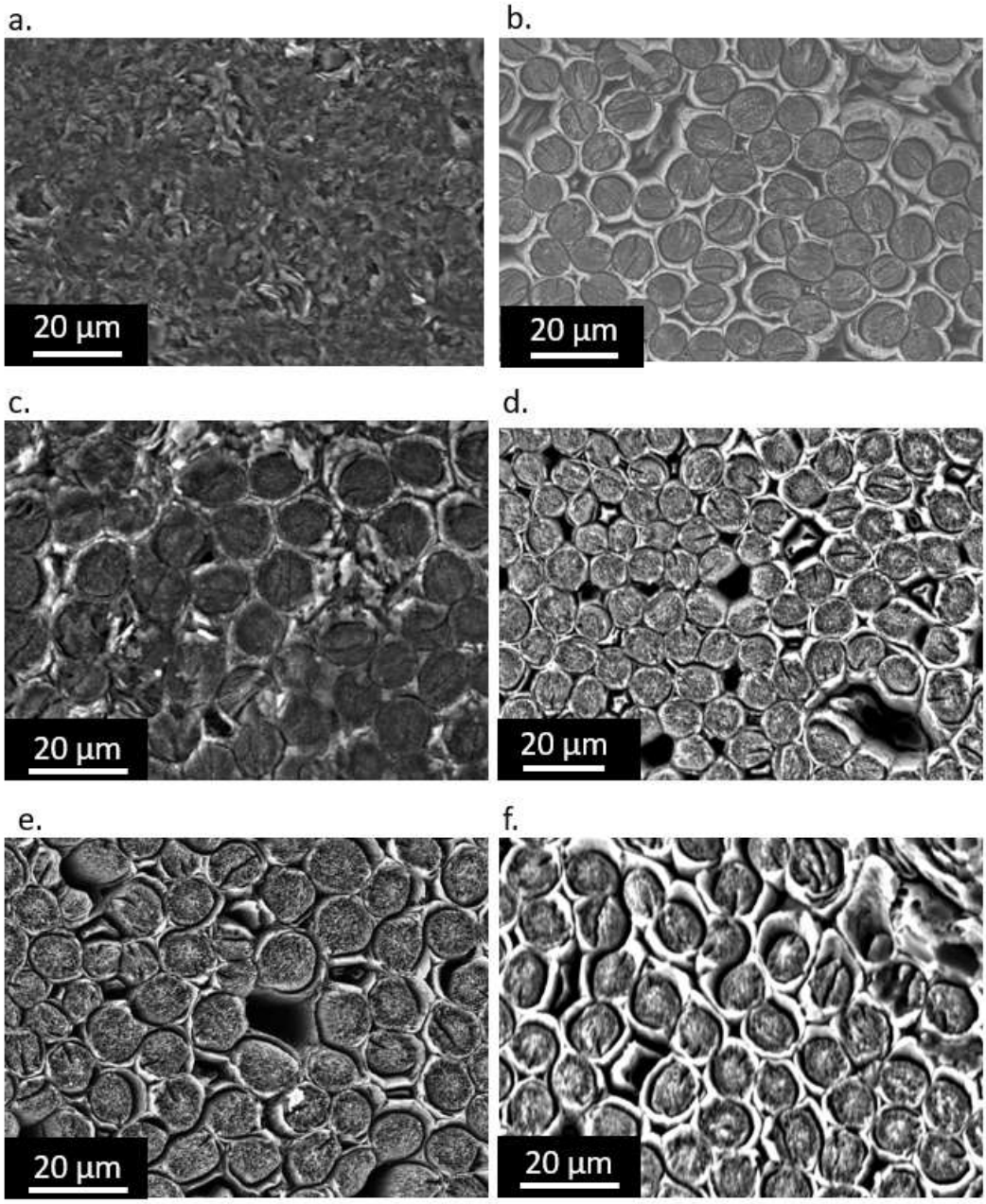

Figure 5-13: Top view of NB31 ZY surface: polished (a), after 30s of APPJ (b), after 5 min (c), after 10 min (d), after 15 min (e) and 20 min (f). Air flow: 1500 l/h. Sample-nozzle distance: approximately 5 mm.

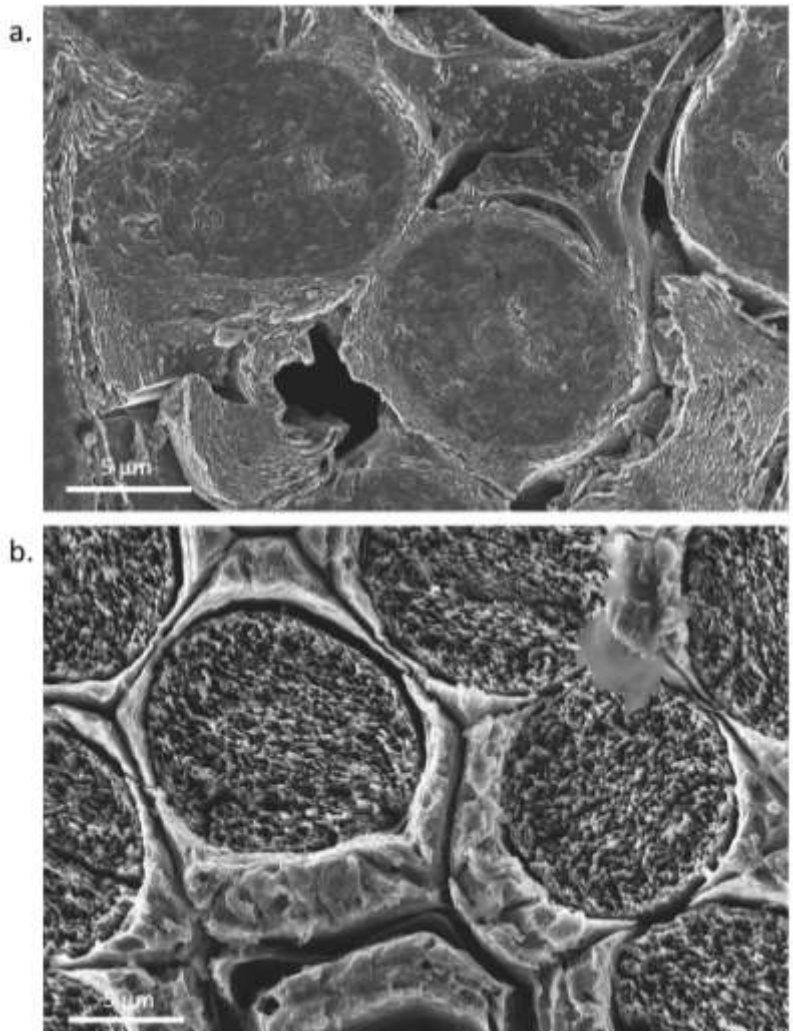

Figure 5-14: Surface of C/C before (a) and after 30s APPJ (b) at higher magnification

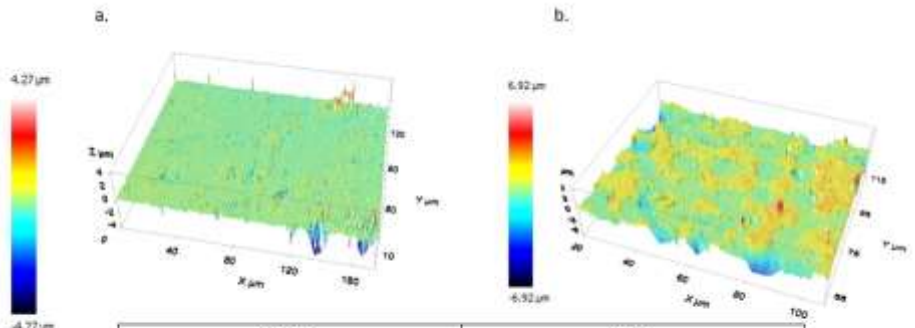

Sample	SdR
Polished C/C	11 %
APPJ-treated C/C (30 s)	190 %

Figure 5-15: roughness maps for polished C/C (a) and 30s APPJ C/C (b). Under each map the related Sdr value is reported.

Further confirmation for the selective removal came from the analysis of the height distribution, shown in Fig. 5-16. The distribution for untreated and 30 s APPJ

treated C/C is completely different. Indeed, a single-peak distribution was reported for untreated samples, while treated C/C exhibited a double-peak curve. The The highest peak refers to fibers (lowest points)and the other to the matrix. The presence of these two peaks denoted a clear distinction between the two constituents.

The average height gap between fibers and matrix after the plasma-enhanced selective removal was calculated to be 1.4 µm. Similar observations were collected with the line analysis carried out tomeasure a profile of the surface (Fig. 5-17) Steps between matrix and fibers are visible and the profile appeared to be brush-like as targeted.

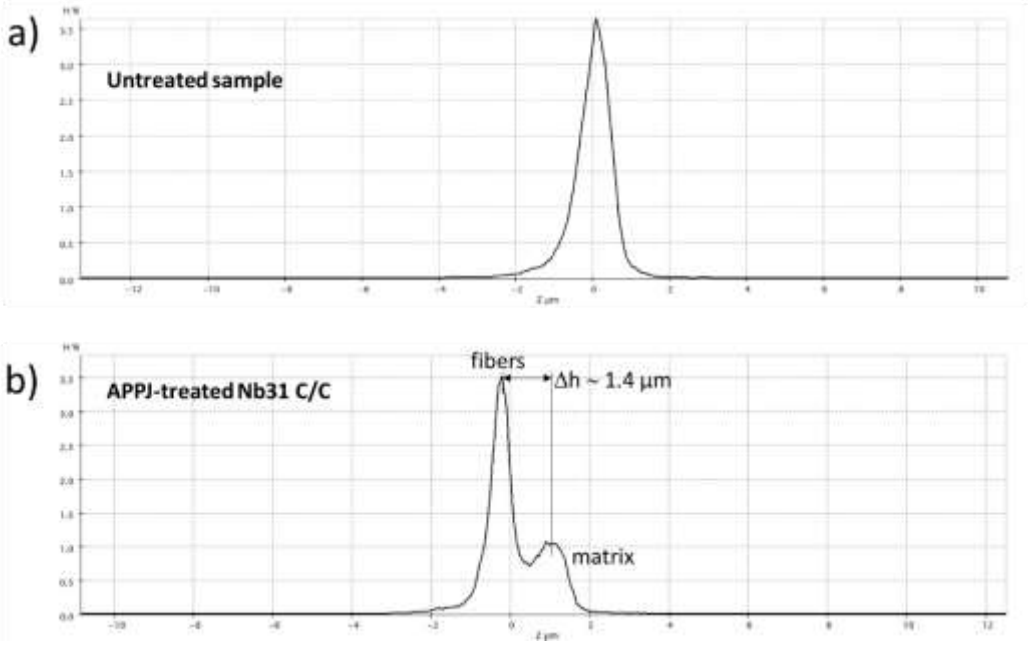

Figure 5-16: height distribution of polished C/C (a) and 30 s APPJ C/C (b)

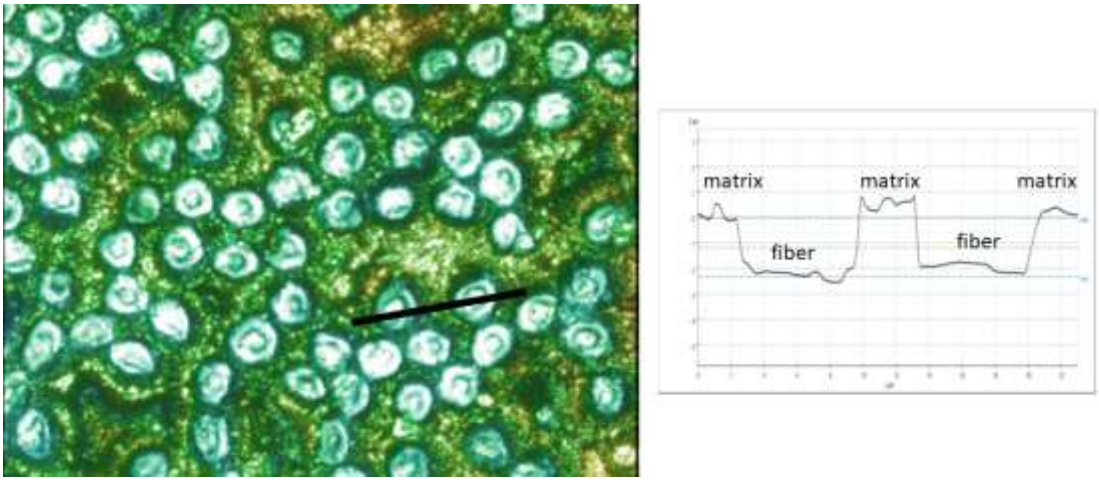

Figure 5-17: Confocal line analysis on 30 s APPJ-treated surface. The profile reported refers to the line identified by the segment.

The SEM analysis and profilometer characterizations confirmed that the APPJ treatment was effective in producing the desired brush-like structure on the surface of the composite. The second part of the experimental activity focused on the evaluation on how the new brush-like surface texture affected the interaction with the TiCuNi brazing alloy. Fig. 5-18 reports the contact angle evolution for the polished C/C and for a sample after plasma treatment. No detectable differences were observed: the wettability is good for both of them and the contact angle decreased with the same trend. Thus, the plasma-induced texture did not affect the wettability of the TiCuNi alloy on the composite.

According to the SEM investigation of the APPJ-treated surface after wetting tests (Fig. 5-19), the TiCuNi droplet seemed to wet the matrix first and then infiltrate the cavities left by the fibers. This is visible in Fig. 5-19, where there were regions close to the front of the droplet, with matrix completely covered by the braze surrounded by clean fibers. To the aim of understanding better the wettability behavior, further investigations may be carried to clarify this observation.

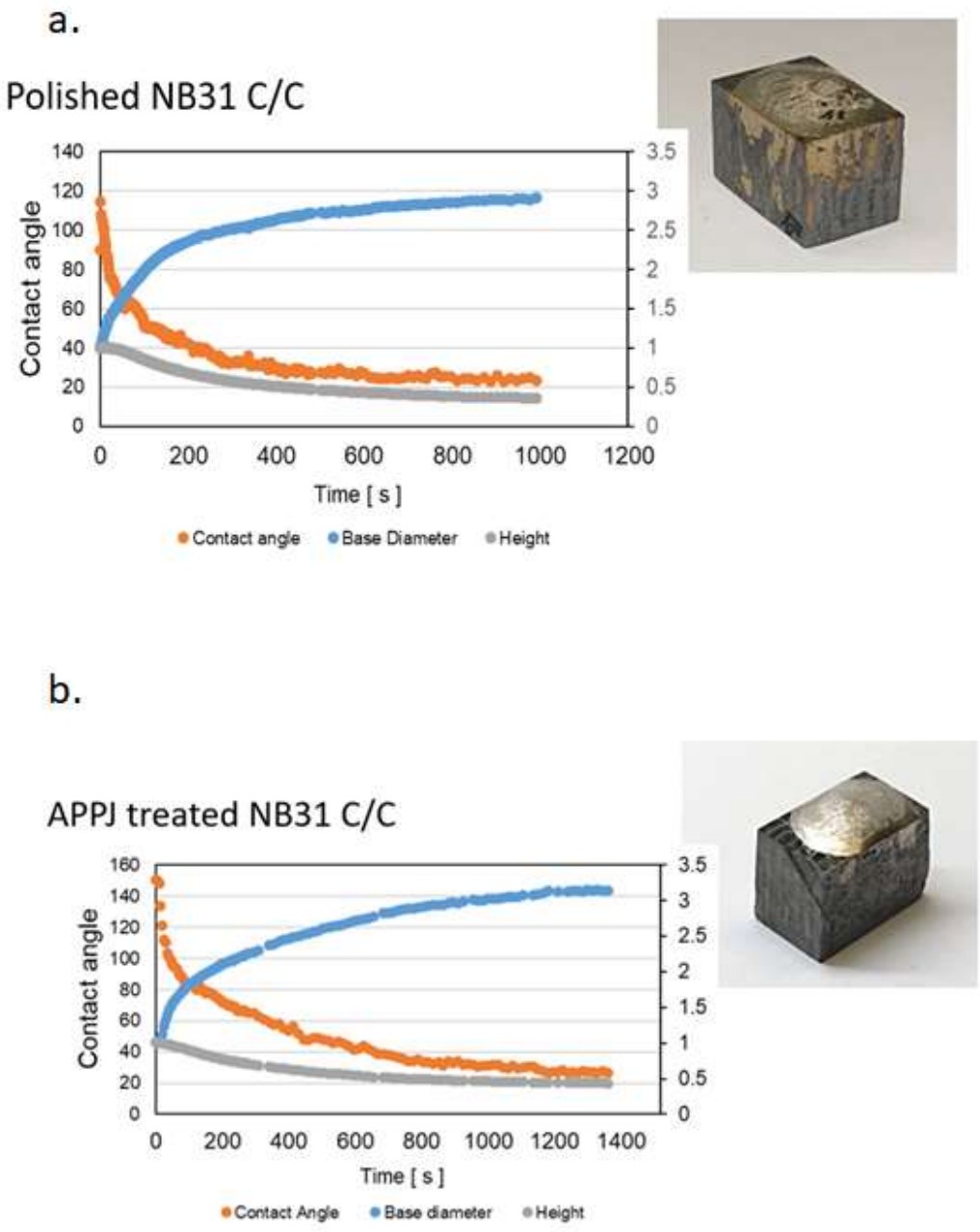

Figure 5-18: contact angle evolution of TiCuNi on untreated (a) and 30 s APPJ treated (b) C/C

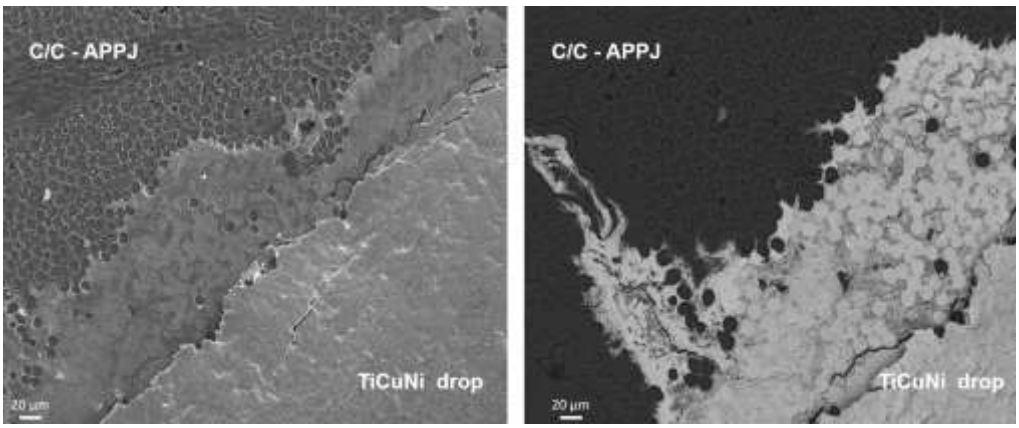

Figure 5-19: TiCuNi drop front on APPJ-treated C/C

After the wettability tests, the samples were cross-cut to inspect the TiCuNi-composite interface. The comparison between the cross-section of the untreated (Fig. 5-20) and APPJ-treated (Fig. 5-21) after is provided. Some large voids and porosities were present in the composite because of the manufacturing process and they were completely filled by the braze. New infiltration channels were observed for the plasma treated samples suggesting that the new texture may be beneficial for promoting alloy infiltration and therefore interlocking mechanism.

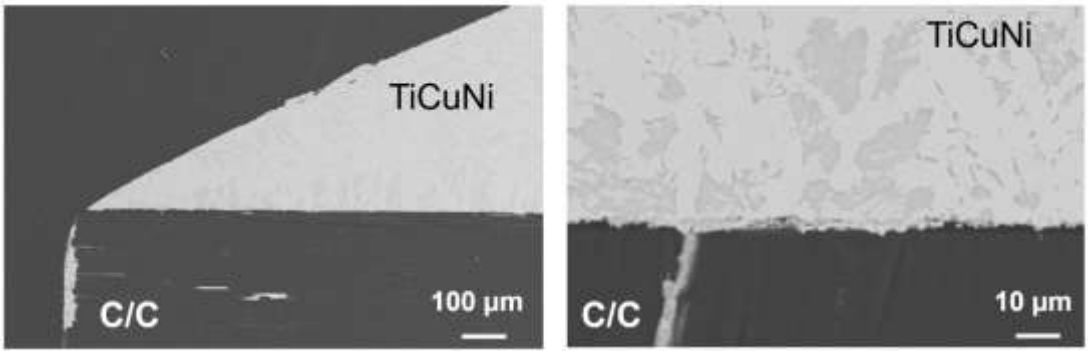

Figure 5-20: cross-section of untreated C/C after TiCuNi wetting test.

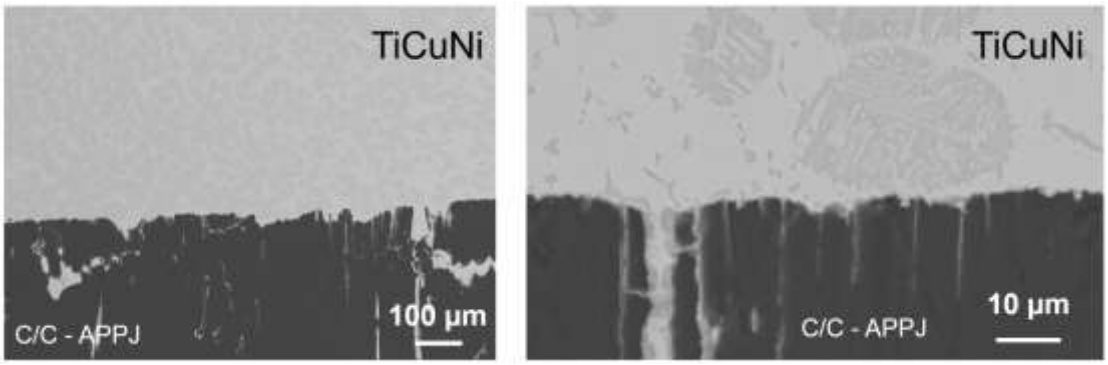

Figure 5-21: cross-section of untreated C/C after TiCuNi wetting test.

Cross-sections of joined samples for both untreated (Fig. 5-22) and APPJ treated C/C are shown in Fig. 5-23. The thickness of TiCuNi, given by overlapping the three foils, was 150 µm. The joint thickness calculated by analyzing the cross-sections of the joined samples is far thinner, around 10 µm. The thickness was approximately the same for both APPJ treated and untreated samples, suggesting a similar degree of infiltration in the voids of the composite and a similar depletion of the joining material from the joint area. It is interesting to observe that the joint interface of the untreated C/C was rather flat, while the APPJ treated C/C presented an evident brush-like structure that enhance the interlocking with the braze. The reactive layer in both cases was formed at the interface with the composite. In the case of the APPJ treated samples, the reactive layer had a saw-tooth appearance given by the underlying plasma-induced texture.

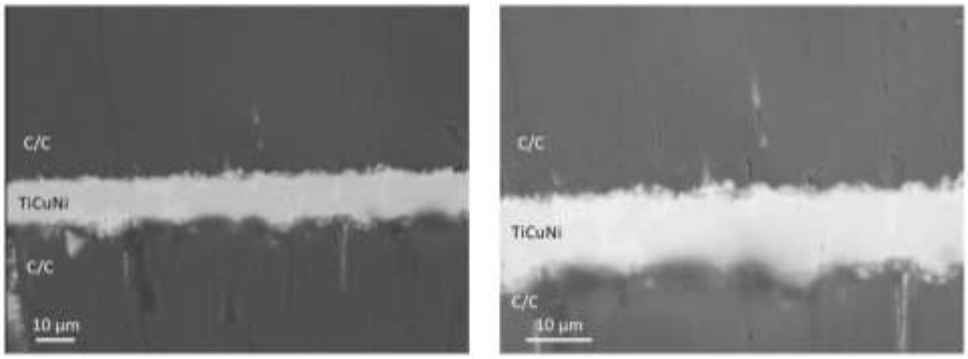

Figure 5-22: cross-section of TiCuNi joined C/C

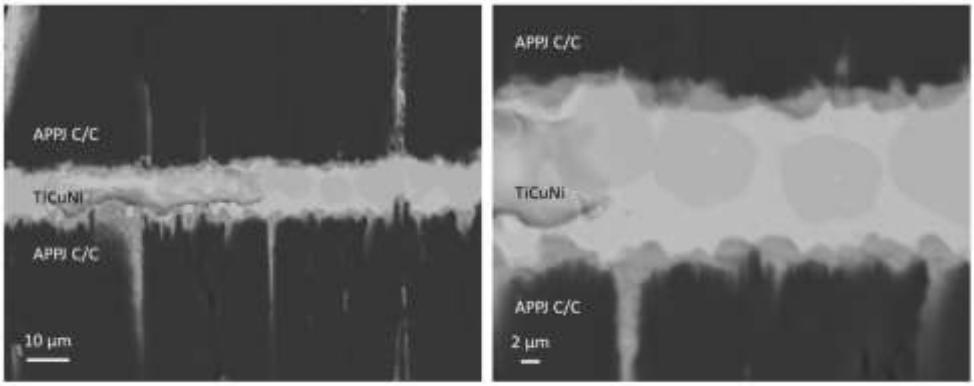

Figure 5-23: cross-section of TiCuNi joined APPJ C/C

The quality of the joint, according to the SEM characterization of the cross-section, looked good for both materials and the interlocking effect expected as a

consequence of the APPJ surface texturing was confirmed. However, the remarkable infiltration of the alloy in the composite was identified as a potential weakness. The residual thickness of the joining material of approximately 10 μm was quite low compared with those reported in similar works[148,149]. After joining C/C samples with 3 TiCuNi foils, Salvo et al.[148] reported a joint thickness between 90 and 100 μm and a joint strength, after SLO shear stress test, of 17 ± 3 MPa. A higher joint strength was reported by Salvo et al. for the use of a single foil of TiCuNi that provided a final thickness of 30-35 μm with a resulting joint strength of 24 ± 2 MPa. The infiltration of the braze in the composite used in that work was far lower than that observed in this work, probably because of the use of different types of C/C.

The mechanical performances of the joints were evaluated via SLO shear stress strength test. Overall recorded values were much lower than those presented in [148] for both untreated and treated samples. Untreated samples provided an average joint strength of 2.3 ± 0.8 MPa . Similarly, treated samples provided a value of 2.0 ± 0.3 MPa. Both treated and untreated samples showed a cohesive failure since the joining material can be find on each failure surface after the test, even if more material can be found on the surface of the APPJ samples (Fig. 5-24, Fig 5-25), probably because of a higher retention given by the texture. Usually, a cohesive failure suggests that the adhesion with the substrate is optimal and therefore that high mechanical performances can be expected. In this case, the low performances and the similar behavior between the two types of sample may be due to the insufficient quantity of brazing alloy in the joint. The strong infiltration may eventually result in voids at the interface that act as weak points. Three foils of TiCuNi reasonably were not enough for joining these composites along the ZY face. Increasing the number of foils, guaranteeing a larger reservoir of joining material, can be effective, but it is not practical. Alternatively, the alloy can be deposited in the form of a paste or thicker foils. However, extending the study to other C/C architectures and to other brazing systems may provide additional insights.

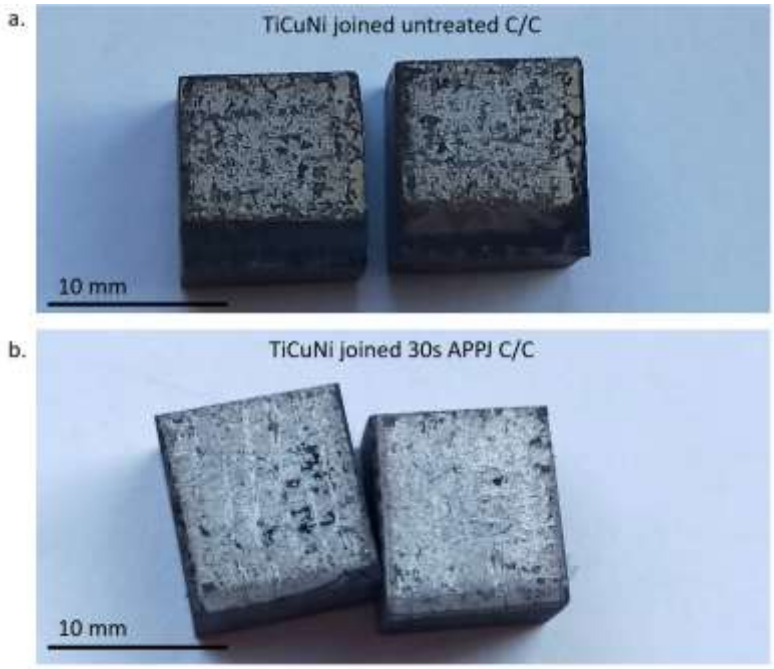

Figure 5-24: fracture surfaces of joined C/C samples: untreated (a) and APPJ-treated (b)

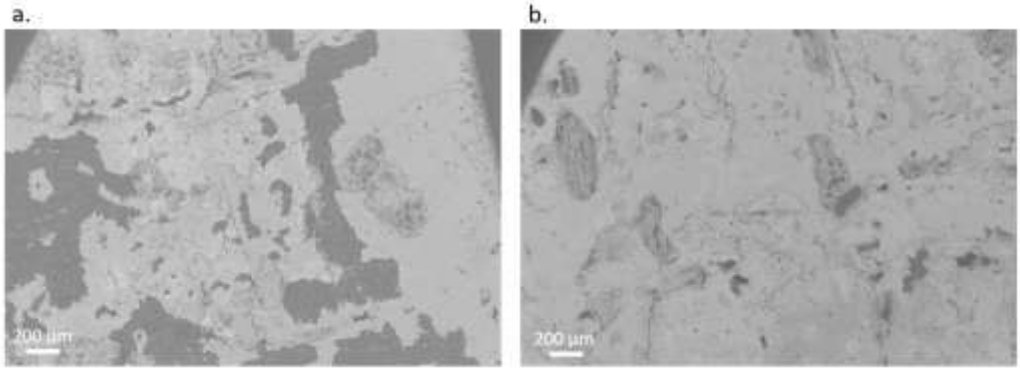

Figure 5-25: ***SEM micrographs of the fracture surfaces of joined C/C: untreated (a) and APPJ-treated (b)***

Evaluations on the effectiveness of the APPJ plasma treatment on dissimilar joints were investigated carrying out SLO mechanical test on TiCuNi joined C/C-copper. Results were different compared with those reported for C/C-C/C.. In the case of C/C-C/C joined, the joint was depleted of the braze because of the presence of cavities to fill on both parts and capillarity effects promoted by the vacuum degree imposed for the process. The copper plate, instead, is massive and no infiltration of braze occurred, so the depletion was confined on C/C side. Furthermore, copper formed a eutectic with titanium [153] and therefore at the interface additional material is supplied by the local melting. The interface between

copper and TiCuNi cannot be distinguished after the joining process as can be seen in Fig. 5-26.

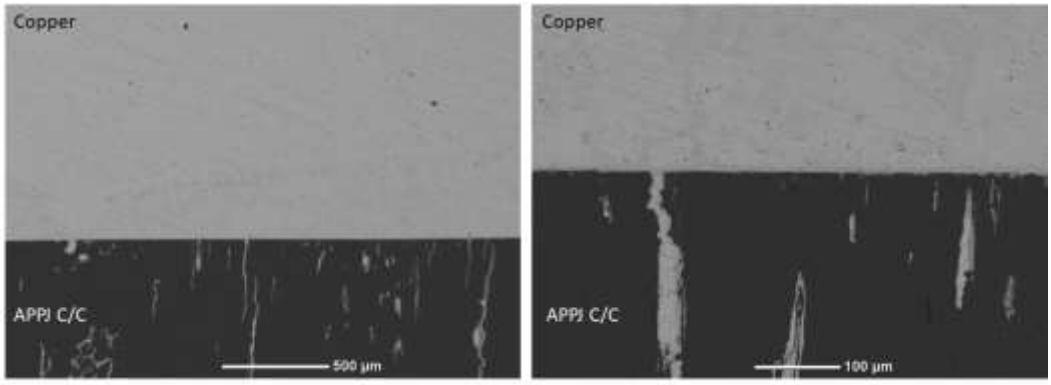

Figure 5-26: cross-section of TiCuNi joined APPJ C/C-copper at different magnifications.

Mechanical tests showed an increase of the joint strength after the treatment. Joined C/C-copper samples failed at τ=9.5 ± 5.6 MPa, while APPJ C/C-copper at τ=22.8 ± 6.9 MPa, 140% higher than the value observed with the untreated composite. The standard deviation is relatively high and it may be due to the differences in the distribution of fibers at the surface from one sample to another.

For both samples, delamination occurred, even if for untreated C/C-copper the detached layer looked discontinuous. The higher mechanical strength recorded for APPJ C/C-copper may be due to a higher contribution of the interlocking given by the joining process.

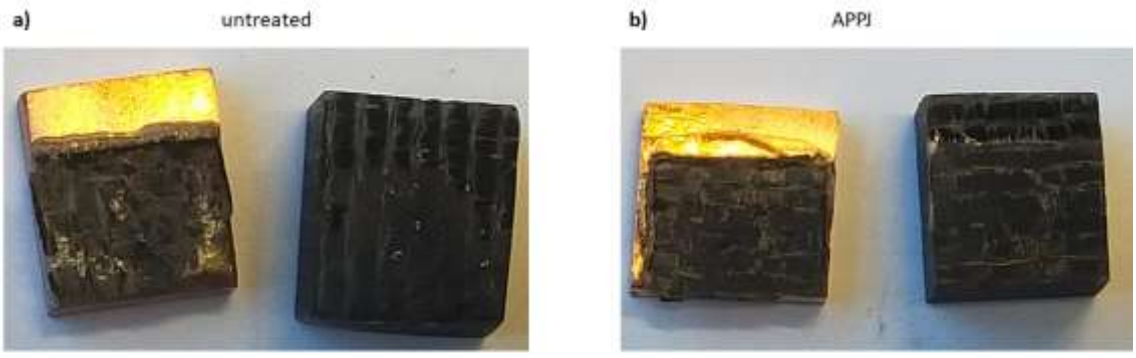

Figure 5-27: fracture surfaces of untreated C/C-copper (a) and APPJ C/C-copper (b) joints

The results collected for C/C-copper were encouraging and it is reasonable to suppose that if the problem of depletion of the joining materials is solved, the brush-

like texture can result in higher mechanical performances also for C/C-C/C joints. To this aim, a braze that can provide higher wettability and higher viscosity can be proposed.

Modeling of C/C – an opportunity to get better insights on the plasma etching process

Multiscale modeling has the potential to accelerate the development of new materials, the design of new processes and the interactions of the material at multiple scales of time and space. When coupled with experimental activity such methods can reduce costs and accelerate the acquisition of information and its quality[154].

The work presented in this chapter on the plasma etching of C/C was based exclusively on experimental observations. A trend was identified, but in order to get a better understanding of the plasma-material interactions and the difference in the etching resistance of each constituent, coupling these results with modeling can provide additional insights. In particular, modeling strategies have been developed to address the surface roughness evolution of composites when they undergo ablation.

Previously, the use of C/C as TPS was described. TPS protects the vehicle by its progressive ablation and a critical understanding of its behavior is critical for a safe re-entry. Therefore, modeling studies have been carried out to evaluate TPS ablative mechanisms during re-entry phase, in terms of pure thermal ablation and oxidation.

During the ablation, the surface of the composite progressively recedes as a result of chemical/physical actions. The original superficial layer is removed and the surface evolves influenced by the different contribution of each constituents (fibers, matrix and interphase). Roughness affects the ablation process and predicting its evolution is necessary for assessing the viability of the TPS[155].

Laboratoire des Composites Thermo Structuraux (LCTS), based in Bordeaux, has an expertise on ablation modeling of C/C and on the evaluation of surface roughness evolution[136]. They have published several works on modeling of surface recession[156–159]. These works were focused on ablation of C/C and

results from models were checked with experimental results. C/C for TPS cannot be tested in real in-service conditions, but similar environments can be reproduced at laboratory scale.

Experimental equipment used are plasma arc jets, oxyacetylene torches, and lasers. High-speed gas is fluxed onto the surface, temperature is in the range of 3000-4000 °C and an oxidizing atmosphere is employed[136].

Ablation-induced roughness evolution can be studied at different length scales on composites: micro-scale (single fiber and matrix/fiber region), meso-scale (bundle of fibers) and macro-scale (composite architecture). This distinction is schematized in Fig. 5-28.

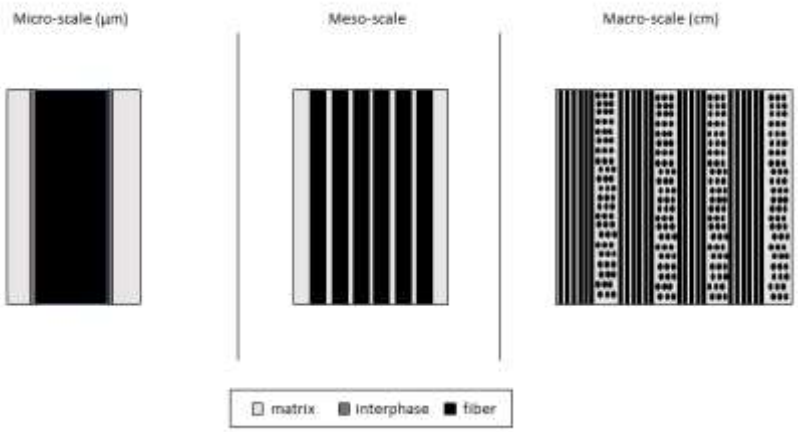

Figure 5-28:length scales of interest for modeling composite behavior under ablation.

Thus, LCTS studies focused on high-temperature ablation, while the work carried out using an APPJ dealt with rather different conditions. However, the ablation takes place during APPJ treatment as indicated by the mass loss. Therefore, a modeling tool developed by LCTS can be also applied for the plasma-based texturing.

The image-based modeling software (startup screen in Fig. 5-2) is versatile and it can simulate ablation carried out in different conditions. The theoretical model used for the surface regression is shortly presented in [160]. The ablation is simulated considering these four hypotheses:

- Diffusion of the etching species is steady-state.
- Surface recession occurs with a constant velocity.
- The flux of reactive species is approximated as vertical.

- Fixed height for the boundary layer.

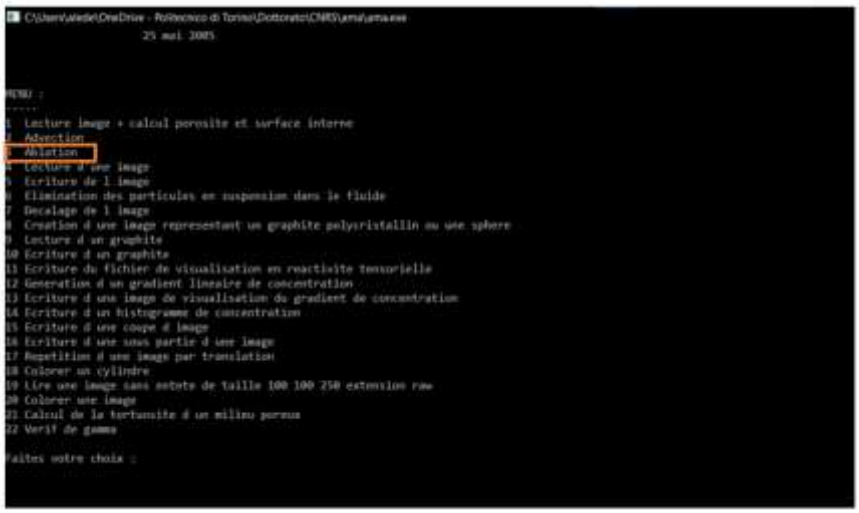

Figure 5-29: startup screen of ama.exe

Starting from these hypotheses, the surface recession depends on three parameters (dimensionless in the software)[160] reported in the table 5-3:

Table 5-3: parameters for the modeling the surface recession

Geometrical parameter	Sherwood number	Reactivity contrast
$r = \frac{r_f}{L}$	$Sh_f = \frac{k_f r_f}{D}$	$k = \frac{k_m}{k_f}$

r_f refers to fiber radius, L to the length of the edge of the unit cell. k_m and k_f are the reaction rate constants for the matrix and fibers.

The workflow of ama.exe is reported in Fig. 5-30. Parameters are inserted when the software is run and a 3D image (stack) of the surface, previously generated, is fed to the algorithm. The image is then discretized and random walkers [161] are generated. Random walkers were generated by the software and they randomly move in the void spaces until they meet the surface. When the single random walker hits the surface, if it sticks (depending on the probability), it dies and the superficial voxel involved in the interaction experiences a reduction in its greyscale value. If the voxel reaches a value of zero it is removed and the surface is updated consistently. The software then checks if one of the layers of the stack is removed.

In case, the ablation rate is calculated and an image is taken. This cycle runs iteratively until a steady state is reached.

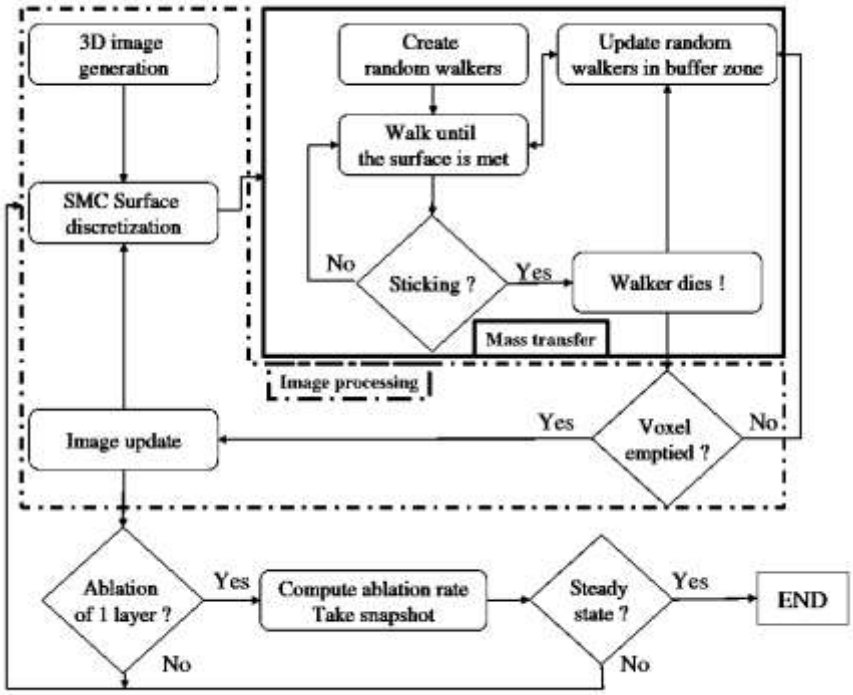

Figure 5-30: Workflow of the simulation carried out using ama.exe software, developed by Vignoles' team at LCTS Bordeaux (adapted from [136]***).***

The input 3D image is generated from SEM microscopy top view 2D image of the pristine surface via FIJI, an ImageJ variant[162]. The original image is simplified, through the application of masks, to assign to each constituent of the composite a different greyscale value (from 0 to 255) that identifies its resistance against the action of the etchant species. An example is shown in Fig. 5-31. The higher the grey-scale value, the higher the number of random walkers that have to stick onto the voxel. Since experimental observation for APPJ-treated C/C showed that the matrix is slightly more resistant, a higher grey-scale value was assigned.

The single image is then transformed into a stack of images by overlapping. Pixels, therefore, become voxels. The image has to be as simple as possible in order to make the calculation faster. It is not important to obtain a perfect replica of the original surface, but to replicate its basic elements to study their evolution according to the proposed model and then check it with the experimental data for checking the validity of the hypothesis.

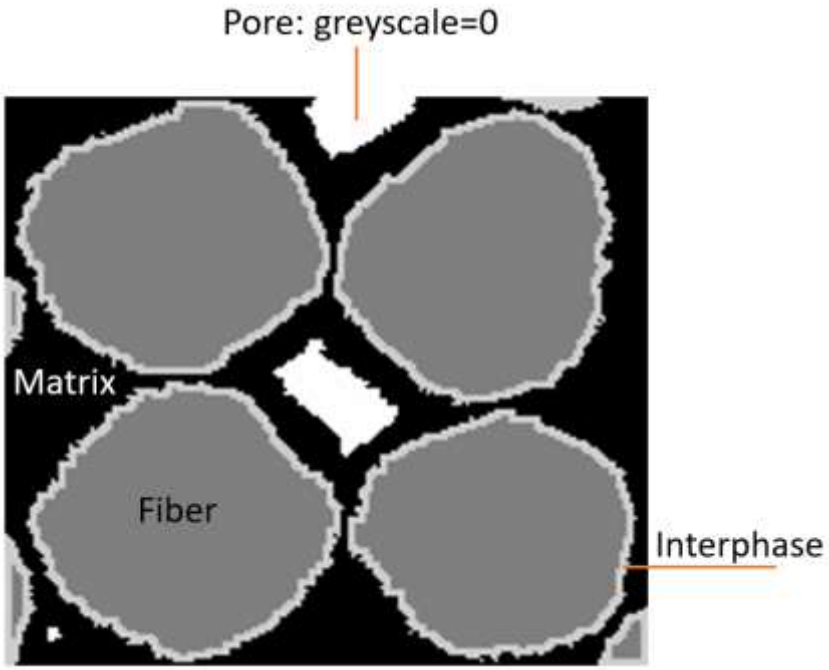

Figure 5-31: examples of a simplified 2D image of the surface with different greyscale values for each constituent.

Once the 3D image is built, the software can load it and simulations can be run.

Some first attempts to model the evolution of the surface of C/C under APPJ were done to evaluate the opportunity to extend this solution from the high-temperature ablation domain to low-temperature. Fig. 5-32 shows one of these first investigations.

Keeping the same parameters used for previous studies on ablation for TPS and changing the grey-scale value, surfaces similar to real ones were obtained in a qualitative way

It can be expected that the application of the model can be successful in describing the surface recession of the C/C under APPJ. However, a detailed study has to be carried out and this is a promising future activity. Input parameters have to be optimized in accordance with the experimental observation iteratively, collecting many data.

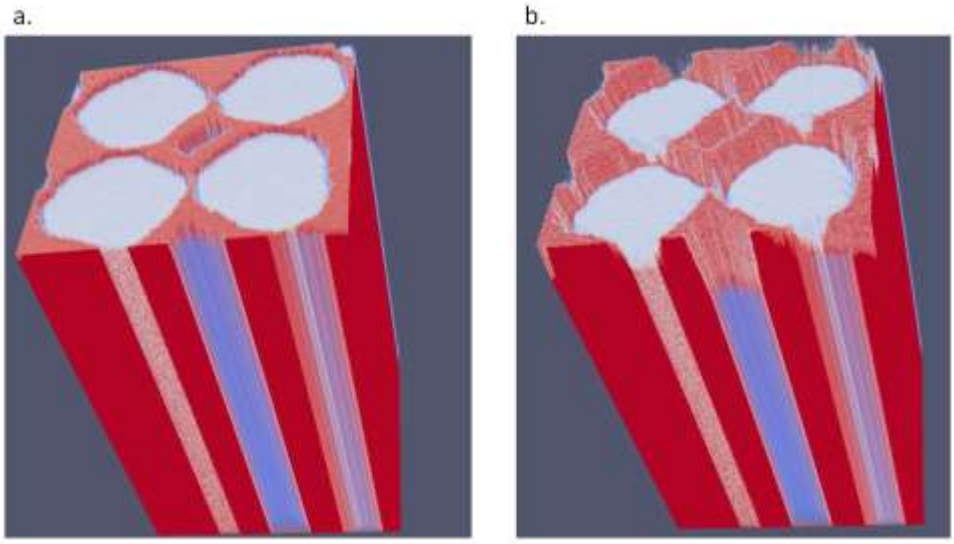

Figure 5-32: surface at t=0 (a) and after several iterations (b).

Conclusions

APPJ proved to be a viable treatment for the surface texturing of C/C. The small differences between the matrix and fiber resulted in different etch rates when exposed to the etching species of the plasma plume.

A brush-like texture was successfully manufactured on the surface of the C/C after 30 s. Longer treatment lengths result in a high mass removal (an undesired effect). Furthermore, the shorter the treatment, the higher may be the interest in its transfer to industrial applications.

The texture did not affect the evolution of the contact angle, but more anchoring points available for interlocking were formed on the surface and the surface area dramatically increased.

Those results suggested that the new texture may be able to improve the joint strength of TiCuNi joined C/C-C/C samples, but when mechanically tested both treated and untreated samples performed poorly. The analysis of the failure surfaces suggested cohesive failure mode, but recorded values were too low. The intense infiltration of TiCuNi in the existing cavities of C/C depleted the joint of the braze, resulting in a thickness of about 10 μm, probably too thin for guaranteeing reliable joining performances.

6. APPJ as surface modifier for C/SiC

As described in Chapter 5, carbon fiber-reinforced materials are among the most performing material for structural applications because of their exceptional specific modulus and specific resistance. C/C materials, however, suffer from fast and detrimental oxidation when the temperature exceeds 400°C in presence of oxygen. In order to overcome this limitation of C/C composites, carbon fiber-reinforced silicon carbide (C/SiC) materials were developed. High-performing carbon fibers are embedded in a SiC matrix and an external CVD SiC dense coating is deposited to protect from oxidation.

The higher oxidation resistance of SiC makes these composites able to cope oxidizing atmosphere, extending the range of applications. Joining this material is not trivial and several methods have been proposed according to the service conditions for the final component[163]. Among the viable solutions, many rely on the use of indirect joining techniques, as described in Chapter 1. Since C/SiC materials, like other CMCs, are often integrated with metals, brazing alloys are common solutions for joining[164], improving the retention of the alloy and promoting the formation of anchoring points at the surface is a key point for providing sound and reliable joints.

The APPJ treatment presented in Chapter 5 was effective in inducing a brush-like surface texture on C/C. Similarly, the same treatment was proposed for the surface modification of C/SiC composites. The presence of two different constituents, the carbon fibers, and the SiC matrix, with very different oxidation resistance[165], suggested the opportunity of using the same technique with a different outcome.

The work presented in this chapter aimed to demonstrate the validity of these two hypotheses:

1. The difference in oxidation resistance between the carbon reinforcing phase and the silicon carbide matrix can lead to the formation of a reverse brush-like structure.

2. The reverse brush-like structure is beneficial for enhancing the joint strength of brazed C/SiC.

Materials and methods

2D Keraman C/SiC (MT Aerospace, Germany) were used as materials to be joined. 100 mm x 100 mm plates with a thickness of 4 mm were cut into smaller samples with a size of 10 mm x 10 mm. Thickness was unchanged.

Since the objective was to produce a brush-like structure, the lateral surface – the thickness – of the samples was chosen for the treatment in order to have fibers perpendicular to the plasma jet. This surface was then polished using SiC grinding papers up to 2400 grit to obtain flat surfaces.

Fig. 6-1 and Fig. 6-2 shows the top-view and the as-cut lateral surface for Keraman C/SiC respectively.

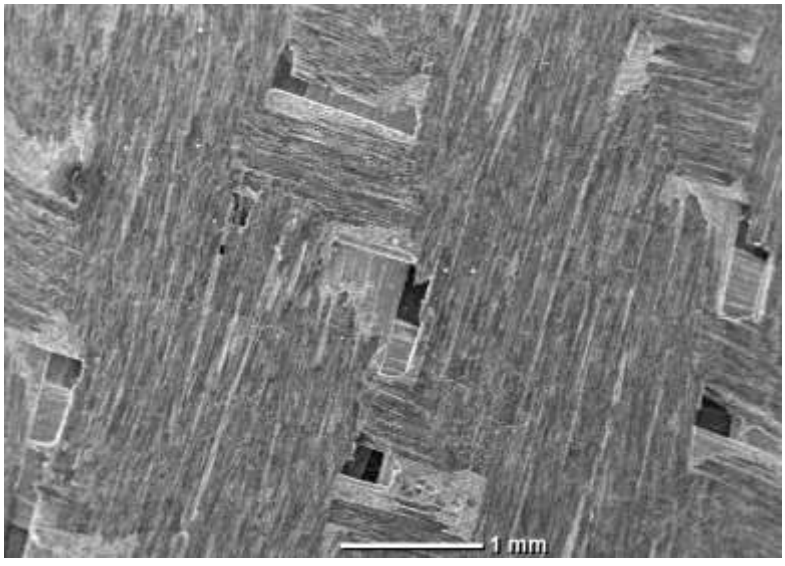

Figure 6-1: top-view of uncoated Keraman C/SiC.

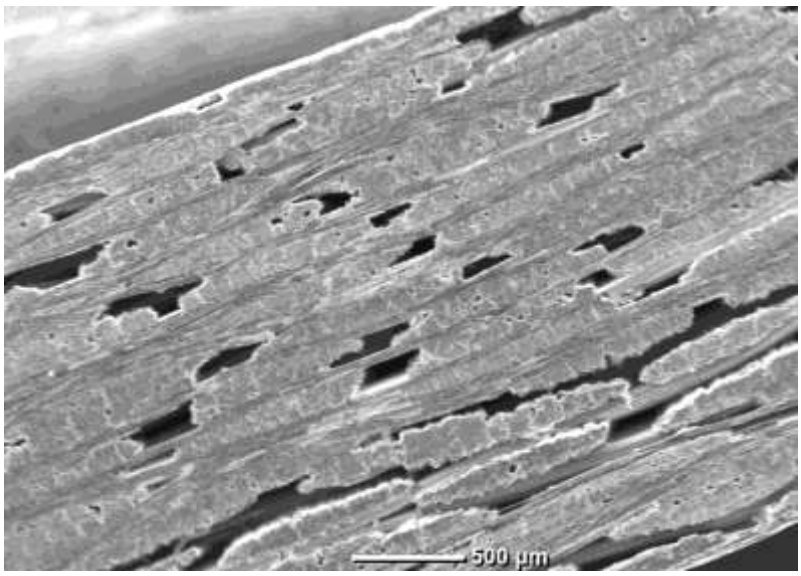

Figure 6-2: lateral surface of the as-cut Keraman C/SiC

The plasma equipment used for the activity is the PlasmaTec-X (Tantec, Denmark), the same utilized the activity on C/C. For further details, revise the information presented in Chapter 5. The lateral surface was treated by working with the following conditions: surface-nozzle distance of approximately 5 mm, air flux of 1500 l/h and variable time length. Again, the effect of various exposure time lengths was investigated in order to identify the most promising. Therefore, treatments of 1 min, 5 min, 10 min and 20 min were carried out.

Temperature was monitored during the plasma treatment via a thermal image camera E6 (FLIR, USA).

Samples were weighted before and after the treatment and the mass loss was averaged to get information on material removal. Then, SEM inspections of the surface were carried out to evaluate changes on the surface. Surface layers were then removed by cutting (depth of approximately 400 µm) to observe the integrity of the underlying material after the treatment.

According to the results of the preliminary characterization the treatment conditions for the second part of the activity were identified: 30 s, 1500 l/h, 5 mm distance. Untreated surfaces and APPJ treated surfaces, modified using the chosen plasma settings, were characterized via confocal microscope (Sensofar S-neox, Spain) to observe the changes in texture. Then the wettability of the braze used for this study was evaluated on the surface of treated and untreated samples. A metallic sphere having the same composition of the joining material was generated by arc melting and then placed on the surface. The samples were then inserted in a vacuum

furnace and the evolution of the contact area was done at the temperature selected for the joining treatment: 950°C.

The braze used for joining is the BrazeTec CB4 (Saxonia, Germany) and its nominal composition is: 70.5 wt% Ag; 26.5 wt% Cu; 3 wt% Ti[166]. Like other active brazing systems, this alloy has been already used for joining non-oxide ceramics [105,167,168]. CB4 was supplied as foils with a thickness of approximately 100 μm.

Samples were joined in SLO configuration for testing the joint strength. C/SiC-CB4-C/SiC sandwiches were manufactured according to the geometry described in [115]. One single foil was used as joining material. The joining process was performed at 950 °C for 10 min (heating rate 10°C/min). At least 3 samples for each type, untreated and APPJ-treated, were tested using a universal testing machine (Sintec D10). The test was conducted using a 50kN load cell and a crosshead speed of 1 mm/min. The fracture surfaces were then inspected and compared.

Results and Discussion

The mass loss recorded for C/SiC after APPJ was less intense compared with the one reported for C/C in the previous chapter. While for C/C both constituents, fibers and matrix, were sensitive to oxidation, in this case the matrix has a higher resistance compared with carbon fibers. Therefore, the recession reasonably affected only the carbon fiber and was negligible for SiC, on contrary of C/C.

The graph reports in Fig. 6-3 shows the weight loss recorded for the APPJ treated C/SiC.

After 1 minute of APPJ the C/SiC lost 0.42% of their mass, then, after 5 minutes, the value reached the 0.55% and, after 10 minutes, 0.82%. The mass loss vs time is linear, as observed for C/C, but, for C/SiC, the removal rate was far lower.

.

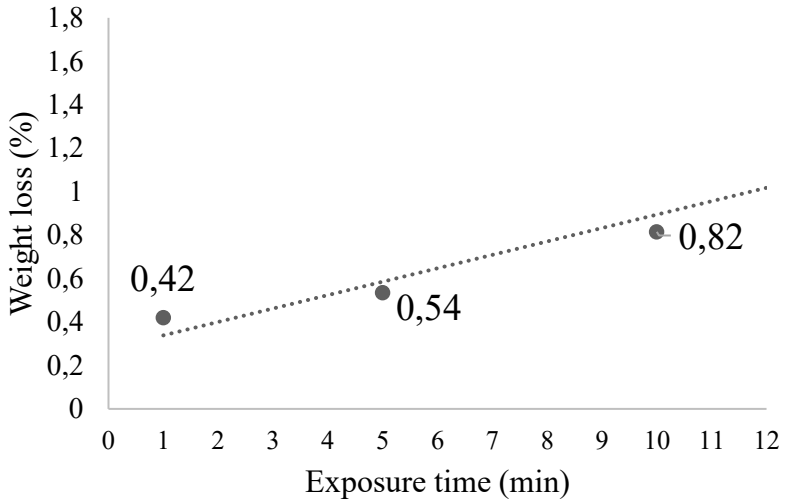

Figure 6-3: weight loss of C/SiC under APPJ as function of the exposure time.

Assumptions made for weight loss data were supported by micrographs collected via SEM The carbon fibers were preferentially eroded, leaving holes surrounded by the SiC matrix. Therefore, channels were produced in correspondence to the carbon fibers, while the matrix seemed to be very little affected by the plasma-induced oxidation. This effect is evident for all the time length: 1 min, 5 min and 10 min (Figs. 6-4, 6-5).

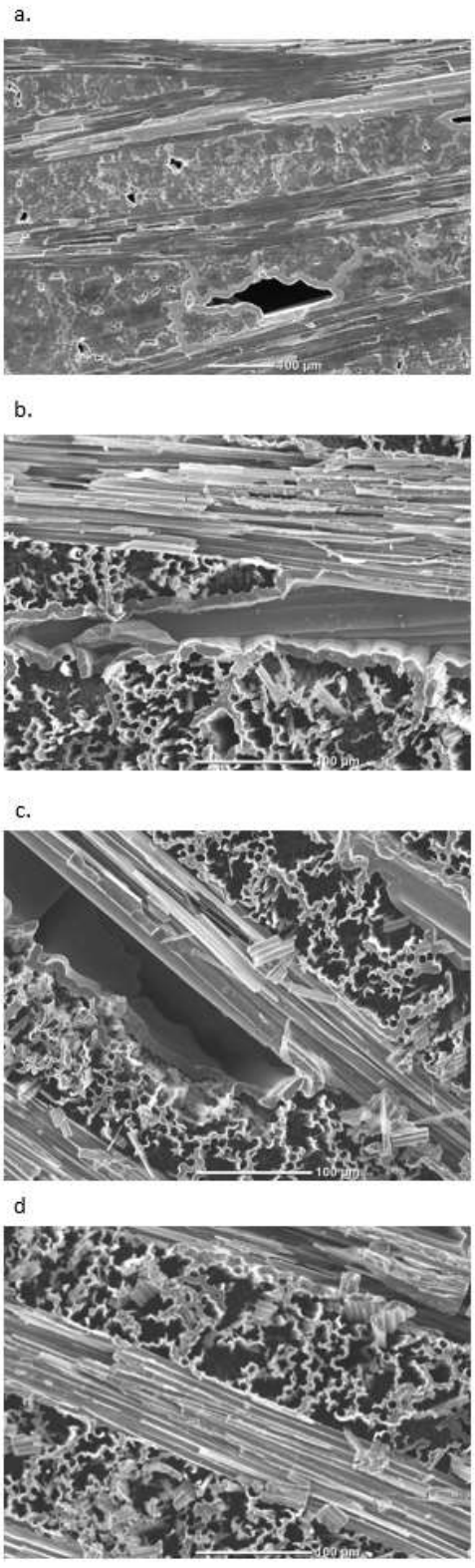

Figure 6-4: Comparison of the top views of untreated polished C/SiC (a) and after APPJ: 1 min (b), 5 min (c) and 10 min (d).

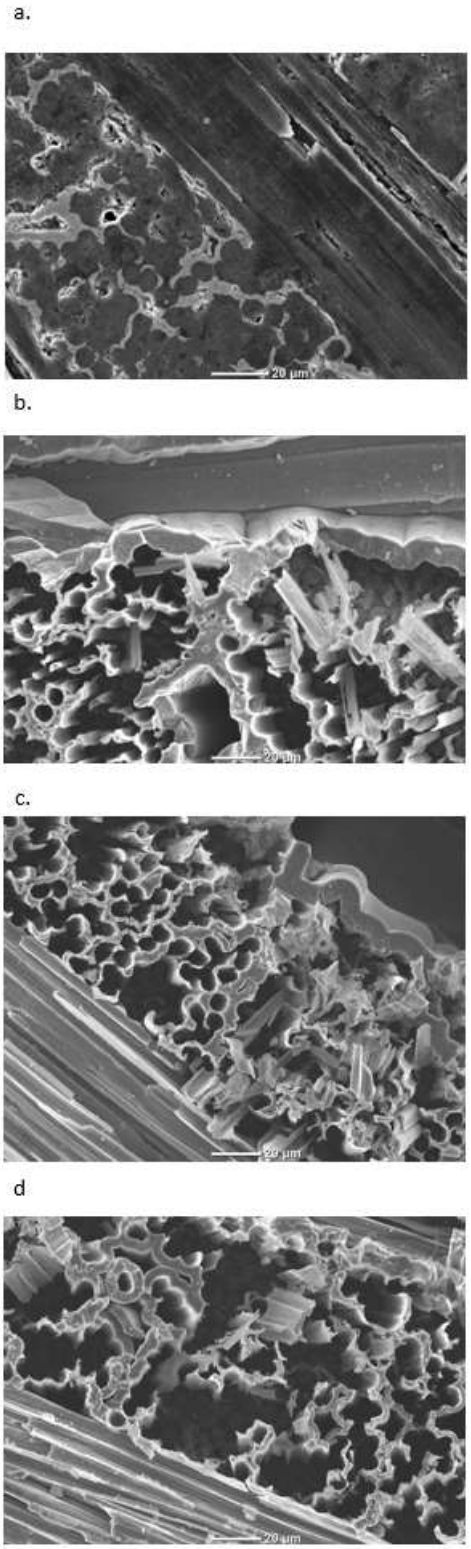

Figure 6-5: Comparison of the top views of untreated C/SiC (a) and after APPJ: 1 min (b), 5 min (c) and 10 min (d), at higher magnification.

The erosion of the fibers was already remarkable after 1 minute of treatment. The matrix seemed not to recess, in accordance with its higher oxidation resistance. From the top view images it was still possible to see carbon fibers at the bottom of

the APPJ-drilled channels. Some pieces of matrix collapsed because of the loss of contact with the carbon fibers, but, globally, the matrix did not look affected by the APPJ treatment. Similar structures were formed for longer APPJ treatment lengths.

The dry etching of the fibers can be explained by the high oxidation action provided by the air-fed APPJ, as reported in Chapter 5. As for C/C, the overall temperature during the treatment was lower than 300°C (Fig.6-6). The APPJ-generated plasma environment is rich in strongly oxidizing ion species [169] derived from ionization of the fed pressurized air and the air and humidity present in the environment where the treatment is carried out. Contrary to what was observed for the corona treatment on SiC, described in Chapter 2, the formation of a silica layer was not originated from the matrix [76].

Figure 6-6: Thermal image of APPJ treatment on C/SiC (after 10 min of treatment).

The removal of carbon fibers from the surface was significant, raising some concerns about the integrity of fibers inside the composite. However, no damages were noticed on fibers after the cut of a slice of approximately 400 µm. The composite appearance can be compared to the as-received composites: fibers were unaffected by the treatment inside the composite and the matrix-fiber interface looked well preserved. In Fig. 6-7 is shown one of these cut surfaces for a 5 min APPJ-treated C/SiC.

It can be concluded that only the surface was affected by the APPJ treatment. The presence of the APPJ-induced channels can constitute preferential paths for

oxidation paths for carbon fibers as commonly reported[170], however in this case the temperature was lower than 400°C and the availability of reactive oxygen species decrease while the distance with the nozzle increase[171], hindering the progressive removal of fibers while they recede from the surface.

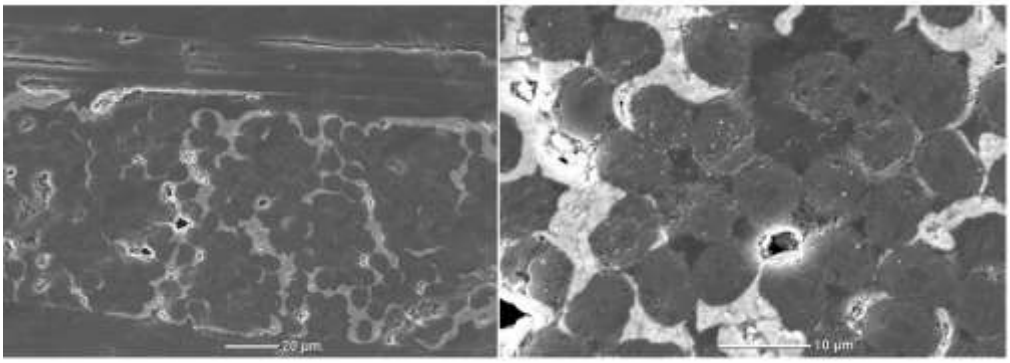

Figure 6-7: Underling surface (400 µm below) of a 5 min APPJ-treated C/SiC.

The strong oxidation of the carbon fibers, observed even for 1 min of APPJ treatment, suggested that the treatment would be effective even further reducing the plasma exposure length. Therefore, for investigating the effectiveness of the treatment to improve the joining process, the time was reduced to 30 s, keeping all the other parameters constant.

As aspected, the oxidation of the 30-second APPJ treated C/SiC surface was less severe compared to that observable for longer time lengths (Fig. 6-8). Channels appeared shorter in depth and the matrix, which appeared in lighter grey, came out lightly fragmented after the channels digging. These pieces of matrix were observed despite the cleaning operation in ultrasonic bath, but their presence is not expected to be detrimental to the joining process, since they might act as a reinforcing phase within the junction.

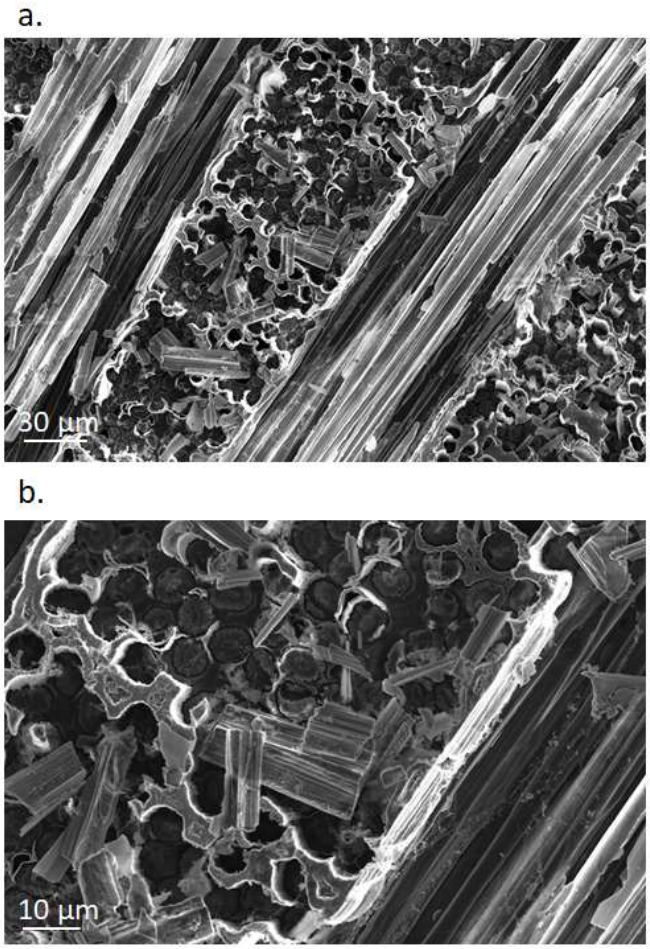

Figure 6-8: 30 s APPJ-treated surface at lower (a) and higher magnification (b).

The eroded fibers, shown in Fig. 6.9, looked slightly blunt at its center and detached at the interface with the matrix. This is coherent with what was observed for C/C after APPJ. The vertical erosion of the fibers was prevalent compared with the progressive oxidation from the external regions close to the interphase. The fiber surface was flat, not sharp. The latter morphology is commonly described in the case of thermal oxidation[172].

To provide additional information on the modification occurring at the surface, profilometer characterization was carried out.

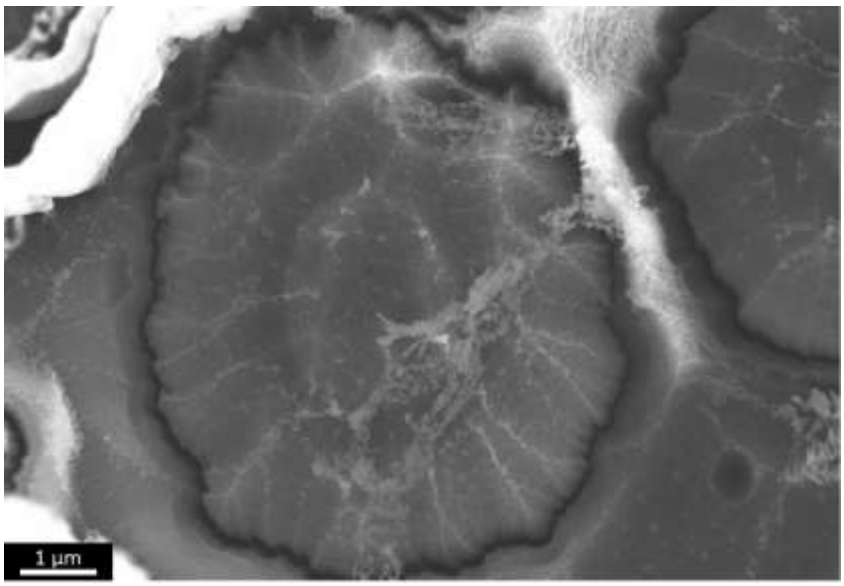

Figure 6-9: APPJ-etched carbon fiber after 30 s of APPJ treatment.

In Fig. 6-10 the roughness map of a polished untreated C/SiC sample is compared with the one of a 30 s APPJ treated C/SiC and their relative Sdr values are provided.

The polished C/SiC had a relatively high Sdr value (288%), but its surface structure looked pretty homogeneous since slight color variations are visible in the profilometer reconstruction. On the other side, the 30 s APPJ etched composite presented a more remarkable color distribution with two areas easily detectable: the yellow-green, constitute by the higher points and the blue, related to the lower points. What was observed for the 30 s APPJ etched C/SiC is coherent with the electron microscopy analysis; the oxidation-resistant SiC matrix can be associated to the areas having the highest altitudes and the etched channels to the lowest. The APPJ induced structure provided a striking rise in the Sdr value, which was more than doubled (780%), pointing out a remarkable increase of the exposed area.

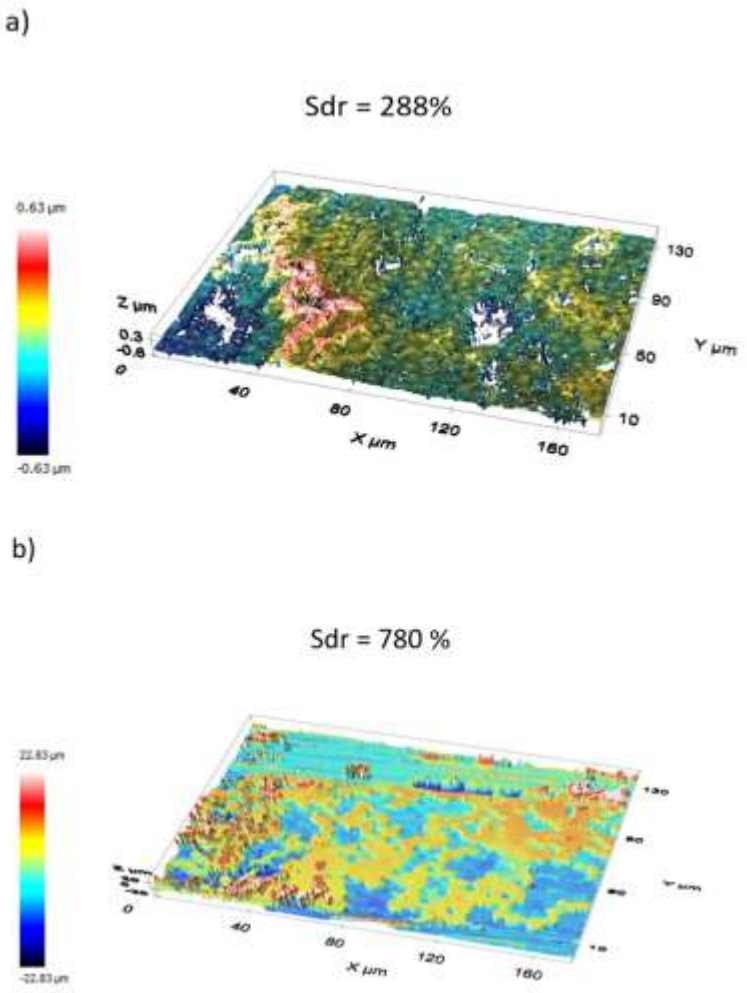

Figure 6-10: Height maps and relative value of Sdr for a polished C/SiC (a) and a 30-s APPJ etched C/SiC (b).

The presence of two separate regions with at different elevation is even more evident by observing the height distribution graph shown in Fig. 6-11. On the contrary to observations carried out on the polished sample, characterized by a single-peak Gaussian shaped curve (Fig. 6-11.a), the APPJ etched samples provided a completely different distribution. Two peaks can be identified (Fig 6-11.b): the lowest one referring to etched fibers and the highest to the matrix. The difference in height between the two peaks was estimated to be approximately 15 µm.

Similar values were reported for all the analyzed samples and therefore 15 µm may be considered as the average etching depth given by the treatment after 30 s.

a) C/SiC

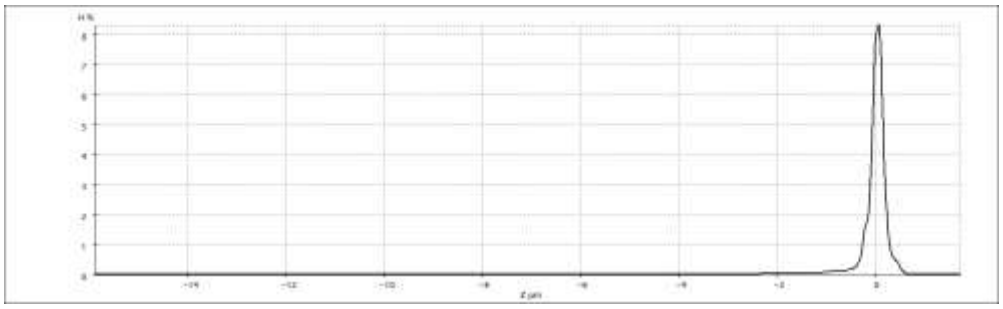

b) 30s APPJ C/SiC

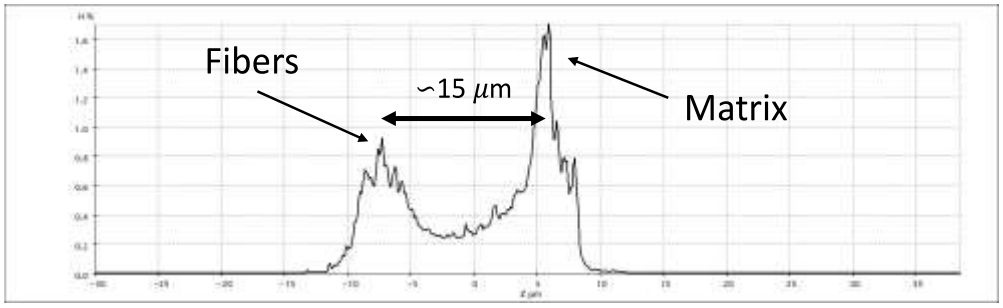

Figure 6-11: Height distribution for untreated C/SiC (a) and 30s APPJ treated C/SiC (b).

The multiple investigations carried out confirmed the same surface evolution for all the treated samples, suggesting a good degree of reproducibility of the treatment. However, it must be remembered that the distribution of pores, fibers and matrix of each specimen has an influence in the surface modification obtained withthe APPJ treatment.

A 30 s treatment was enough to introduce the brush-like texture on the surface and the desired selective removal was obtained without damaging the composite.

The wettability of the CB4 braze was then evaluated on the polished and 30 s APPJ treated C/SiC surface,. Fig. 6-12 shows the evolution of the contact angle at 950°C on untreated C/SiC (a) and 30 s APPJ-treated C/SiC (b). No remarkable differences can be noticed in wettability behaviour between treated and untreated samples. CB4 already wet well the composite and no further improvement were given by the plasma treatment.

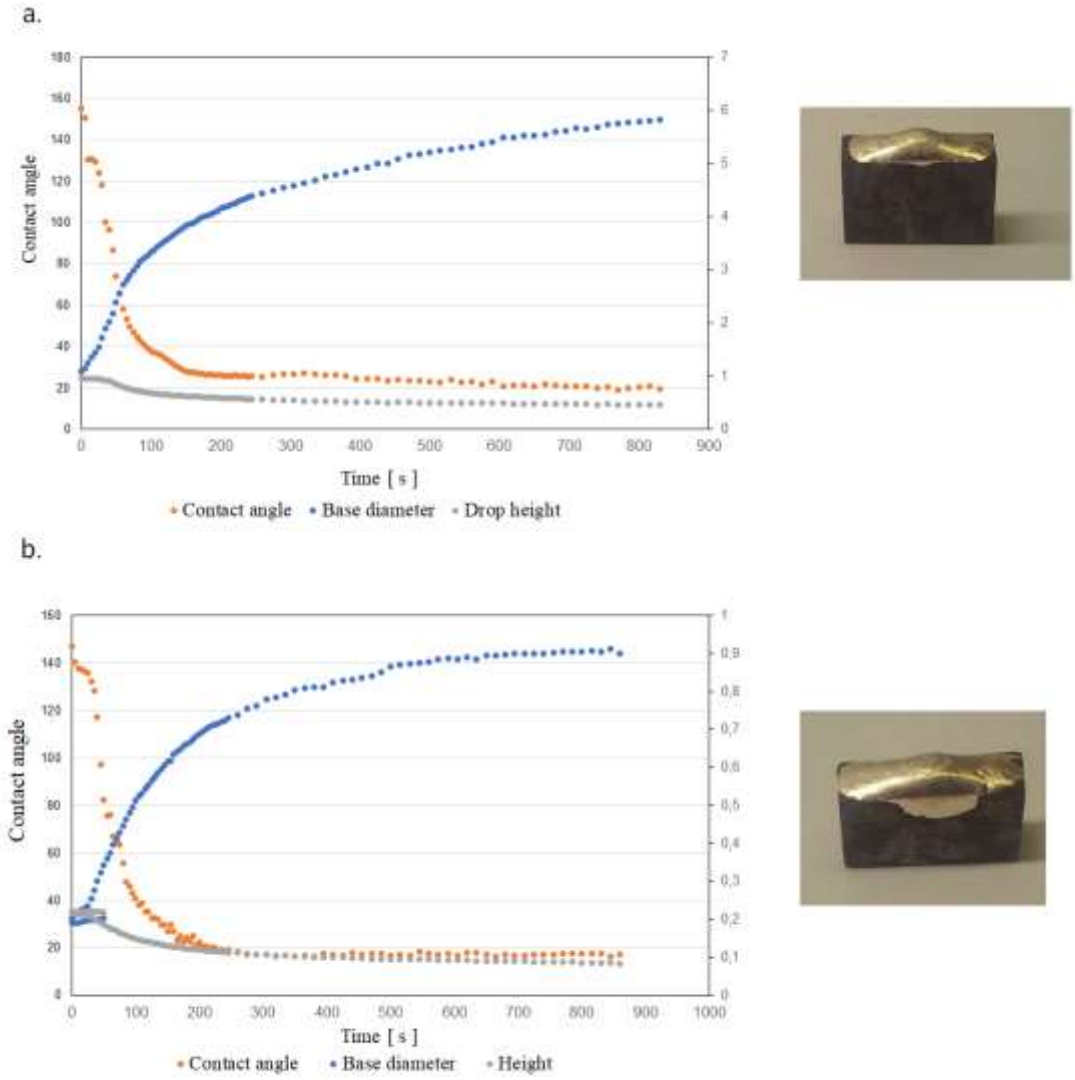

Figure 6-12: contact angle evolution of CB4 on untreated C/SiC (a) and 30 s APPJ C/SiC (b) at 950°C.

The cross-section analysis of the C/SiC samples after the wetting tests (Fig. 6-13) showed that the AgCuTi braze infiltrated available porosities left by the manufacturing process and formed a sound and continuous interface with carbon fibers and SiC matrix. The C/SiC flat surface did not provide additional anchoring points for mechanical interlocking. Instead, after 30 s of APPJ, the brush-like texture was visible and the enhanced interlocking between the braze and C/SiC.

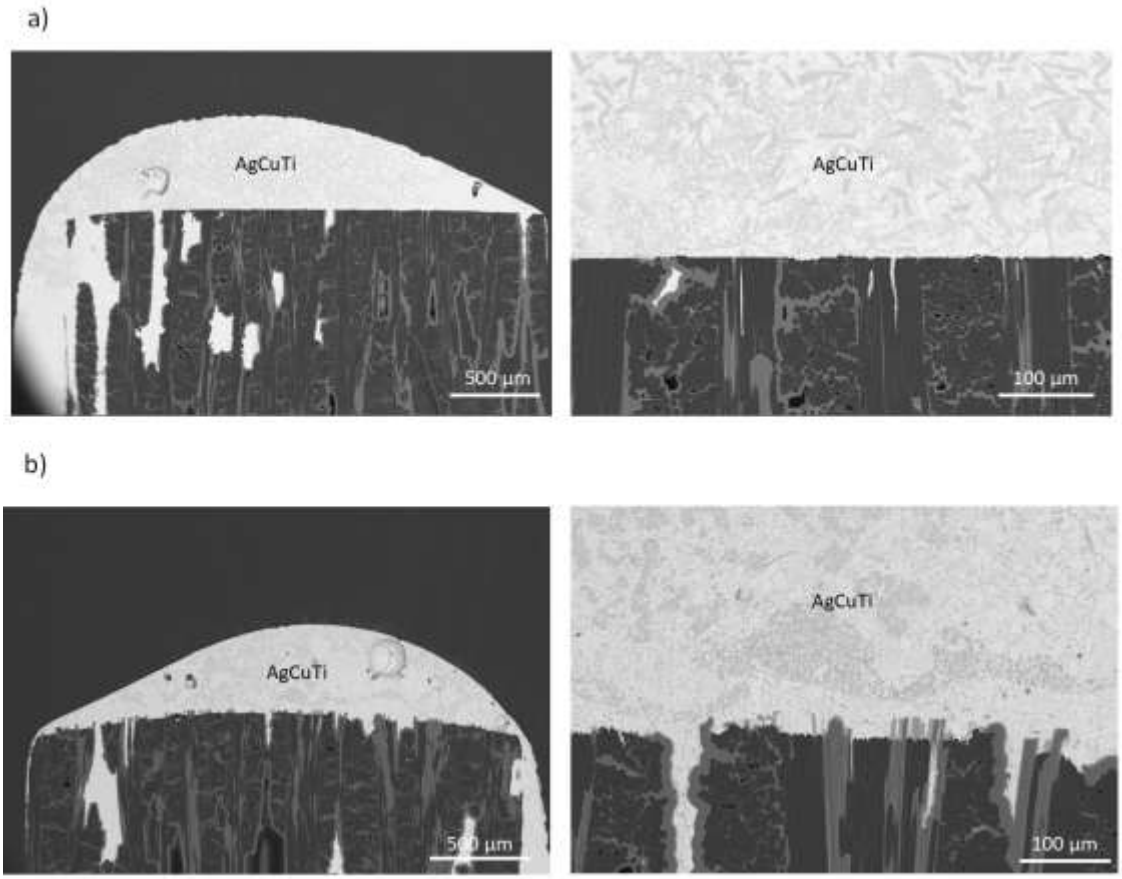

Figure 6-13: cross-section of CB4 AgCuTi wet untreated C/SiC (a) and CB4 AgCuTi wet APPJ-treated C/SiC (b).

Fig. 6-14 shows the cross-section of a CB4 joined APPJ-treated C/SiC. The interface was sound and continuous, with enhanced interlocking where fibers were etched. Existing cavities due to manufacturing process of the composites were infiltrated by the braze. Thickness of the joint was around 60 µm.

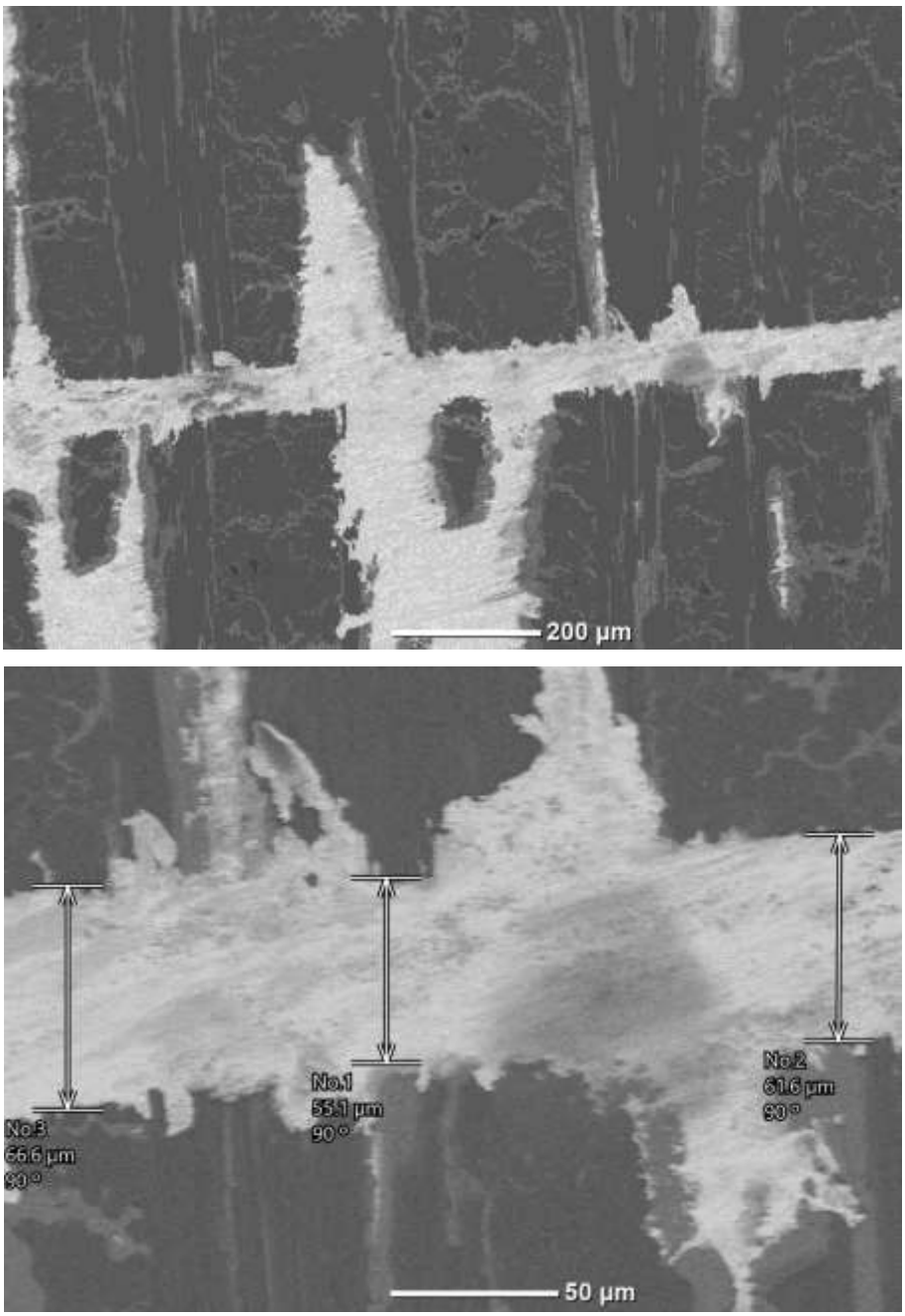

Figure 6-14: Cross-section of joined CB4 AgCuTi joined APPJ C/SiC at different magnification.

After being joined with the CB4 braze through a thermal treatment (950°C, 10 min), both types of C/SiC were mechanically tested in SLO configuration. The joined samples produced with polished C/SiC failed at $\tau = 45.5 \pm 0.6$ MPa, while the ones produced with 30 s APPJ treated C/SiC showed an apparent shear strength of 65.8 ± 2.5 MPa, corresponding to an increase of almost 45 %). In both cases

(Fig. 6-15) the joined samples failed with a mixed mode (cohesive/adhesive) and the composite delamination can be spotted in some regions.

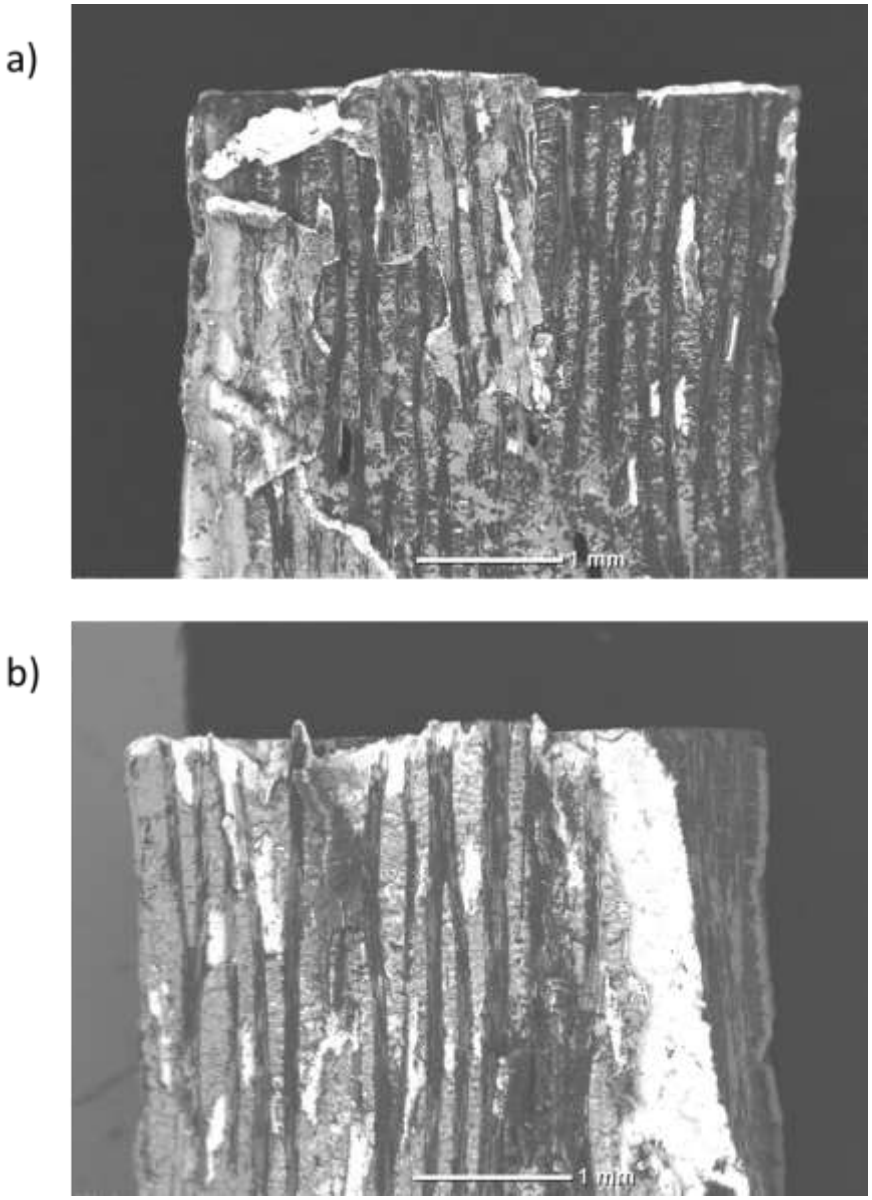

Figure 6-15: fracture surface of CB4-AgCuTi joined C/SiC (a) and CB4-AgCuTi joined APPJ C/SiC (b).

Furthermore, it was possible to observe a higher retention of the braze (brightest areas in Fig. 6-16) where fibers are perpendicular to the surface on the fracture surfaces of joined 30 s APPJ C/SiC, compared with the untreated (Fig. 6-16). The EDS analysis supported such observation. Similar findings were reported in Chapter 4 for the brush-like textured SiC/SiC.

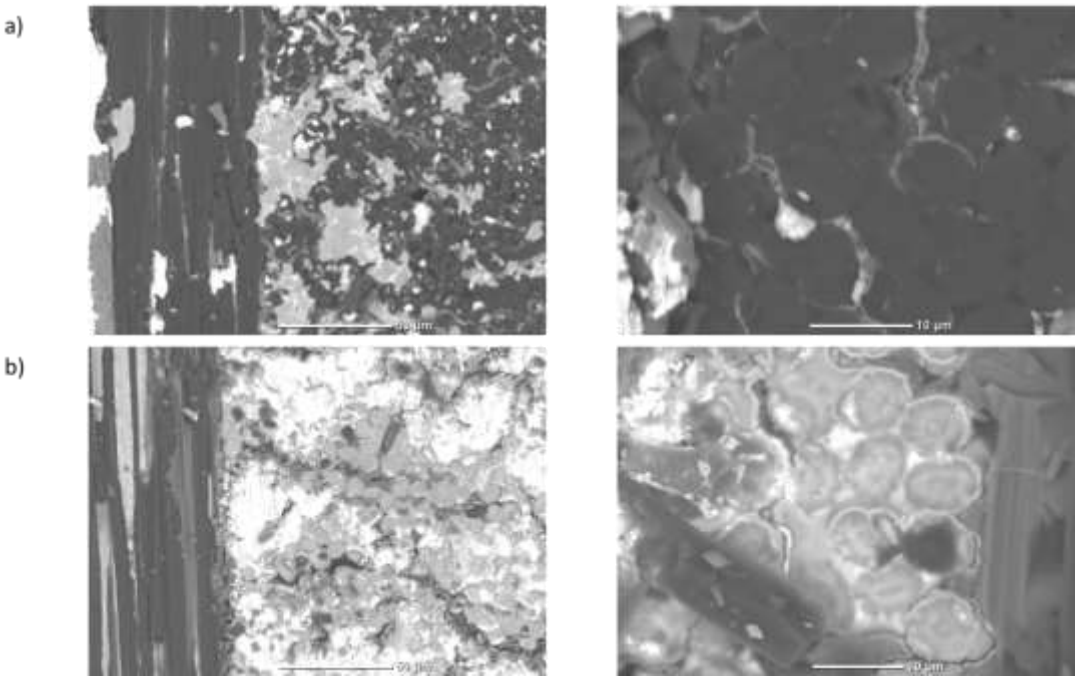

Figure 6-16: fracture surface (details on fibers) of CB4-AgCuTi joined C/SiC (a) and CB4-AgCuTi joined APPJ C/SiC (b).

Conclusions

As for C/C, APPJ proved to be a promising treatment for the surface engineering of C/SiC composites. In this case, the remarkable difference in terms of oxidation resistance between matrix and fiber led to the removal of the C fibers, while SiC was unaffected, thus resulting in a brush-like superficial texture.

Several APPJ treatment lengths were tested, keeping the other settings fixed (1500 l/h air flow and 5 mm nozzle-surface distance) and then 30 s was chosen as viable for the assessment of the effects on the joint strength when CB4-AgCuTi brazing system is used for joining. The wettability of the braze was tested at 950°C and changes in the evolution of the contact angle were reported to be negligible after the APPJ treatment.

Compressive mechanical tests confirmed the beneficial effect of the APPJ treatment on the joint strength. Joined 30s APPJ joined C/SiC samples failed at 65.8 ± 2.5 MPa, outperforming untreated samples that yielded at 45.5 ± 0.6 MPa. The interlocking effect given by the plasma-induced brush-like texture was significant.

These results opened to new opportunities for the exploitation of APPJ in industrial settings, after optimization.

7. Conclusions

The goal of this thesis was to investigate new strategies for the pre-treatment of the surface of advanced ceramics and composites before joining to improve joint strength and, therefore, provide more reliable components. In particular, existing plasma techniques were evaluated to find viable solutions for surface pre-treatment for industrial implementation. Both atmospheric-pressure plasma (corona and atmospheric-pressure plasma jet) and low-pressure plasma techniques were tested. Fig. 7-1 summarizes all the treatments carried out, the material processing, and the main effects.

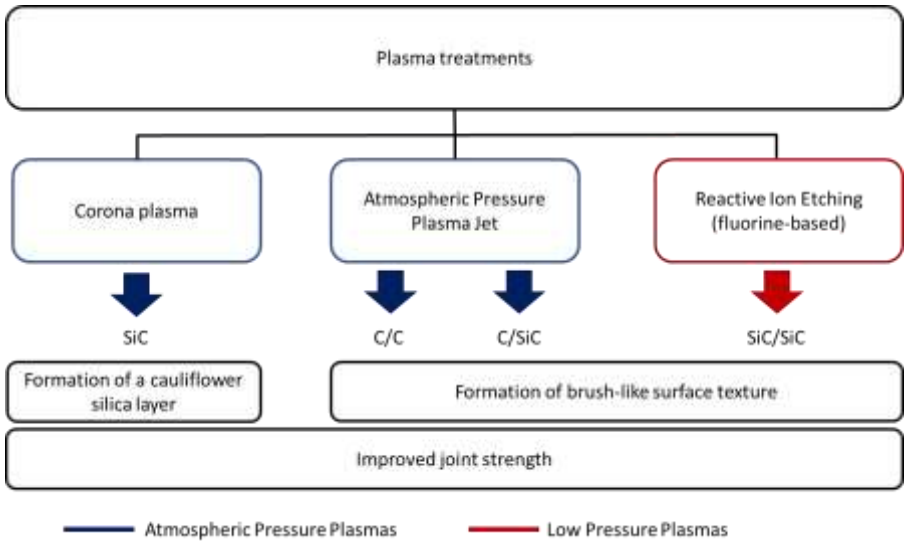

Figure 7-1: summary of plasma treatments investigated in this thesis

Corona plasma was applied for the very first time as a surface modifier for SiC. The surface was characterized before and after the treatment, showing the formation of a silica layer on the surface as a result of the treatment. Surface chemistry changed, but also the surface topography was different since the silica showed a cauliflower-like texture able to promote interlocking with the epoxy glue used for adhesive bonding. The combination of the two effects resulted in a remarkable

increase in the joint strength after the corona treatment and the fracture mode changed from adhesive to cohesive. Furthermore, zeta potential analysis was proposed, for the first time, as a characterization technique to evaluate the chemical affinity between the surface and the epoxy glue before and after the corona treatment. It pointed out higher compatibility with the adhesive of the corona-treated SiC that exposed more acidic groups at the surface, available for the basic groups contained by the epoxy adhesive.

These results were very promising and suggested the viability of the corona treatment, an established technique for processing other materials, as a surface treatment for SiC, opening new research and industrial opportunities (e.g. the corona treatment is a cheap and versatile alternative to laser).

The brush-like texture was previously explored as a mean for increasing the adhesion of the joining material on CMCs by promoting infiltration of the braze. In this work the goal was to replicate such a surface structure, resulting from the selective removal of one of the constituents, confining the effects of the treatment at the surface. To achieve this result, the different etching resistance between fibers and matrix was critical.

A low-pressure reactive ion etching was successfully used to engineer a brush-like surface texture on SiC/SiC composites. SiC fibers, indeed, were preferentially etched leaving channels for braze infiltration originating and then interlocking.

CF_4 alone and mixed with H_2 was used for the plasma treatment. Several conditions were tested and one (pure CF_4, 20 sscm, 200 W, 30 min) was selected for testing the effects on the joint performances of brazed components. The braze was Cusil-ABA, a commercial AgCuTi system.

After treatment, the joint strength increased by 55%, indicating a remarkable effect.

Comparable results were given by the application of a commercially available APPJ on C/SiC and C/C before joining. C/C samples were joined to themselves and to copper using a TiCuNi braze. C/SiC composites were joined to themselves using a commercial AgCuTi system (CB4). The APPJ was air-fed and the etching effect was given by the formation of reactive oxidizing species generated by the plasma.

APPJ removed preferentially carbon fibers in both cases. For C/C, the removal of carbon fibers was faster than for the matrix, while the SiC matrix of C/SiC was unaffected. Plasma conditions selected for testing the joint strength were the

following: 30 s, 1500 l/h, and 5 mm distance between the nozzle and surface. After the plasma treatment, the interlocking at the composite/braze interface was improved and the joint strength significantly increased for both C/SiC-C/SiC and C/C-copper joints.

Fig. 7-2 schematizes how the brush-like texture was obtained for each composite.

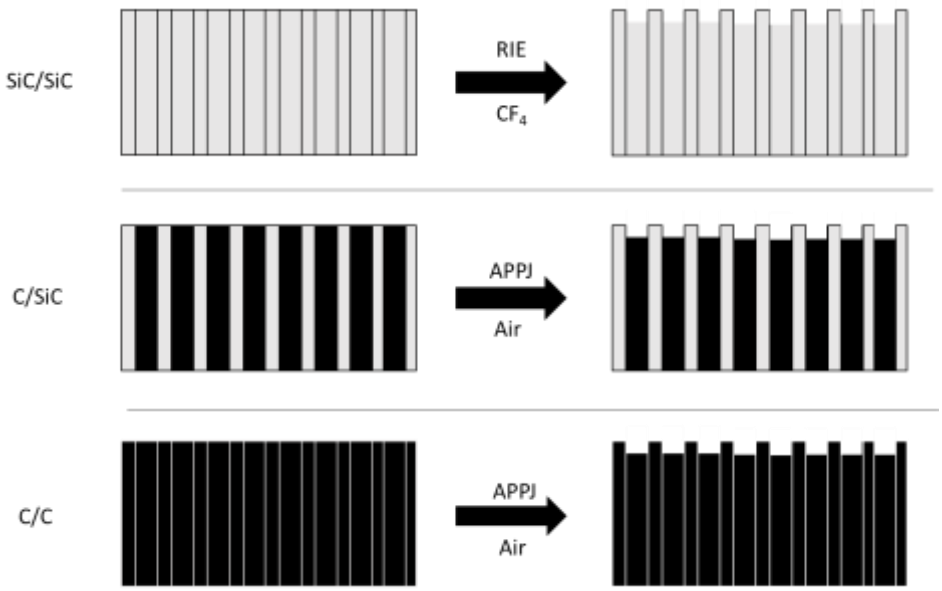

Figure 7-2: Summary of brush-like texturing plasma treatments

Engineering a brush-like texture proved to be an effective strategy for increasing the performance of the joining process of advanced ceramics and CMCs. Since the formation of brush-like texture is dependent on the selective removal of one of the constituents, the properties of materials have a dramatic influence on the final result. Plasma treatments can prevent any damage to the material integrity and can save cost and time compared with other processes, such as laser pre-treatments and thermal selective removal.

The investigation of new methods, carried out within this Doctoral research, opened new opportunities for the surface preparation of CMC before joining, but further research has to be dedicated to collecting information on other types of composites.

8. Appendix: Mo-wrap joining of SiC-base receivers for CSP

Part of the activity presented in the following chapter was published as a regular article [173] *on Materials (MDPI).*

Among renewable energy sources, solar is one of the most promising for powering the world[174]. Most popular solutions are based on photovoltaics, which convert energy from sunlight directly into electricity. However, other technologies can exploit solar radiation to generate power from solar radiation. Concentrated Solar Power is one of them. In this case, the sunlight is converted to heat and then to electricity through turbines. Some designs for a CSP plant are shown in Fig. 1.

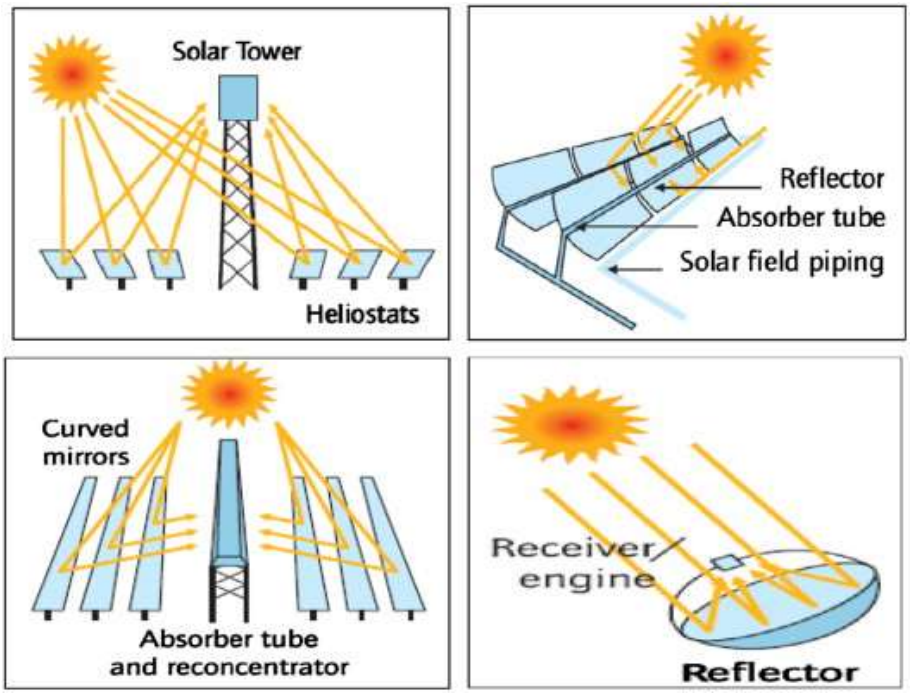

Figure 8-1: CSP designs [175]

As can be observed in Fig.1 the geometry of the component can be very different, but the principle is always the same. The incident sun rays are reflected by the mirrors and collected on an antenna concentrating a large amount of solar energy on a small area. There, the incident energy is converted to heat and transferred to a working fluid. Such fluid is then used for exchanging heat with water and producing steam. The latter then produces electricity when passes through the turbine.

The receiver is a key component of the entire system. Indeed, it absorbs the incident energy generating heat and then it exchanges heat with the working fluid (Fig 7-2). The temperature of the working fluid varies up to 800°C, according to its type.

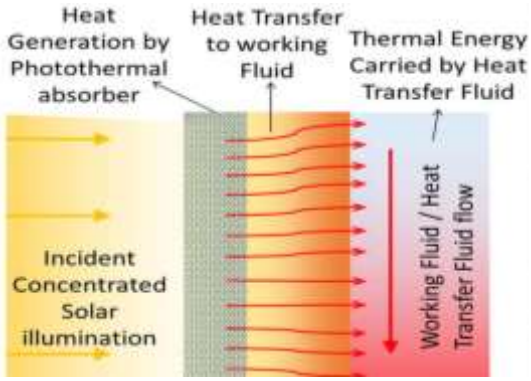

Figure 8-2: Generation of heat and its transfer to the working fluid by the absorber. Adapted from [176]

To date, two main issues have to be addressed to exploit better CSP. The first is related to the material of the solar receiver, which is the core of the collectors and the second to the methods for thermal storage[177]. The receiver has to convert the radiation into heat and then transfer it to the fluid. Most commercial CSP plants work with molten salt that enables peak temperature up to 600°C.

Several types of receivers can be used. Among those, volumetric receivers are made of porous structures that heat the air (or another fluid) by convective heating. According to the chosen material for the receiver, the system can work in different temperature ranges [178].

For air-based CSP the solar receiver can be considered one of the main limiting factors for the technology, since pre-term failures are often reported[179]. Such

issues are generally due to the material that inevitably is key in determining the working temperatures, heat transfer and capacity features of the plant.

According to the available state-of-the-art knowledge on air volumetric receivers [180], two main solutions are identified: metallic wire-mesh and porous ceramic absorbers. The first can operate at a lower temperature (slightly over 500°C) because of the high oxidation of the absorber material. The latter can withstand higher temperatures (< 850°C). Ceramic foams show interesting mechanical properties when compared with bulk, after optimizing porosity, pore size distribution and microstructure.

A viable volumetric receiver has to respect requirements related both to thermophysical and optical properties, to absorb and convey heat. The material has to be able to guarantee the expected performances for a long time.

Using a porous microstructure provides many advantages like a high surface area that promotes contact between the solid receiver and the gas, high gas flow rate, low-pressure drop and good heat transfer, as reported in literature[181–183]. Silicon carbide provides high thermal performance, as already introduced in the previous chapter. It is stable, and highly thermal conductive and its color (black) makes it an interesting material for addressing CSP absorber applications. However, as other ceramics, thermal fatigue due to thermal cycling can lead to premature mechanical failure, mainly in two points: cup-tile joints and the cup[180].

The H2020 NEXTOWER (advanced materials solutions for next generation high efficiency concentrated solar power (csp) tower systems*)* [184] project proposed novel porous SiC-based receivers that may provide higher resistance against thermal shock and thermal fatigue, extending the lifetime of the components up to 20-25 years. This has the potential to improve the performances of solar tower CSP plants (an example reported in Fig 8-3). The solar receiver designed by NEXTOWER consortium (of which POLITO was member) consisted by multiple single units, each of them made of three parts: a tile, a venturi-shaped cup and a cup support. The tile and the cup need to be joined.

Figure 8-3: Example of a CSP plant based on solar tower concept [185]

The work hereby described the manufacturing process of SiC-based receivers, with a focus on joining, and the evaluation of their performances. Such receivers were tested for the very first time and they showed interesting opportunities for future application in CSPs.

Two concepts were proposed, according to two proprietary technologies:

- All-SiC honeycomb open volumetric receivers manufactured by LiqTech Ceramics A/S (Ballerup, Denmark). This design was adapted to manufacture a monolithic component after a SiC-based joining process above 2000°C.
- Joined silicon infiltrated silicon carbide ceramics (SiSiC). SiSiC components were manufactured by EngiCer (Balerna, Switzerland) and they were then joined at Politecnico di Torino. This concept is shown in Fig. -4. A SiC-based is bonded together with the SiSiC foam through indirect joining and fastening (SiSiC pin), to provide higher mechanical strength.

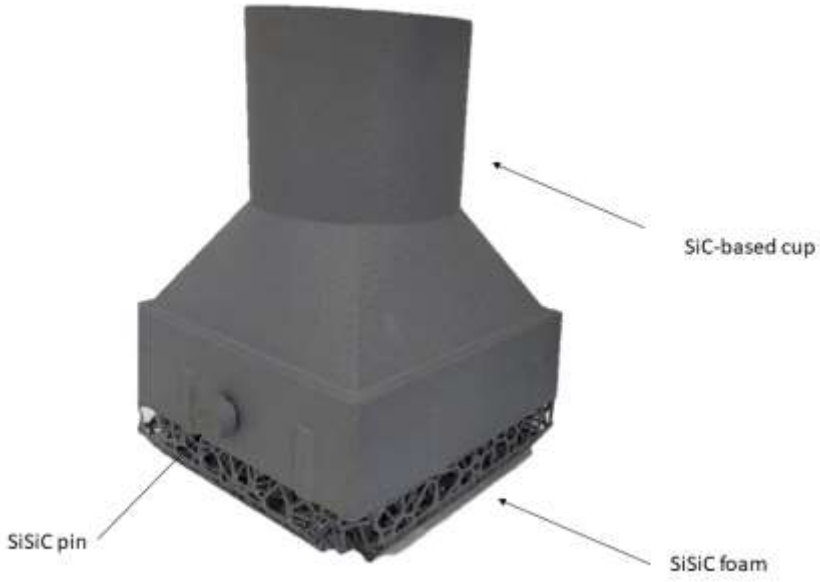

Figure 8-4: design of the SiSiC solar receiver

The next paragraphs describe the manufacturing of the SiSiC solar receiver, in which Politecnico was directly involved. While the joining process was consolidated by previous work, the presence of a foam together with the complex geometry due to the SiSiC solar receiver design, raised challenges in manufacturing the final part.

Materials and methods

The joining process for bonding the SiC cup with the SiSiC foam was carried out using a technique known as Mo-wrap[186,187]. It relies on the coupling of silicon with a refractory metal, in this case, molybdenum, for the manufacturing of a composite joint made of a silicon matrix with embedded silicides. Such a technique proved to be effective for bonding SiC-based components and can withstand high temperatures like those targeted by NEXTOWER project. An example of a Mo-wrap joint is reported in Fig. 8-5. The darkest regions refer to silicon carbide, the intermediate to silicon matrix and the brighter ones correspond to $MoSi_2$ particles. The process is carried out in argon flow at 1450°C for 5 min (heating rate 1000°C/h). The joint is formed when silicon melts and reacts with molybdenum. In order to maximize the contact between molybdenum and silicon,

and simultaneously minimise the depletion of liquid silicon from the joint, the wrap technique was used. A silicon wafer is placed in an envelope made with molybdenum foil, forming the wrap as shown in Fig. 8-6. To successfully form the Mo-wrap joint, the amount of silicon and molybdenum has to be 65-68 wt% and 32-35 wt% respectively. Further and detailed information on the joining process is available in [188].

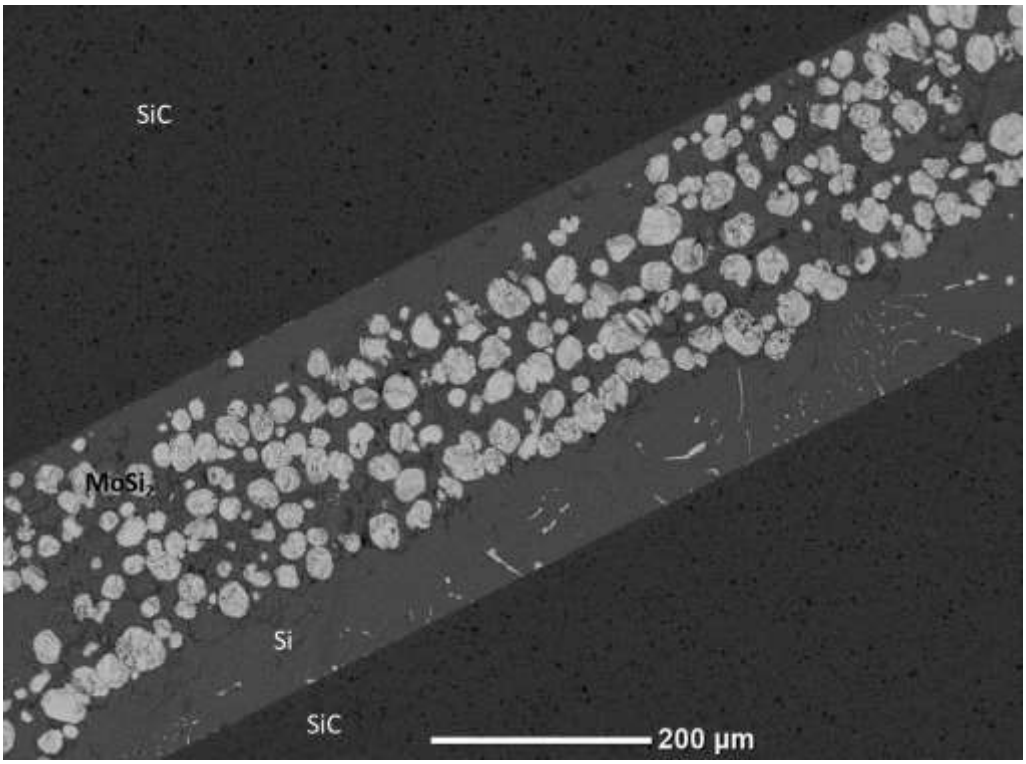

Figure 8-5: Example of a Mo-wrap joint

To assess the feasibility of this joining process 10 samples were prepared cutting SiSiC foam and flat SiC surfaces. Samples of a size of approximately 10 mm x 10 mm x 10 mm were prepared. Before joining, they were cleaned in ultrasonic bath using ethanol.

In addition, mock-up samples designed for simulating the real geometry of the SiSiC receiver were manufactured. The mock-up (Fig. 8.6) consisted of: SiSiC foam, a L-shaped SiC substrate and a SiSiC pin. The foam and the substrate have a hole for accommodating the pin.

All samples were joined via Mo-wrap process. A silicon wafer (MEMC Electronic Materials, S.p.A, Novara, Italy, 584 microns thick, 99.95% Si) was wrapped in a Mo-foil ((Alfa Aesar Germany, 25.4 microns thick, 99.95% Mo) and the joining treatment was carried out in a tubular furnace (BICASA, Bernareggio,

Italy). Samples to be joined were placed in the furnace and the process was done under pure argon flow. The heating rate was set at 1000 °C and a dwell of 5 min at 1450°C was programmed. The process was pressure-less.

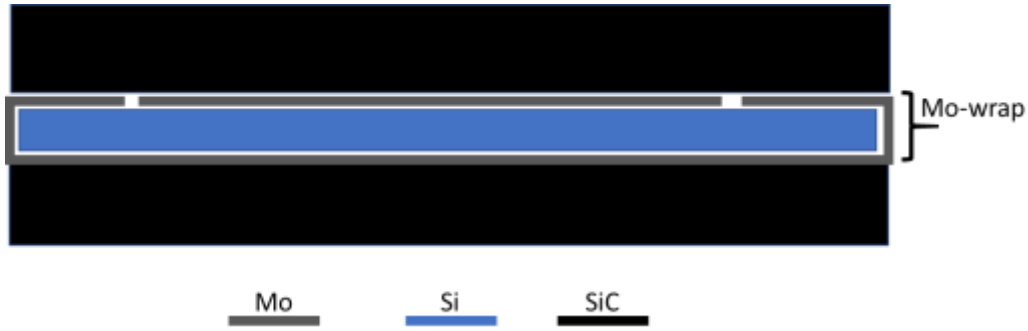

Figure 8-6: sketch of the Mo-wrap joint

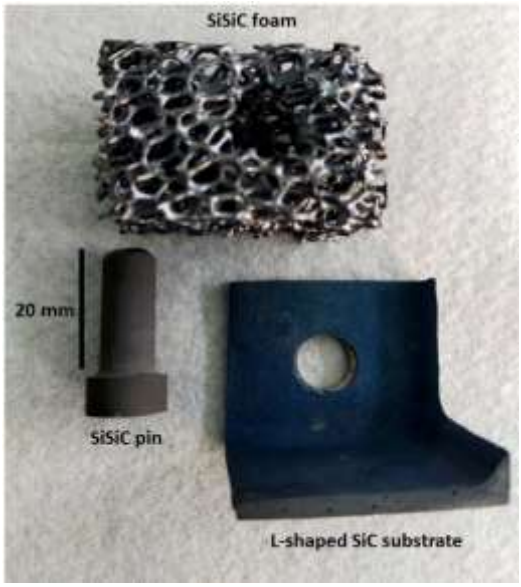

Figure 8-7: mock-up samples to be joined: SiSiC pin, L-shaped SiC substrate and SiSiC foam

After joining samples were investigated via a scanning electron microscope (Zeiss SUPRA TM 40) together with an energy-dispersive X-ray spectroscope (EDAX PV 9900). Finally, micro-CT (Phoenix v|tome|x m 300, Waygate Technologies) inspection was conducted with these settings: 270 kV (filament voltage), 125 A (filament current), 500 ms (exposure time for each projection), 1500 projections for 360° rotation. As prefilters 0.5 mm-thick Sn and 0.5 mm-thick Cu were used. The tomography was registered by 3D translations and rotations and a digital volume correlation (30 µm/voxel resolution) was set.

Results and discussion

The cross-section of a SiSiC foam/SiC joint is reported in Fig. 8-7. The joint thickness was rather constant along the joining area and was compromised between 200-250 μm for all the 10 samples. The typical microstructure of Mo-wrap joint ($MoSi_2$ particles dispersed in the silicon matrix) was observed.

Compared with flat surfaces, the foam provided less contact points with the joining material, but those looked well joined by the Si/$MoSi_2$. No infiltration of silicon in the foam was reported. This was a positive finding because the low viscosity of silicon after melting would result in a depletion of materials from the joining area that can affect the formation of disilicides and the consolidation of the matrix. However, some degree of infiltration would provide additional contact with the foam. Finding a balance between the need of supplying enough material for the consolidation of the joint and leaving silicon free for partial ingress in the porosities of the foam, may be a good strategy to improve the joining process.

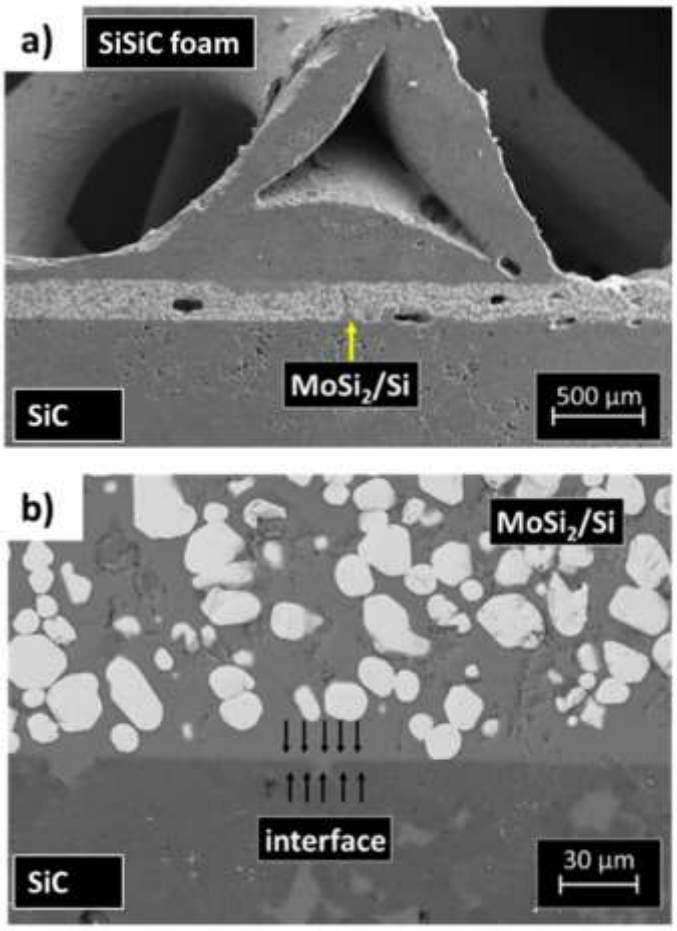

Figure 8-8: cross-section of Mo-wrap joined SiSiC/SiC at lower (a) and higher magnification (b).

The 10 mm x 10 mm x 10 mm SiSiC/SiC were effectively joined using the Mo-wrap process, but the actual parts are larger and more complex (Fig. 8-4). The final part requires the joining of the SiSiC foam to the four walls of the SiC cup and SiSiC fasteners are used as additional joining strategy. Upscaling is tricky: the surface to be joined are larger, bigger furnaces are required and the introduction of the pins introduce challenges for their integration with the Mo-wrap.

More in detail, the use of bigger furnaces, when transferring the process from laboratory to industry, can raise issues related to temperature control of the joining process resulting in incomplete melting of silicon and ineffective reaction with molybdenum that can prevent the formation of the joint. Overheating has to be prevented too, otherwise, silicon could massively leak from the joint area.

The presence of the mechanical fasteners mitigates the presence of issues related to the Mo-wrap joint but they require to be joint with the SiC and the SiSiC foam to guarantee the additional reinforcement. The combination of Mo-wrap and SiSiC pin, therefore, is expected to enable upscaling of such a solution.

The mockup samples were the first attempt to join SiC with the SiSiC using this mixed joining (pin together with Mo-wrap) approach. Several configurations were tested to identify the most promising placement for the joining material to fix the pin. The best findings were given by the positioning of the Mo-wrap envelope on both the end of the pin (where it is surrounded by the foam) and the bottom surface of the L-shaped substrate. As for the previous samples, the foam legs were embedded in the joining material and the interface was sound and continuous. Foam legs were not of the same length and this resulted in the presence of regions where there is no contact with the substrate or the pin. $Si/MoSi_2$ joining material had the expected morphology, identical to that observed in the previous works. This result highlighted the feasibility of the Mo-wrap for upscaling.

Through the micro-CT scan, the joined interfaces were analyzed to identify critical areas where cracks and pores are present or the joining area was depleted.

The soundness of the joints was confirmed (Fig. 8-8). No cracks were detected. The confinement of the molten silicon was successfully achieved. Indeed, no signs of joining material were visible on the vertical portion of the pin. Similarly, no silicon was detected inside the open porosity of the foam, confirming that the configuration prevents leakage.

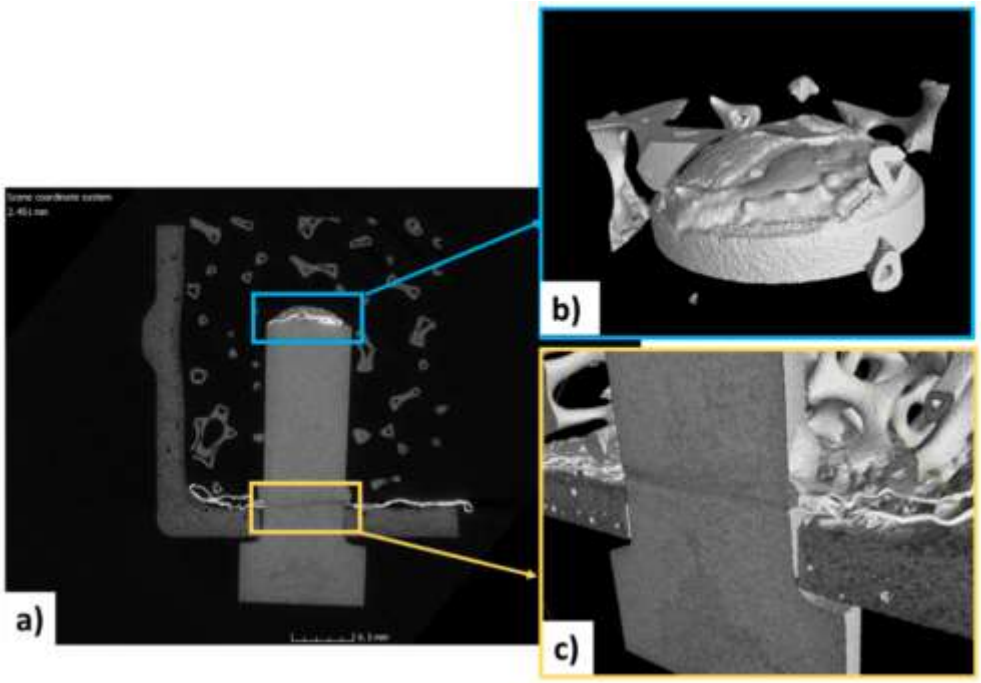

Figure 8-9: CT-scan reconstruction of Mo-wrap joined mock-up sample. Cross-section of the sample (a), and details of Mo-wrap at the end of the pin in contact with the foam (b) and close to the hole of the SiC substrate (b).

Conclusions

SiC-based solar receiver has the potential for being disruptive for the technology of CSP plants. The manufacturing route of the parts together with the joining process hereby proposed gave good results.

In particular, no remarkable issues were raised when the mock-up samples were joined. The Mo-wrap process, coupled with the SiSiC pins, fit as a solution for bonding the foam and the substrate.

Further research has to be carried out to scale the solutions to real-size components, however, these first observations were promising. The next activities will focus also on the thermo-physical characterization of the two types of SiC-based receivers. Thermal age tests on the samples are ongoing in the facilities of the Plataforma Solar de Almeria in Spain.

According to the results of thermo-physical characterization, the joining process and, overall, the entire manufacturing route will be optimized.

List of Publications

- A. De Zanet, V. Casalegno, M. Salvo, Lasersurface texturing of ceramics and ceramiccomposite materials – A review, Ceram.Int. 47 (2021) 7307–7320. https://doi.org/10.1016/j.ceramint.2020.11.146.

- A. De Zanet, M. Salvo, V. Casalegno, Surfacemodification of SiC to improve jointstrength via a Corona plasma treatment,Ceram. Int. 48 (2022) 23492–23497. https://doi.org/10.1016/j.ceramint.2022.04.344.

- V. Casalegno, L. Ferrari, M. JimenezFuentes, A. De Zanet, S. Gianella, M.Ferraris, V.M. Candelario, High-Performance SiC–Based Solar Receiversfor CSP: Component Manufacturing andJoining, Materials (Basel). 14 (2021) 4687. https://doi.org/10.3390/ma14164687.

- Malinverni, M. Salvo, A. De Zanet, F.D'Isanto, F. Smeacetto, P. Bertrand, G.Puchas, S. Schafföner, V. Casalegno,Glass-ceramics for joining oxide-basedceramic matrix composites (Al2O3/Al2O3-ZrO2) operating under direct flameexposure, J. Eur. Ceram. Soc. 43 (2023)3621–3629. https://doi.org/10.1016/j.jeurceramsoc.2023.02.019.

- A. De Zanet, M. Pedroni, M. Salvo, E. Vassallo,V. Casalegno, Plasma etching as a surfaceengineering technique for SiC/SiCcomposites to improve joint strength,Ceram. Int. (2022). https://doi.org/10.1016/j.ceramint.2022.11.248.

- A. De Zanet, F. Valenza, V. Casalegno, S. Gambaro, M. Salvo, Atmospheric pressure plasma jet for surface texturing of C/SiC, Ceramics International. 49 (2023) 32136–32143. https://doi.org/10.1016/j.ceramint.2023.07.182.

List of Conferences

- Oral presentation - 45th International Conference and Expo on Advanced Ceramics and Composites (virtual).
  Title: Plasma-based surface modification of carbon fibre-reinforced ceramics to improve joint strength through interlocking mechanism.

- Oral presentation - EUROMAT 2021 (virtual)
  Title: Assessment on the effectiveness of APPJ treatment in improving jointstrength of joined CMC materials.

- Oral presentation - XXV AIV CONFERENCE (Napoli, Italy)
  Title: Plasma etching of SiC/SiC composites to improve joint strength.

- Oral presentation - CIMTEC 2022 15th Ceramics Congress (Perugia, Italy).
  Title: Atmospheric plasmas forimproving mechanical performances of joined SiC components.

- Poster – Le mille vite del vetro 2022 (Venezia, Italy)
  Title: Glass-ceramics as joining material for novel MW-CVI manufactured SiC/SiC

References

[1] S. Sömiya, Advanced Technical Ceramics, ACADEMIC PRESS, INC., San Diego, California, 1989. https://doi.org/10.1016/b978-0-12-654630-9.x5001-3.

[2] I.W. Donald, P.W. McMillan, Ceramic-matrix composites, J. Mater. Sci. 11 (1976) 949–972. https://doi.org/10.1007/BF00542312.

[3] United Nations, THE 2030 AGENDA FOR SUSTAINABLE DEVELOPMENT, 2015. https://sdgs.un.org/sites/default/files/publications/21252030 Agenda for Sustainable Development web.pdf.

[4] N.P. Padture, Advanced structural ceramics in aerospace propulsion, Nat. Mater. 15 (2016) 804–809. https://doi.org/10.1038/nmat4687.

[5] R.A.J. Sambell, The technology of ceramic-fibre ceramic-matrix composites, Composites. 1 (1970) 276–285. https://doi.org/10.1016/0010-4361(70)90094-7.

[6] S.-J. Park, History and Structure of Carbon Fibers, in: 2018: pp. 1–30. https://doi.org/10.1007/978-981-13-0538-2_1.

[7] T. Ishikawa, Recent developments of the SiC fiber Nicalon and its composites, including properties of the SiC fiber Hi-Nicalon for ultra-high temperature, Compos. Sci. Technol. 51 (1994) 135–144. https://doi.org/10.1016/0266-3538(94)90184-8.

[8] A. Misra, Composite materials for aerospace propulsion related to air and space transportation, in: Light. Compos. Struct. Transp., Elsevier, 2016: pp. 305–327. https://doi.org/10.1016/B978-1-78242-325-6.00012-8.

[9] X. Wang, X. Gao, Z. Zhang, L. Cheng, H. Ma, W. Yang, Advances in modifications and high-temperature applications of silicon carbide ceramic matrix composites in aerospace: A focused review, J. Eur. Ceram. Soc. 41 (2021) 4671–4688. https://doi.org/10.1016/j.jeurceramsoc.2021.03.051.

[10] Q. Zhang, G. Li, A Review of the Application of C/SiC Composite in Thermal Protection System, Multidiscip. Model. Mater. Struct. 5 (2009) 199–203. https://doi.org/10.1163/157361109787959903.

[11] Z. Duan, H. Yang, Y. Satoh, K. Murakami, S. Kano, Z. Zhao, J. Shen, H.

Abe, Current status of materials development of nuclear fuel cladding tubes for light water reactors, Nucl. Eng. Des. 316 (2017) 131–150. https://doi.org/10.1016/j.nucengdes.2017.02.031.

[12] T. Koyanagi, Y. Katoh, T. Nozawa, L.L. Snead, S. Kondo, C.H. Henager, M. Ferraris, T. Hinoki, Q. Huang, Recent progress in the development of SiC composites for nuclear fusion applications, J. Nucl. Mater. 511 (2018) 544–555. https://doi.org/10.1016/j.jnucmat.2018.06.017.

[13] S.G. Nair, V. Vijay, M.S. Siva, R. Devasia, F. Mohamed, M.K. Suresh, K.J. Sreejith, Development of C/PyC/SiC CMCs by CVI Process for Hypersonic Vehicle Application, Trans. Indian Natl. Acad. Eng. 6 (2021) 79–85. https://doi.org/10.1007/s41403-020-00180-0.

[14] H2020 - CEM-WAVE project, (n.d.). https://www.cem-wave.eu/ (accessed August 29, 2022).

[15] F. Leleu, P. Watillon, J. Moulin, A. Lacombe, P. Soyris, The thermo-mechanical architecture and TPS configuration of the pre-X vehicle, Acta Astronaut. 56 (2005) 453–464. https://doi.org/10.1016/j.actaastro.2004.05.073.

[16] R.W. Messler, Introduction to Joining, in: Join. Adv. Mater., Elsevier, 1993: pp. 3–24. https://doi.org/10.1016/B978-0-7506-9008-9.50004-X.

[17] E.H. Penilla, L.F. Devia-Cruz, A.T. Wieg, P. Martinez-Torres, N. Cuando-Espitia, P. Sellappan, Y. Kodera, G. Aguilar, J.E. Garay, Ultrafast laser welding of ceramics, Science (80-.). 365 (2019) 803–808. https://doi.org/10.1126/science.aaw6699.

[18] M. Tokita, Progress of Spark Plasma Sintering (SPS) Method, Systems, Ceramics Applications and Industrialization, Ceramics. 4 (2021) 160–198. https://doi.org/10.3390/ceramics4020014.

[19] O. Gavalda Diaz, G. Garcia Luna, Z. Liao, D. Axinte, The new challenges of machining Ceramic Matrix Composites (CMCs): Review of surface integrity, Int. J. Mach. Tools Manuf. 139 (2019) 24–36. https://doi.org/10.1016/j.ijmachtools.2019.01.003.

[20] H. Böhrk, U. Beyermann, Secure tightening of a CMC fastener for the heat shield of re-entry vehicles, Compos. Struct. 92 (2010) 107–112. https://doi.org/10.1016/j.compstruct.2009.07.002.

[21] Y. Kondo, K. Deguchi, Y. Hayashi, F. Obata, Reversibility and disassembly

time of part connection, Resour. Conserv. Recycl. 38 (2003) 175–184. https://doi.org/10.1016/S0921-3449(02)00153-2.

[22] A. Marques, A. Mocanu, N. Tomić, S. Balos, E. Stammen, A. Lundevall, S. Abrahami, R. Günther, J. de Kok, S. Teixeira de Freitas, Review on Adhesives and Surface Treatments for Structural Applications: Recent Developments on Sustainability and Implementation for Metal and Composite Substrates, Materials (Basel). 13 (2020) 5590. https://doi.org/10.3390/ma13245590.

[23] M. Ferraris, V. Casalegno, F. Smeacetto, M. Salvo, Glass as a joining material for ceramic matrix composites: 25 years of research at Politecnico di Torino, Int. J. Appl. Glas. Sci. 11 (2020) 569–576. https://doi.org/10.1111/ijag.15032.

[24] K. Nogi, The role of wettability in metal–ceramic joining, Scr. Mater. 62 (2010) 945–948. https://doi.org/10.1016/j.scriptamat.2010.03.007.

[25] S.J. Marshall, S.C. Bayne, R. Baier, A.P. Tomsia, G.W. Marshall, A review of adhesion science, Dent. Mater. 26 (2010) e11–e16. https://doi.org/10.1016/j.dental.2009.11.157.

[26] S.N. Grigoriev, T.N. Soe, K. Hamdy, Y. Pristinskiy, A. Malakhinsky, I. Makhadilov, V. Romanov, E. Kuznetsova, P. Podrabinnik, A.Y. Kurmysheva, A. Smirnov, N.W. Solís Pinargote, The Influence of Surface Texturing of Ceramic and Superhard Cutting Tools on the Machining Process—A Review, Materials (Basel). 15 (2022) 6945. https://doi.org/10.3390/ma15196945.

[27] Y. Zhang, H. Qiao, J. Zhao, Z. Cao, Surface topography by water jet-guided laser texturing on wettability of monocrystalline silicon, Int. J. Adv. Manuf. Technol. 120 (2022) 2747–2761. https://doi.org/10.1007/s00170-022-08712-4.

[28] Y. Hu, Feasibility of using wet abrasive jet machining to produce flat and crack-free micro-textures on reaction bonded silicon carbide, J. Mater. Process. Technol. 300 (2022) 117423. https://doi.org/10.1016/j.jmatprotec.2021.117423.

[29] H.T. TING, K.A. ABOU-EL-HOSSEIN, H.B. CHUA, Review of micromachining of ceramics by etching, Trans. Nonferrous Met. Soc. China. 19 (2009) s1–s16. https://doi.org/10.1016/S1003-6326(10)60237-3.

[30] M. Katsuno, N. Ohtani, J. Takahashi, H. Yashiro, M. Kanaya, Mechanism of Molten KOH Etching of SiC Single Crystals: Comparative Study with Thermal Oxidation, Jpn. J. Appl. Phys. 38 (1999) 4661–4665. https://doi.org/10.1143/JJAP.38.4661.

[31] E.G. Gamaly, A. V. Rode, B. Luther-Davies, V.T. Tikhonchuk, Ablation of solids by femtosecond lasers: Ablation mechanism and ablation thresholds for metals and dielectrics, Phys. Plasmas. 9 (2002) 949–957. https://doi.org/10.1063/1.1447555.

[32] T.H. Maiman, Stimulated Optical Radiation in Ruby, Nature. 187 (1960) 493–494. https://doi.org/10.1038/187493a0.

[33] N.B. Dahotre, S.P. Harimkar, Laser Materials Interactions, in: Laser Fabr. Mach. Mater., Springer US, Boston, MA, n.d.: pp. 34–65. https://doi.org/10.1007/978-0-387-72344-0_2.

[34] J.-W. Jeon, S. Yoon, H. Choi, J. Kim, D. Farson, S.-H. Cho, The Effect of Laser Pulse Widths on Laser—Ag Nanoparticle Interaction: Femto- to Nanosecond Lasers, Appl. Sci. 8 (2018) 112. https://doi.org/10.3390/app8010112.

[35] K. Mitra, S. Miller, Introduction, in: Short Pulse Laser Syst. Biomed. Appl., 2017: pp. 1–12. https://doi.org/10.1007/978-3-319-54253-9_1.

[36] F. Claverie, Laser ablation, Elsevier B.V., 2020. https://doi.org/10.1016/b978-0-444-59482-2.00010-5.

[37] F.L. Palmieri, C.J. Wohl, Topographical Modification of Polymers and Metals by Laser Ablation to Create Superhydrophobic Surfaces, in: K.L. Mittal, W.-S. Lei (Eds.), Laser Technol. Appl. Adhes. Relat. Areas, John Wiley & Sons, Inc., Hoboken, NJ, USA, 2018: pp. 1–68. https://doi.org/10.1002/9781119185031.ch1.

[38] L.T. Cangueiro, T. Le Quang, R. Vilar, Laser surface modification of biological hard tissues, in: Laser Surf. Modif. Biomater. Tech. Appl., Elsevier Ltd, 2016: pp. 221–251. https://doi.org/10.1016/B978-0-08-100883-6.00008-3.

[39] R. Stoian, D. Ashkenasi, A. Rosenfeld, E.E.B. Campbell, Coulomb explosion in ultrashort pulsed laser ablation of Al2O3, Phys. Rev. B. 62 (2000) 13167–13173. https://doi.org/10.1103/PhysRevB.62.13167.

[40] Z. Zhang, G. Gogos, Theory of shock wave propagation during laser

ablation, Phys. Rev. B. 69 (2004) 235403. https://doi.org/10.1103/PhysRevB.69.235403.

[41] A. De Zanet, V. Casalegno, M. Salvo, Laser surface texturing of ceramics and ceramic composite materials – A review, Ceram. Int. 47 (2021) 7307–7320. https://doi.org/10.1016/j.ceramint.2020.11.146.

[42] A. Carvalho, L. Grenho, M.H. Fernandes, A. Daskalova, A. Trifonov, I. Buchvarov, F.J. Monteiro, Femtosecond laser microstructuring of alumina toughened zirconia for surface functionalization of dental implants, Ceram. Int. 46 (2020) 1383–1389. https://doi.org/10.1016/j.ceramint.2019.09.101.

[43] M.L. Wu, C.Z. Ren, Active control of the anisotropic wettability of the carbon fiber reinforced carbon and silicon carbide dual matrix composites (C/C-SiC), Appl. Surf. Sci. 327 (2015) 424–431. https://doi.org/10.1016/j.apsusc.2014.11.183.

[44] M.L. Wu, C.Z. Ren, H.Z. Xu, C.L. Zhou, Fabrication of a bionic microstructure on a C/SiC brake lining surface: Positive applications of surface defects for surface wetting control, Appl. Surf. Sci. 440 (2018) 669–679. https://doi.org/10.1016/j.apsusc.2018.01.093.

[45] M.L. Wu, C.Z. Ren, H.Z. Xu, On the wettability diversity of C/SiC surface: Comparison of the ground C/SiC surface and ablated C/SiC surface from three aspects, Appl. Surf. Sci. 385 (2016) 391–399. https://doi.org/10.1016/j.apsusc.2016.05.061.

[46] S. Pan, Q. Li, Z. Xian, N. Su, F. Zeng, The effects of laser parameters and the ablation mechanism in laser ablation of c/sic composite, Materials (Basel). 12 (2019). https://doi.org/10.3390/ma12193076.

[47] Z. Zhai, C. Wei, Y. Zhang, Y. Cui, Q. Zeng, Investigations on the oxidation phenomenon of SiC/SiC fabricated by high repetition frequency femtosecond laser, Appl. Surf. Sci. 502 (2020) 144131. https://doi.org/10.1016/j.apsusc.2019.144131.

[48] J. Chen, Q. An, W. Ming, M. Chen, Investigations on continuous-wave laser and pulsed laser induced controllable ablation of SiCf/SiC composites, J. Eur. Ceram. Soc. 41 (2021) 5835–5849. https://doi.org/10.1016/j.jeurceramsoc.2021.04.061.

[49] J. Wei, S. Yuan, J. Zhang, N. Zhou, W. Zhang, J. Li, W. An, M. Gao, Y. Fu, Removal mechanism of SiC/SiC composites by underwater femtosecond

laser ablation, J. Eur. Ceram. Soc. 42 (2022) 5380–5390. https://doi.org/10.1016/j.jeurceramsoc.2022.05.041.

[50] K. Zimmer, M. Ehrhardt, P. Lorenz, X. Wang, P. Wang, S. Sun, Etching of SiC–SiC-composites by a laser-induced plasma in a reactive gas, Ceram. Int. 48 (2022) 90–95. https://doi.org/10.1016/j.ceramint.2021.09.084.

[51] F. Rossi, O. Kylián, M. Hasiwa, Decontamination of Surfaces by Low Pressure Plasma Discharges, Plasma Process. Polym. 3 (2006) 431–442. https://doi.org/10.1002/ppap.200600011.

[52] A. Belkind, S. Krommenhoek, H. Li, Z. Orban, F. Jansen, Removal of oil from metals by plasma techniques, Surf. Coatings Technol. 68–69 (1994) 804–808. https://doi.org/10.1016/0257-8972(94)90257-7.

[53] R. Ghobeira, P.S. Esbah Tabaei, R. Morent, N. De Geyter, Chemical characterization of plasma-activated polymeric surfaces via XPS analyses: A review, Surfaces and Interfaces. 31 (2022) 102087. https://doi.org/10.1016/j.surfin.2022.102087.

[54] G. Franz, Plasma roughening of polished SiC substrates, Mater. Sci. Semicond. Process. 5 (2002) 525–527. https://doi.org/10.1016/S1369-8001(02)00115-4.

[55] J. Izdebska-Podsiadły, Application of Plasma in Printed Surfaces and Print Quality, in: Non-Thermal Plasma Technol. Polym. Mater., Elsevier, 2019: pp. 159–191. https://doi.org/10.1016/B978-0-12-813152-7.00006-8.

[56] A.S. Katsigiannis, N. Hojnik, M. Modic, D.L. Bayliss, J. Kovač, J.L. Walsh, Continuous in-line decontamination of food-processing surfaces using cold atmospheric pressure air plasma, Innov. Food Sci. Emerg. Technol. 81 (2022) 103150. https://doi.org/10.1016/j.ifset.2022.103150.

[57] S. Bekeschus, A. Schmidt, K.D. Weltmann, T. von Woedtke, The plasma jet kINPen – A powerful tool for wound healing, Clin. Plasma Med. 4 (2016) 19–28. https://doi.org/10.1016/j.cpme.2016.01.001.

[58] V. Scholtz, J. Pazlarova, H. Souskova, J. Khun, J. Julak, Nonthermal plasma — A tool for decontamination and disinfection, Biotechnol. Adv. 33 (2015) 1108–1119. https://doi.org/10.1016/j.biotechadv.2015.01.002.

[59] P. Vanraes, A. Bogaerts, The essential role of the plasma sheath in plasma–liquid interaction and its applications—A perspective, J. Appl. Phys. 129 (2021) 220901. https://doi.org/10.1063/5.0044905.

[60] F.L. Tabares, I. Junkar, Cold Plasma Systems and Their Application in Surface Treatments for Medicine, Molecules. 26 (2021) 1903. https://doi.org/10.3390/molecules26071903.

[61] S. Samal, Thermal plasma technology: The prospective future in material processing, J. Clean. Prod. 142 (2017) 3131–3150. https://doi.org/10.1016/j.jclepro.2016.10.154.

[62] M.I. Boulos, P. Fauchais, E. Pfender, The Plasma State, in: Therm. Plasmas, Springer US, Boston, MA, 1994: pp. 1–47. https://doi.org/10.1007/978-1-4899-1337-1.

[63] A. Schutze, J.Y. Jeong, S.E. Babayan, Jaeyoung Park, G.S. Selwyn, R.F. Hicks, The atmospheric-pressure plasma jet: a review and comparison to other plasma sources, IEEE Trans. Plasma Sci. 26 (1998) 1685–1694. https://doi.org/10.1109/27.747887.

[64] S. kumar, A review on Zerodur material strength behaviour with lightweighted design, Mater. Today Proc. 37 (2021) 3643–3645. https://doi.org/10.1016/j.matpr.2020.09.785.

[65] Schott, Zerodur® Data, (n.d.). https://www.schott.com/en-us/products/zerodur-p1000269.

[66] H.-K. Sung, T. Qiang, Z. Yao, Y. Li, Q. Wu, H.-K. Lee, B.-D. Park, W.-S. Lim, K.-H. Park, C. Wang, Vertical and bevel-structured SiC etching techniques incorporating different gas mixture plasmas for various microelectronic applications, Sci. Rep. 7 (2017) 3915. https://doi.org/10.1038/s41598-017-04389-y.

[67] F. Karouta, A practical approach to reactive ion etching, J. Phys. D. Appl. Phys. 47 (2014) 233501. https://doi.org/10.1088/0022-3727/47/23/233501.

[68] M. Huff, Recent Advances in Reactive Ion Etching and Applications of High-Aspect-Ratio Microfabrication, Micromachines. 12 (2021) 991. https://doi.org/10.3390/mi12080991.

[69] C. Richter, K. Espertshuber, C. Wagner, M. Eickhoff, G. Krötz, Rapid plasma etching of cubic SiC using NF3/O2 gas mixtures, Mater. Sci. Eng. B. 46 (1997) 160–163. https://doi.org/10.1016/S0921-5107(96)01969-1.

[70] C. Weigel, M. Schulze, H. Gargouri, M. Hoffmann, Deep etching of Zerodur glass ceramics in a fluorine-based plasma, Microelectron. Eng. 185–186 (2018) 1–8. https://doi.org/10.1016/j.mee.2017.10.013.

[71] C. Weigel, H.B. Phi, F.A. Denissel, M. Hoffmann, S. Sinzinger, S. Strehle, Highly Anisotropic Fluorine-Based Plasma Etching of Ultralow Expansion Glass, Adv. Eng. Mater. 23 (2021) 2001336. https://doi.org/10.1002/adem.202001336.

[72] M. Huff, Process Variations in Microsystems Manufacturing, Springer International Publishing, Cham, 2020. https://doi.org/10.1007/978-3-030-40560-1.

[73] J. Izdebska, Corona Treatment, in: Print. Polym., Elsevier, 2016: pp. 123–142. https://doi.org/10.1016/B978-0-323-37468-2.00008-7.

[74] U. Lommatzsch, D. Pasedag, A. Baalmann, G. Ellinghorst, H.-E. Wagner, Atmospheric Pressure Plasma Jet Treatment of Polyethylene Surfaces for Adhesion Improvement, Plasma Process. Polym. 4 (2007) S1041–S1045. https://doi.org/10.1002/ppap.200732402.

[75] Y.X. Yao, B. Wang, J.H. Wang, H.L. Jin, Y.F. Zhang, S. Dong, Chemical machining of Zerodur material with atmospheric pressure plasma jet, CIRP Ann. - Manuf. Technol. 59 (2010) 337–340. https://doi.org/10.1016/j.cirp.2010.03.118.

[76] A. De Zanet, M. Salvo, V. Casalegno, Surface modification of SiC to improve joint strength via a Corona plasma treatment, Ceram. Int. 48 (2022) 23492–23497. https://doi.org/10.1016/j.ceramint.2022.04.344.

[77] V. Casalegno, M. Ferraris, S. Perero, M. Suess, C. Wilhelmi, M. Pedroni, E. Vassallo, M. Salvo, A plasma pre-treatment to improve adhesion on SiC and Si3N4 ceramics, Mater. Lett. 272 (2020) 127855. https://doi.org/10.1016/j.matlet.2020.127855.

[78] M. Suess, C. Wilhelmi, M. Salvo, V. Casalegno, P. Tatarko, M. Funke, Effect of pulsed laser irradiation on the SiC surface, Int. J. Appl. Ceram. Technol. 14 (2017) 313–322. https://doi.org/10.1111/ijac.12655.

[79] B. Akgul, M. Kul, F. Erden, The puzzling thermal expansion behavior of invar alloys: a review on process-structure-property relationship, Crit. Rev. Solid State Mater. Sci. (2023) 1–54. https://doi.org/10.1080/10408436.2023.2170975.

[80] M. Kotani, Y. Muta, A. Yoshimura, S. Ogihara, T. Imai, H. Katayama, Y. Yui, Y. Tange, K. Enya, H. Kaneda, T. Nakagawa, Evaluation of Spaceborne SiC Mirror Materials Using Samples Cut from the Periphery of a Mirror

Body, J. Mater. Eng. Perform. 23 (2014) 850–858. https://doi.org/10.1007/s11665-013-0827-1.

[81] A. Fridman, A. Chirokov, A. Gutsol, Non-thermal atmospheric pressure discharges, J. Phys. D. Appl. Phys. 38 (2005) R1–R24. https://doi.org/10.1088/0022-3727/38/2/R01.

[82] A. Hsu, H.-H. Chien, C.-Y. Liao, C.-C. Lee, J.-H. Tsai, C.-C. Hsu, I.-C. Cheng, J.-Z. Chen, Scan-Mode Atmospheric-Pressure Plasma Jet Processed Reduced Graphene Oxides for Quasi-Solid-State Gel-Electrolyte Supercapacitors, Coatings. 8 (2018) 52. https://doi.org/10.3390/coatings8020052.

[83] R.S. Goldman, M., Goldman, A. and Sigmond, The corona discharge, its properties and specific uses, Pure Appl. Chem. 57 (1985) 1353–1362. https://doi.org/https://doi.org/10.1351/pac198557091353.

[84] P. Cools, L. Astoreca, P.S. Esbah Tabaei, M. Thukkaram, H. De Smet, R. Morent, N. De Geyter, Surface Treatment of Polymers by Plasma, in: Surf. Modif. Polym., Wiley-VCH Verlag GmbH & Co. KGaA, Weinheim, Germany, 2019: pp. 31–65. https://doi.org/10.1002/9783527819249.ch2.

[85] Tantec: Corona treaters, (n.d.). https://tantec.com/corona-treaters/ (accessed September 1, 2023).

[86] Diener -PLASMA APC 500, (n.d.). https://www.plasma.com/en/atmospheric-pressure-plasma-plasma-apc-500/ (accessed September 1, 2023).

[87] Enercon: Corona treaters, (n.d.). https://www.enerconind.com/web-treating/corona-treatment.aspx (accessed September 1, 2023).

[88] Y. Komagata, H. Ikeda, Y. Fujio, Y. Nagamatsu, H. Shimizu, Surface modification of feldspar porcelain by corona discharge and its effect on bonding to resin cement with silane coupling agent, J. Mech. Behav. Biomed. Mater. 105 (2020) 103708. https://doi.org/10.1016/j.jmbbm.2020.103708.

[89] H. Ikeda, D. Sakai, S. Funatsu, K. Yamamoto, T. Suzuki, K. Harada, J. Nishii, Generation of alkali-free and high-proton concentration layer in a soda lime glass using non-contact corona discharge, J. Appl. Phys. 114 (2013) 063303. https://doi.org/10.1063/1.4817760.

[90] Mersen BOOSTEC® Silicon Carbide Datasheet, (n.d.). https://www.mersen.com/fileadmin/user_upload/pdf/ht/21-silicon-carbide-

sic-boostec-mersen.pdf (accessed October 12, 2021).

[91] Tantec SpotTEC - product information, (n.d.). https://mk0tantec25go4oy6kbt.kinstacdn.com/wp-content/uploads/2020/06/SpotTEC-GB.pdf (accessed October 9, 2021).

[92] Hysol EA9321 Datasheet, (n.d.). https://tdsna.henkel.com/americas/na/adhesives/hnauttds.nsf/web/1B38A9E963F1BB0B85257BC60067B1AE/$File/LOCTITE EA 9321 AERO-EN.pdf (accessed October 12, 2021).

[93] M. Salvo, V. Casalegno, M. Suess, L. Gozzelino, C. Wilhelmi, Laser surface nanostructuring for reliable Si3N4/Si3N4 and Si3N4/Invar joined components, Ceram. Int. 44 (2018) 12081–12087. https://doi.org/10.1016/j.ceramint.2018.03.226.

[94] S. Bhattacharjee, DLS and zeta potential – What they are and what they are not?, J. Control. Release. 235 (2016) 337–351. https://doi.org/10.1016/j.jconrel.2016.06.017.

[95] T. Luxbacher, The ZETA Guide Principles of the Streaming Potential Technique, Anton Paar, n.d. https://www.anton-paar.com/corp-en/the-zeta-guide/.

[96] S. Spriano, V. Sarath Chandra, A. Cochis, F. Uberti, L. Rimondini, E. Bertone, A. Vitale, C. Scolaro, M. Ferrari, F. Cirisano, G. Gautier di Confiengo, S. Ferraris, How do wettability, zeta potential and hydroxylation degree affect the biological response of biomaterials?, Mater. Sci. Eng. C. 74 (2017) 542–555. https://doi.org/10.1016/j.msec.2016.12.107.

[97] M.R. Madani, P.K. Ajmera, Characterization of silicon oxide films grown at room temperature by point-to-plane corona discharge, J. Electron. Mater. 22 (1993) 1147–1152. https://doi.org/10.1007/BF02817687.

[98] D.-K. Kim, K.-S. Jeong, Y.-S. Kang, H.-K. Kang, S.W. Cho, S.-O. Kim, D. Suh, S. Kim, M.-H. Cho, Controlling the defects and transition layer in SiO2 films grown on 4H-SiC via direct plasma-assisted oxidation, Sci. Rep. 6 (2016) 34945. https://doi.org/10.1038/srep34945.

[99] A. Piri, H.R. Kim, J. Hwang, Prevention of damage caused by corona discharge-generated reactive oxygen species under electrostatic aerosol-to-hydrosol sampling, J. Hazard. Mater. 384 (2020) 121477. https://doi.org/10.1016/j.jhazmat.2019.121477.

[100] A.J. Harris, B. Vaughan, J.A. Yeomans, P.A. Smith, S.T. Burnage, Surface preparation of silicon carbide for improved adhesive bond strength in armour applications, J. Eur. Ceram. Soc. 33 (2013) 2925–2934. https://doi.org/10.1016/j.jeurceramsoc.2013.05.026.

[101] A. Lazaro, K. Sato, H.J.H. Brouwers, J.W. Geus, Pore structure development of silica particles below the isoelectric point, Microporous Mesoporous Mater. 267 (2018) 257–264. https://doi.org/10.1016/j.micromeso.2018.03.031.

[102] Henkel, Safety Data Sheet - LOCTITE EA 9321 AERO PART A QT, n.d. https://www.ellsworth.com/products/adhesives/epoxy/henkel-loctite-hysol-ea-9321-aero-epoxy-adhesive-1-qt-kit/.

[103] Henkel, Safety Data Sheet - LOCTITE EA 9321 AERO PART B PT, n.d. https://www.ellsworth.com/products/adhesives/epoxy/henkel-loctite-hysol-ea-9321-aero-epoxy-adhesive-1-qt-kit/.

[104] F. Valenza, V. Casalegno, S. Gambaro, M.L. Muolo, A. Passerone, M. Salvo, M. Ferraris, Surface engineering of SiCf/SiC composites by selective thermal removal, Int. J. Appl. Ceram. Technol. 14 (2017) 287–294. https://doi.org/10.1111/ijac.12618.

[105] V. Casalegno, F. Valenza, C. Balagna, R. Sedlák, V. Girman, M. Salvo, S. De la Pierre des Ambrois, M. Ferraris, Characterisation of joined surface modified SiCf/SiC composites, Ceram. Int. 46 (2020) 4159–4166. https://doi.org/10.1016/j.ceramint.2019.10.133.

[106] A. De Zanet, M. Pedroni, M. Salvo, E. Vassallo, V. Casalegno, Plasma etching as a surface engineering technique for SiC/SiC composites to improve joint strength, Ceram. Int. (2022). https://doi.org/10.1016/j.ceramint.2022.11.248.

[107] E. Vassallo, M. Pedroni, S.M. Pietralunga, R. Caniello, A. Cremona, F. Di Fonzo, F. Ghezzi, F. Inzoli, G. Monteleone, G. Nava, V. Spampinato, A. Tagliaferri, M. Zani, G. Angella, Black-silicon production process by CF4/H2 plasma, Thin Solid Films. 603 (2016) 173–179. https://doi.org/10.1016/j.tsf.2016.02.008.

[108] Wesgo Cusil-ABA Data Sheet, (n.d.). https://www.morganbrazealloys.com/media/6941/wesgo_cusil-aba_technical-data-sheet-2018.pdf (accessed June 15, 2022).

[109] J.K. Boadi, T. Yang, T. Iseki, Brazing of pressureless-sintered SiC using Ag-Cu-Ti alloy, J. Mater. Sci. 22 (1987) 2431–2434. https://doi.org/10.1007/BF01082127.

[110] Y. Liu, Z.R. Huang, X.J. Liu, Joining of sintered silicon carbide using ternary Ag–Cu–Ti active brazing alloy, Ceram. Int. 35 (2009) 3479–3484. https://doi.org/10.1016/j.ceramint.2009.03.016.

[111] Y. Liu, Y. Zhu, Y. Yang, X. Liu, Z. Huang, Microstructure of reaction layer and its effect on the joining strength of SiC/SiC joints brazed using Ag-Cu-In-Ti alloy, J. Adv. Ceram. 3 (2014) 71–75. https://doi.org/10.1007/s40145-014-0095-z.

[112] M.C. Halbig, B.P. Coddington, R. Asthana, M. Singh, Characterization of silicon carbide joints fabricated using SiC particulate-reinforced Ag–Cu–Ti alloys, Ceram. Int. 39 (2013) 4151–4162. https://doi.org/10.1016/j.ceramint.2012.10.271.

[113] R. Asthana, M. Singh, N. Sobczak, Wetting behavior and interfacial microstructure of palladium- and silver-based braze alloys with C–C and SiC–SiC composites, J. Mater. Sci. 45 (2010) 4276–4290. https://doi.org/10.1007/s10853-010-4647-5.

[114] M. Singh, R. Asthana, N. Sobczak, Active Brazing of SiC-Base Ceramics to High-Temperature Alloys, J. Mater. Eng. Perform. 29 (2020) 4898–4912. https://doi.org/10.1007/s11665-020-04934-3.

[115] M. Salvo, V. Casalegno, S. Rizzo, F. Smeacetto, A. Ventrella, M. Ferraris, Glasses and glass-ceramics as brazing materials for high-temperature applications, Woodhead Publishing Limited, 2013. https://doi.org/10.1533/9780857096500.3.525.

[116] D.R. Patel, T. Koyanagi, High-Temperature Creep Properties of SiC Fibers with Different Compositions, Fusion Sci. Technol. 75 (2019) 636–641. https://doi.org/10.1080/15361055.2019.1647029.

[117] D. Schawaller, B. Clauß, M.R. Buchmeiser, Ceramic Filament Fibers - A Review, Macromol. Mater. Eng. 297 (2012) 502–522. https://doi.org/10.1002/mame.201100364.

[118] R. d'Agostino, F. Cramarossa, V. Colaprico, R. D'Ettole, Mechanisms of etching and polymerization in radiofrequency discharges of CF 4 –H 2 , CF 4 –C 2 F 4 , C 2 F 6 –H 2 , C 3 F 8 –H 2, J. Appl. Phys. 54 (1983) 1284–

1288. https://doi.org/10.1063/1.332193.

[119] S. Nasrazadani, S. Hassani, Modern analytical techniques in failure analysis of aerospace, chemical, and oil and gas industries, in: Handb. Mater. Fail. Anal. with Case Stud. from Oil Gas Ind., Elsevier, 2016: pp. 39–54. https://doi.org/10.1016/B978-0-08-100117-2.00010-8.

[120] S. Pestchanyi, V. Safronov, I. Landman, Estimation of carbon fibre composites as ITER divertor armour, J. Nucl. Mater. 329–333 (2004) 697–701. https://doi.org/10.1016/j.jnucmat.2004.04.189.

[121] T. Hirai, S. Panayotis, V. Barabash, C. Amzallag, F. Escourbiac, A. Durocher, M. Merola, J. Linke, T. Loewenhoff, G. Pintsuk, M. Wirtz, I. Uytdenhouwen, Use of tungsten material for the ITER divertor, Nucl. Mater. Energy. 9 (2016) 616–622. https://doi.org/10.1016/j.nme.2016.07.003.

[122] A.T. Peacock, M. Merola, M.A. Pick, R. Tivey, Status of CFC development in Europe for ITER, Phys. Scr. T128 (2007) 23–28. https://doi.org/10.1088/0031-8949/2007/T128/005.

[123] L.L. SNEAD, Fusion Energy Applications, in: Carbon Mater. Adv. Technol., Elsevier, 1999: pp. 389–427. https://doi.org/10.1016/B978-008042683-9/50014-5.

[124] J. Linke, J. Du, T. Loewenhoff, G. Pintsuk, B. Spilker, I. Steudel, M. Wirtz, Challenges for plasma-facing components in nuclear fusion, Matter Radiat. Extrem. 4 (2019) 056201. https://doi.org/10.1063/1.5090100.

[125] M. Salvo, V. Casalegno, S. Rizzo, F. Smeacetto, M. Ferraris, M. Merola, One-step brazing process to join CFC composites to copper and copper alloy, J. Nucl. Mater. 374 (2008) 69–74. https://doi.org/10.1016/j.jnucmat.2007.07.010.

[126] P. Appendino, M. Ferraris, V. Casalegno, M. Salvo, M. Merola, M. Grattarola, Direct joining of CFC to copper, J. Nucl. Mater. 329–333 (2004) 1563–1566. https://doi.org/10.1016/j.jnucmat.2004.04.313.

[127] S. Roccella, E. Cacciotti, D. Candura, A. Mancini, A. Pizzuto, A. Reale, A. Tatì, E. Visca, Ultrasonic test of carbon composite/copper joints in the ITER divertor, Fusion Eng. Des. 88 (2013) 1802–1807. https://doi.org/10.1016/j.fusengdes.2013.05.078.

[128] Z. Yi, L. Ran, M. Yi, Differences in microstructure and properties of C/C composites brazed with Ag-Cu-Ti and Ni-Cr-P-Ti pasty brazing filler,

Vacuum. 168 (2019) 108804. https://doi.org/10.1016/j.vacuum.2019.108804.

[129] X. Song, H. Li, V. Casalegno, M. Salvo, M. Ferraris, X. Zeng, Microstructure and mechanical properties of C/C composite/Ti6Al4V joints with a Cu/TiCuZrNi composite brazing alloy, Ceram. Int. 42 (2016) 6347–6354. https://doi.org/10.1016/j.ceramint.2016.01.026.

[130] A.A. Shokati, N.Y. Zhou, J.Z. Wen, Dissimilar joining of carbon/carbon composites to Ti6Al4V using reactive resistance spot welding, J. Alloys Compd. 772 (2019) 418–428. https://doi.org/10.1016/j.jallcom.2018.09.018.

[131] E. Frank, F. Hermanutz, M.R. Buchmeiser, Carbon Fibers: Precursors, Manufacturing, and Properties, Macromol. Mater. Eng. 297 (2012) 493–501. https://doi.org/10.1002/mame.201100406.

[132] Manufacturing of fibre–polymer composite materials, in: Introd. to Aerosp. Mater., Elsevier, 2012: pp. 303–337. https://doi.org/10.1533/9780857095152.303.

[133] B. Clauß, Fibers for Ceramic Matrix Composites, in: Ceram. Matrix Compos., Wiley-VCH Verlag GmbH & Co. KGaA, Weinheim, Germany, n.d.: pp. 1–20. https://doi.org/10.1002/9783527622412.ch1.

[134] T. Nakagawa, Applications of Carbon/Carbon Composites Prepared by Yarn Method, in: Compr. Compos. Mater., Elsevier, 2000: pp. 47–55. https://doi.org/10.1016/B0-08-042993-9/00210-2.

[135] S. Dietrich, J.-M. Gebert, G. Stasiuk, A. Wanner, K.A. Weidenmann, O. Deutschmann, I. Tsukrov, R. Piat, Microstructure characterization of CVI-densified carbon/carbon composites with various fiber distributions, Compos. Sci. Technol. 72 (2012) 1892–1900. https://doi.org/10.1016/j.compscitech.2012.08.009.

[136] G.L. Vignoles, J. Lachaud, Y. Aspa, Environmental Effects: Ablation of C/C Materials-Surface Dynamics and Effective Reactivity, in: Ceram. Matrix Compos., John Wiley & Sons, Inc., Hoboken, NJ, USA, 2014: pp. 353–388. https://doi.org/10.1002/9781118832998.ch12.

[137] L. Xiaowei, R. Jean-Charles, Y. Suyuan, Effect of temperature on graphite oxidation behavior, Nucl. Eng. Des. 227 (2004) 273–280. https://doi.org/10.1016/j.nucengdes.2003.11.004.

[138] Z.W. Yang, C.L. Wang, Y. Han, Y.T. Zhao, Y. Wang, D.P. Wang, Design

of reinforced interfacial structure in brazed joints of C/C composites and Nb by pre-oxidation surface treatment combined with in situ growth of CNTs, Carbon N. Y. 143 (2019) 494–506. https://doi.org/10.1016/j.carbon.2018.11.047.

[139] S. Niu, Z. Yang, C. Wang, Y. Han, Y. Wang, D. Wang, Improving the Bonding Strength of Nb–C/C Composite Brazed Structures by Preoxidation, Adv. Eng. Mater. 22 (2020) 2000065. https://doi.org/10.1002/adem.202000065.

[140] Enercon, Enercon, (n.d.). https://www.enerconind.com/treating/index.aspx.

[141] Plasma Etch, Plasma Etch, (n.d.). https://www.plasmaetch.com/.

[142] Tantec, Tantec PlasmaTec-X, (n.d.). https://tantec.com/atmospheric-plasma-treatment-system-plasmatec-x/.

[143] J. Xie, D. Xin, H. Cao, C. Wang, Y. Zhao, L. Yao, F. Ji, Y. Qiu, Improving carbon fiber adhesion to polyimide with atmospheric pressure plasma treatment, Surf. Coatings Technol. 206 (2011) 191–201. https://doi.org/10.1016/j.surfcoat.2011.04.016.

[144] X. Liu, J. Yan, F. Chen, B. Wang, Y. Li, J. Liu, Improving the Bonding Strength of CFRP by Atmospheric Pressure Plasma Jet, in: 2022 IEEE Int. Conf. Manip. Manuf. Meas. Nanoscale, IEEE, 2022: pp. 39–42. https://doi.org/10.1109/3M-NANO56083.2022.9941616.

[145] T.. Marshall, R.. Pawelko, R.. Anderl, G.. Smolik, B.. Merrill, R.. Moore, D.. Petti, Oxygen reactivity of a carbon fiber composite, Fusion Eng. Des. 69 (2003) 663–667. https://doi.org/10.1016/S0920-3796(03)00204-7.

[146] P. Appendino, M. Ferraris, V. Casalegno, M. Salvo, M. Merola, M. Grattarola, Proposal for a new technique to join CFC composites to copper, J. Nucl. Mater. 348 (2006) 102–107. https://doi.org/10.1016/j.jnucmat.2005.09.007.

[147] Tantec, PlasmaTec-X - Atmospheric Plasma: Product Information, (n.d.). https://www.tantec.com/wp-content/uploads/2020/05/PlasmaTEC-X-GB.pdf.

[148] M. Salvo, V. Casalegno, Y. Vitupier, L. Cornillon, L. Pambaguian, M. Ferraris, Study of joining of carbon/carbon composites for ultra stable structures, J. Eur. Ceram. Soc. 30 (2010) 1751–1759. https://doi.org/10.1016/j.jeurceramsoc.2009.12.013.

[149] M. Singh, R. Asthana, T.P. Shpargel, Brazing of carbon–carbon composites to Cu-clad molybdenum for thermal management applications, Mater. Sci. Eng. A. 452–453 (2007) 699–704. https://doi.org/10.1016/j.msea.2006.11.031.

[150] J.-H. Lee, K.-N. Kim, Effects of a Nonthermal Atmospheric Pressure Plasma Jet on Human Gingival Fibroblasts for Biomedical Application, Biomed Res. Int. 2016 (2016) 1–9. https://doi.org/10.1155/2016/2876916.

[151] G.E. Conway, A. Casey, V. Milosavljevic, Y. Liu, O. Howe, P.J. Cullen, J.F. Curtin, Non-thermal atmospheric plasma induces ROS-independent cell death in U373MG glioma cells and augments the cytotoxicity of temozolomide, Br. J. Cancer. 114 (2016) 435–443. https://doi.org/10.1038/bjc.2016.12.

[152] K.G. Kostov, T.M.C. Nishime, A.H.R. Castro, A. Toth, L.R.O. Hein, Surface modification of polymeric materials by cold atmospheric plasma jet, Appl. Surf. Sci. 314 (2014) 367–375. https://doi.org/10.1016/j.apsusc.2014.07.009.

[153] V.N. Eremenko, Y.I. Buyanov, S.B. Prima, Phase diagram of the system titanium-copper, Sov. Powder Metall. Met. Ceram. 5 (1966) 494–502. https://doi.org/10.1007/BF00775543.

[154] J. Fish, G.J. Wagner, S. Keten, Mesoscopic and multiscale modelling in materials, Nat. Mater. 20 (2021) 774–786. https://doi.org/10.1038/s41563-020-00913-0.

[155] S.A. Berry, T.J. Horvath, Discrete-Roughness Transition for Hypersonic Flight Vehicles, J. Spacecr. Rockets. 45 (2008) 216–227. https://doi.org/10.2514/1.30970.

[156] J. Lachaud, Y. Aspa, G.L. Vignoles, Analytical modeling of the steady state ablation of a 3D C/C composite, Int. J. Heat Mass Transf. 51 (2008) 2614–2627. https://doi.org/10.1016/j.ijheatmasstransfer.2008.01.008.

[157] G.L. Vignoles, J. Lachaud, Y. Aspa, J.-M. Goyhénèche, Ablation of carbon-based materials: Multiscale roughness modelling, Compos. Sci. Technol. 69 (2009) 1470–1477. https://doi.org/10.1016/j.compscitech.2008.09.019.

[158] J. Lachaud, G.L. Vignoles, A Brownian motion technique to simulate gasification and its application to C/C composite ablation, Comput. Mater. Sci. 44 (2009) 1034–1041.

https://doi.org/10.1016/j.commatsci.2008.07.015.

[159] G.L. Vignoles, Y. Aspa, M. Quintard, Modelling of carbon–carbon composite ablation in rocket nozzles, Compos. Sci. Technol. 70 (2010) 1303–1311. https://doi.org/10.1016/j.compscitech.2010.04.002.

[160] G. Vignoles, J. Lachaud, Y. Aspa, Roughness Evolution in Ablation of Carbon-Based Materials: Multi-Scale Modelling and Material Analysis, in: Proc. 5th Eur. Work. Therm. Prot. Syst. Hot Struct., 2006.

[161] K. Pearson, The Problem of the Random Walk, Nature. 72 (1905) 294–294. https://doi.org/10.1038/072294b0.

[162] J. Schindelin, I. Arganda-Carreras, E. Frise, V. Kaynig, M. Longair, T. Pietzsch, S. Preibisch, C. Rueden, S. Saalfeld, B. Schmid, J.-Y. Tinevez, D.J. White, V. Hartenstein, K. Eliceiri, P. Tomancak, A. Cardona, Fiji: an open-source platform for biological-image analysis, Nat. Methods. 9 (2012) 676–682. https://doi.org/10.1038/nmeth.2019.

[163] K. Zhang, L. Zhang, R. He, K. Wang, K. Wei, B. Zhang, Joining of C f /SiC Ceramic Matrix Composites: A Review, Adv. Mater. Sci. Eng. 2018 (2018) 1–15. https://doi.org/10.1155/2018/6176054.

[164] R. Asthana, M. Singh, Active metal brazing of advanced ceramic composites to metallic systems, in: Adv. Brazing, Elsevier, 2013: pp. 323–360. https://doi.org/10.1533/9780857096500.2.323.

[165] Z. Zhao, K. Li, W. Li, Q. Liu, G. Kou, Y. Zhang, Preparation, ablation behavior and mechanism of C/C-ZrC-SiC and C/C-SiC composites, Ceram. Int. 44 (2018) 7481–7490. https://doi.org/10.1016/j.ceramint.2018.01.125.

[166] Saxonia, BrazeTec CB4 Technical Datasheet, n.d. https://www.saxonia-tm.de/Brazetec/en/datenblaetter/show_TD_BrazeTec_CB_4_EN.pdf.

[167] N.Y. Taranets, H. Jones, Wettability of aluminium nitride based ceramics of different porosity by two active silver based brazing alloys, Mater. Sci. Eng. A. 379 (2004) 251–257. https://doi.org/10.1016/j.msea.2004.02.021.

[168] I. Südmeyer, T. Hettesheimer, M. Rohde, On the shear strength of laser brazed SiC–steel joints: Effects of braze metal fillers and surface patterning, Ceram. Int. 36 (2010) 1083–1090. https://doi.org/10.1016/j.ceramint.2009.12.010.

[169] J. Schäfer, T. Hofmann, J. Holtmannspötter, M. Frauenhofer, J. von Czarnecki, H.-J. Gudladt, Atmospheric-pressure plasma treatment of

polyamide 6 composites for bonding with polyurethane, J. Adhes. Sci. Technol. 29 (2015) 1807–1819. https://doi.org/10.1080/01694243.2015.1037380.

[170] L.F. Cheng, Y. Xu, L. Zhang, X. Yin, Preparation of an oxidation protection coating for c/c composites by low pressure chemical vapor deposition, Carbon N. Y. 38 (2000) 1493–1498. https://doi.org/10.1016/S0008-6223(00)00086-5.

[171] A.J. Knoll, P. Luan, A. Pranda, R.L. Bruce, G.S. Oehrlein, Polymer etching by atmospheric-pressure plasma jet and surface micro-discharge sources: Activation energy analysis and etching directionality, Plasma Process. Polym. 15 (2018) 1700217. https://doi.org/10.1002/ppap.201700217.

[172] W. Guo, H. Xiao, E. Yasuda, Y. Cheng, Oxidation kinetics and mechanisms of a 2D-C/C composite, Carbon N. Y. 44 (2006) 3269–3276. https://doi.org/10.1016/j.carbon.2006.06.027.

[173] V. Casalegno, L. Ferrari, M. Jimenez Fuentes, A. De Zanet, S. Gianella, M. Ferraris, V.M. Candelario, High-Performance SiC–Based Solar Receivers for CSP: Component Manufacturing and Joining, Materials (Basel). 14 (2021) 4687. https://doi.org/10.3390/ma14164687.

[174] N.S. Lewis, Research opportunities to advance solar energy utilization, Science (80-.). 351 (2016). https://doi.org/10.1126/science.aad1920.

[175] H.L. Zhang, J. Baeyens, J. Degrève, G. Cacères, Concentrated solar power plants: Review and design methodology, Renew. Sustain. Energy Rev. 22 (2013) 466–481. https://doi.org/10.1016/j.rser.2013.01.032.

[176] K. Vignarooban, X. Xu, A. Arvay, K. Hsu, A.M. Kannan, Heat transfer fluids for concentrating solar power systems – A review, Appl. Energy. 146 (2015) 383–396. https://doi.org/10.1016/j.apenergy.2015.01.125.

[177] C.K. Ho, Advances in central receivers for concentrating solar applications, Sol. Energy. 152 (2017) 38–56. https://doi.org/10.1016/j.solener.2017.03.048.

[178] C.K. Ho, B.D. Iverson, Review of high-temperature central receiver designs for concentrating solar power, Renew. Sustain. Energy Rev. 29 (2014) 835–846. https://doi.org/10.1016/j.rser.2013.08.099.

[179] A.G. Fernández, J. Gomez-Vidal, E. Oró, A. Kruizenga, A. Solé, L.F. Cabeza, Mainstreaming commercial CSP systems: A technology review,

Renew. Energy. 140 (2019) 152–176. https://doi.org/10.1016/j.renene.2019.03.049.

[180] A.L. Ávila-Marín, Volumetric receivers in Solar Thermal Power Plants with Central Receiver System technology: A review, Sol. Energy. 85 (2011) 891–910. https://doi.org/10.1016/j.solener.2011.02.002.

[181] R. Capuano, T. Fend, H. Stadler, B. Hoffschmidt, R. Pitz-Paal, Optimized volumetric solar receiver: Thermal performance prediction and experimental validation, Renew. Energy. 114 (2017) 556–566. https://doi.org/10.1016/j.renene.2017.07.071.

[182] T. Fend, W. Völker, R. Miebach, O. Smirnova, D. Gonsior, D. Schöllgen, P. Rietbrock, Experimental investigation of compact silicon carbide heat exchangers for high temperatures, Int. J. Heat Mass Transf. 54 (2011) 4175–4181. https://doi.org/10.1016/j.ijheatmasstransfer.2011.05.028.

[183] T. Fend, R.- Pitz-Paal, O. Reutter, J. Bauer, B. Hoffschmidt, Two novel high-porosity materials as volumetric receivers for concentrated solar radiation, Sol. Energy Mater. Sol. Cells. 84 (2004) 291–304. https://doi.org/10.1016/j.solmat.2004.01.039.

[184] H2020 NEXTOWER - website, (n.d.). https://www.h2020-nextower.eu/.

[185] S. Alexopoulos, B. Hoffschmidt, Advances in solar tower technology, Wiley Interdiscip. Rev. Energy Environ. 6 (2017) e217. https://doi.org/10.1002/wene.217.

[186] P.K. Gianchandani, V. Casalegno, F. Smeacetto, M. Ferraris, Pressure-less joining of C/SiC and SiC/SiC by a MoSi2/Si composite, Int. J. Appl. Ceram. Technol. 14 (2017) 305–312. https://doi.org/10.1111/ijac.12631.

[187] P.K. Gianchandani, V. Casalegno, M. Salvo, G. Bianchi, A. Ortona, M. Ferraris, SiC foam sandwich structures obtained by Mo-wrap joining, Mater. Lett. 221 (2018) 240–243.

[188] P.K. Gianchandani, Joining of Ceramics and Ceramic Matrix Composites (CMC) for Aerospace and Energy Applications, Politecnico di Torino, 2018.